Condition Monitoring of Axial Piston Pump

A Thesis Submitted to the
College of Graduate Studies and Research
In Partial Fulfillment of the Requirements for
the Degree of Master of Science
in the Department of Mechanical Engineering
University of Saskatchewan
Saskatoon

_____

Zeliang Li

Permission to Use

In presenting this thesis in partial fulfillment of the requirements for a postgraduate degree from the University of Saskatchewan, I agree that the libraries of this University may make it freely available for inspection. I further agree that the permission for copying this thesis in any manner, in whole or in part for scholarly purposes, may be granted by the professors who supervised this work or, in their absence, by the Head of the Department or Dean of the College in which this thesis work was conducted. It is understood that any copying, publication or use of this thesis or parts thereof for financial gain shall not be allowed without my written permission. It is also understood that due recognition shall be given to me and to the University of Saskatchewan in any scholarly use which may be made of any material in this thesis.

Requests for permission to copy or to make other use of material in this thesis, in whole or in part, should be addressed to:

Head of the Department of Mechanical Engineering
University of Saskatchewan
Engineering Building
57 Campus Drive
Saskatoon, Saskatchewan S7N 5A9
Canada

Abstract

Condition Monitoring is an area that has seen substantial growth in the last few decades. The purpose for implementing condition monitoring in industry is to increase productivity, decrease maintenance costs and increase safety. Therefore, condition monitoring can be used not only for planning maintenance but also for allowing the selection of the most efficient equipment to minimize operating costs.

Hydraulic systems are widely used in industry, aerospace and agriculture and are becoming more complex in construction and in function. Reliability of the systems must be supported by an efficient maintenance scheme. Due to component wear or failure, some system parameters may change causing abnormal behaviour in each component or in the overall circuit. Research in this area has been substantial, and includes specialized studies on artificial fault simulation at the University of Saskatchewan.

In this research, an axial pump was the focus of the study. In an axial piston pump, wear between the various faces of components can occur in many parts of the unit. As a consequence, leakage can occur in locations such as between the valve plate and barrel, the drive shaft and oil wiper, the control piston and piston guide, and the swash plate and slippers. In this study, wear (and hence leakage) between the pistons and cylinder bores in the barrel was of interest. Researchers at the University of Saskatchewan, as well as at other research institutions, have been involved in studies to detect wear in pumps using a variety of condition monitoring algorithms. However, to verify the reliability and indeed, limitations of some of the approaches, it is necessary to test the algorithms on systems with “real” leakage. To introduce actual wear in the piston of pumps can be very difficult and very expensive. Hence, introducing piston wear in an “artificial” manner would be of great benefit in the evaluation of various condition monitoring techniques.

Since leakage is a direct consequence of piston wear, it is logical to conclude that varying the leakage in some prescribed manner can be used to artificially simulate wear. A prime concern, therefore, is to be able to precisely understand the dynamic relationships between the wear and leakage and the effect it has on the output flow or pressure waveform from the pump.

Introducing an artificial leakage to simulate the wear of pistons is a complex task. The creation of an artificial leakage path was not simply a process of providing a resistive short to the tank at the outlet of the pump port as was done in other studies. The objective was to create a leakage environment that would simulate leakage from a single piston (or combination of several pistons thereof). The complexity of the flow and pressure ripple waveforms (which various condition monitoring algorithms require) was such that a more comprehensive leakage behaviour had to be modeled and experimentally created.

A pressure control servo valve with a very high frequency response was employed to divert the flow from the pump outlet with a prescribed waveform directly to the tank to simulate the piston leakage from the high pressure discharge chamber to the pump case drain chamber as the simulated worn piston made contact with the high pressure chamber. The control algorithm could mimic the action of a single worn piston at various degrees of wear. The experimental results indicated that the experimental system could successfully introduce artificial leakage into the pump which was quite consistent with a unit with a “real” worn piston. Comparisons of the pressure ripples from an actual faulty pump (worn piston) and the “artificial” faulty pump (artificial leakage) are presented.

Acknowledgements

The author would like express his sincere gratitude to his supervisors, Dr. Richard Burton and Dr. Peter Nikiforuk, for their valuable guidance, advice and encouragement throughout the course of this study and the writing of this thesis. It was a great pleasure for the author to work with his supervisors. This has been a precious opportunity for the author not only to gain knowledge and skills in the fluid power and control areas, but also to learn much more about approaches, attitudes towards work and interpersonal relations.

In addition, the author would like to extend his sincere thanks to Mr. Doug Bitner for his essential technical assistance during all phases of this research. Additionally, gratitude is also owed to Mr. Tonglin Shang for his physical assistance.

Furthermore, the author wishes to express a lot of thanks to his family, particularly his wife, Hong Jiang, for their encouragement and support during this study.

Last, but not least, the author gratefully acknowledges the financial assistance, from a Discovery Grant from NSERC.

Table of Contents

Permission to Use……..i
Abstract…….ii
Acknowledgements……...iv
Table of Contents……..v
List of Figures…….viii
List of Tables……xi
Nomenclature……...xii

Chapter 1 Introduction…….....1
1.1 Background……....1
1.2 Condition monitoring of hydraulic pumps…….. ..4
1.3 Project objectives…… ……..8
1.4 Thesis outline…….…..10

Chapter 2 Axial Piston Pump…….11
2.1 Introduction of variable axial piston pump……..11
2.2 Failure modes and effects for pump components……....18
2.3 Choice of parameter to be studied: piston wear……...22
2.4 Summary……..…22

Chapter 3 Simulation…….. 23
3.1 Relationships between piston leakage and piston wear……...23
3.2 Simulation model…….26
3.3 Simulation results…….28
3.4 Summary…….....37

Chapter 4 Methodology……...39
4.1 Experimental methodology……..39
4.2 Experimental test system……41
4.2.1 Test circuit system……..41

4.2.2 Data acquisition system……..44
4.2.3 Pressure control servo valve……...…44
4.2.3.1 Pressure control servo valve inner structure and mechanism……44
4.2.3.2 Pressure control servo valve steady state flow……..….47
4.3 Method to measure leakage……..…48
4.3.1 Leakage from the worn piston (real leakage)……..…48
4.3.2 Introduced artificial leakage in the pressure servo valve……....48
4.4 Pressure control servo valve response……..…50
4.5 Test conditions and procedure……..…52
4.6 Summary……..52

Chapter 5 Experimental Results…….54
5.1 Experimental data repeatability……...…54
5.2 Pressure ripples from the normal pump……...56
5.2.1 Pressure ripples……...56
5.2.2 Pressure ripples changes with temperature ……....58
5.2.3 Output flow relationship with pressure……...59
5.3 Pressure ripples from the experimental faulty pump……..….61
5.4 Ripples from the artificial leakage faulty pump……..66
5.4.1 Artificial leakage…….66
5.4.2 Pressure ripple from the artificial faulty pump……...….....70
5.5 Comparison of the normal pump and faulty (artificial) pump pressure waveforms....74
5.6 Variable artificial leakage summary……....83
5.7 Summary……..84

Chapter 6 Conclusions and Future Work…….85
6.1 Introduction……..85
6.2 Summary and Conclusions…….....85
6.2.1 Faults in an axial piston pump, piston wear and its effect
on pump performance…….85

6.2.2 Methodology to introduce leakage……..86

6.2.3 Experimental results……87

6.2.4 Research conclusions……..87

6.3 Recommendations for future work…… ……..…..87

References…….…88

Appendix A Reynolds Number for Piston Leakage Fluid…….....92

Appendix B Derivation of Equations…….……...93

B.1 Derivation of the Equation for Total Pump Kinematical Flow…...93

B.2 Derivation of the Equation for Pump Output Pressure……...97

Appendix C Simulation Parameter…….105

Appendix D Calibration Information……...……..107

D1 Pressure Transducer……..…107

D2 Flow Transducer……..….108

D3 Diaphragm Differential Pressure Transducer…….……..109

Appendix E Experimental Instruments……..111

Appendix F Derivation of the Flow through the Pressure Control Servo Valve……..113

Appendix I Power Spectral Density……...118

Appendix H Normalization Data…….120

List of Figures

Figure 1.1 A basic hydraulic circuit: pump, control valve and actuator……...…2
Figure 1.2 A variable displacement axial piston pump……...….8
Figure 2.1 Variable displacement axial piston pump…….13
Figure 2.2 Pump pumping motion…….15
Figure 2.3 Relief notches in valve plate (Vickers PVB5)……..16
Figure 2.4 Instantaneous cylinder chamber pressure…….17
Figure 3.1 Pumping motion with leakage……..……24
Figure 3.2 Piston leakage passage - Annular leakage path……..…..25
Figure 3.3 Pump kinematical output flow (simulated)……..29
Figure 3.4 Pump output flow waveform (simulated).....30
Figure 3.5 Pump output pressure waveform (simulated).....32
Figure 3.6 Pump output pressure waveform (experimental).....32
Figure 3.7 Comparison of normal and faulty pump flow waveform (simulated)……..33
Figure 3.8 Piston delivered flow related to concave pattern (simulated)……..34
Figure 3.9 Comparison of normal pressure and faulty pump pressure waveforms (simulated)……...…….35
Figure 3.10 Faulty pressure ripples from simulation and experiment ……..35
Figure 3.11 Comparison of pump flow ripples with different worn pistons (simulated)..36
Figure 3.12 Comparison of pump pressure ripples with different worn pistons (simulated)…….…….…….37
Figure 4.1 Schematic of introducing artificial piston leakage for pump……...40
Figure 4.2 Schematic of the experimental setup……42
Figure 4.3 Photograph of the experimental system ……..44
Figure 4.4 Inner structure of the pressure control valve……46
Figure 4.5 Relationships of Fss, Fial and Fal ……..49
Figure 4.6 Pressure control servo valve responses with input signal ……...……51
Figure 5.1 Pressure ripple repeatability (experimental)……55
Figure 5.2 Pressure ripple for the normal pump (experimental)……56
Figure 5.3 Power spectral density of normal pump pressure ripple……..57
Figure 5.4 Comparison of the pump output flow at 26.5^0C and 38^0C (experimental)..…58

Figure 5.5 Comparison of the pump output pressure at 26.5^{0}C and 38.0 ^{0}C (experimental)……59
Figure 5.6 Comparison of pump output flow between 7 MPa and 21 MPa at 30.0^{0}C (experimental)……...60
Figure 5.7 Pressure ripple of the faulty pump (experimental) ……..62
Figure 5.8 Real faulty pump power spectral density…….63
Figure 5.9 Pressure ripple comparison between normal pump and faulty pump (experimental)……..…....64
Figure 5.10 Power spectral density comparisons of normal pump and faulty pump pressure……..……...64
Figure 5.11 Pressure comparison of normal and real faulty pumps (experimental)……..65
Figure 5.12 Comparison of normal pump and faulty pump power spectral density……..66
Figure 5.13 Introduced additional artificial leakage (experimental)…….67
Figure 5.14 Comparison of the additional artificial leakage and simulated theoretical piston leakage ……..…...68
Figure 5.15 Servo valve input signal ……69
Figure 5.16 Introduced additional artificial leakages from different valve inputs (experimental)…….70
Figure 5.17 Pressure ripple from artificial faulty pump (experimental)……71
Figure 5.18 Power spectral density of the pressure ripple from the artificial faulty pump……..72
Figure 5.19 Pressure ripples from different artificial faulty pumps (experimental)……..73
Figure 5.20 Pressure ripples from different artificial faulty pumps (detailed, experimental)……...……..73
Figure 5.21 Comparison of the experimental pressure waveforms for the pump with a real fault (not artificially created) and a normal pump …….74
Figure 5.22 Normalized data of a pump with a real fault (60 microns) with respect to the normal pump……...75
Figure 5.23 Comparison of the artificial faulty pressure and the normal pressure waveforms (experimental)……..…..…..76
Figure 5.24 Normalized pressure data of artificial faulty pump……..…..76

Figure 5.25 Comparison of pressure ripple between normal pump and faulty pump pressure waveforms (experimental)……77
Figure 5.26 Comparison of normalization data of real fault and artificial fault pressure (60 microns)……..…….78
Figure 5.27 Pressure ripple waveform comparison of a normal and real faulty pump (30 microns) (experimental)……..79
Figure 5.28 Normalized data of the real faulty pump (30 microns)……..80
Figure 5.29 Pressure comparison of a normal and artificial faulty pump (30 microns)....81
Figure 5.30 Normalized data of artificial faulty pump (30 microns)…….81
Figure 5.31 Comparison of the normalized data of the real faulty and the artificial faulty pump pressure waveform (30 microns)……..82
Figure 5.32 Comparison of real faulty and artificial faulty pump pressure waveforms (30 microns) (experimental)……83
Figure A.1 The schematic for piston leakage ……...92
Figure B.1 Scheme of axial piston pump for derivation of the flow equation ……..94
Figure B.2 Scheme for simple hydraulic circuit ……...97
Figure B.3 Control volume for the instantaneous piston flow ……..98
Figure B.4 Scheme for derivation of pump output pressure equation ……..99
Figure B.5 Discharge area of the piston port opening to the discharge chamber in the valve plate …….104
Figure D.1 Calibration of pressure transducer..……...107
Figure D.2 Calibration of flow transducer ……..109
Figure D.3 Calibration of diaphragm pressure transducer (used to measure calculate artificial leakage flow)…….……..110
Figure F.1 Equivalent circuit of the servo valve torque motor ……...113
Figure F.2 Simplified block diagram Model 15-010 pressure control servo valve..…...114
Figure F.3 Simplified block diagram Model 15-010 pressure control servo valve with needle valve as load ……..116
Figure H.1 Definition of data normalization ……..121
Figure H.2 Normalized data plot. ……...……121

List of Tables

Table 1.1Typical components' faults and their effects on circuit performance …….3
Table 2.1 Pump components' possible faults (causes) and effects ……...19
Table 5.1 Comparison indicator of four data sets ……...…….…..…55
Table 5.2 Artificial fault data ……84
Table 5.3 Real fault pump data …….84
Table C.1 Simulation parameter list ……...105
Table E.1 Summary of equipment for experiment …….111

Nomenclature

A_{dn} The discharge area for P_n piston port opening to the discharge chamber in valve plate [m^2]

A_p Piston of area [m^2]

A_v The discharge orifice area of the needle valve [m^2]

B Bulk modulus [Pa]

C_{d1} Flow discharge coefficient of the discharge area for piston port opening to discharge chamber

C_{d2} Discharge coefficient of needle valve orifice

d Diameter of piston [m]

h_g Gap (radial clearance) between piston and cylinder bore [m]

L Length of leakage passage [m]

m Number of pistons in pump

n 1, 2, 3….. m

ρ Flow density [kg/m^3]

P_c Case drain chamber pressure [Pa]

Pfp Faulty pressure ripple [Pa]

Pnd Pressure normalization data

Pnp Normal pressure ripple [Pa]

P_{pn} Instantaneous pressure in P_n piston chamber [Pa]

P_s Pump output pressure (discharge chamber pressure) [Pa]

Q_{kpn} Kinematical flow delivered by P_n piston [m^3/s]

Q_{lpn} Internal leakage from P_n piston to case chamber [m^3/s]

Q_p Flow from piston chamber to discharge chamber [m^3/s]

Q_{pn} Flow from P_n piston chamber to discharge chamber [m^3/s]

Q_s Pump output flow [m^3/s]

r Radius of piston [m]

R_p Piston pitch radius on barrel [m]

S_{pn} Stroke for P_n piston [m]

t Time [second]

V_0 Piston initial volume [m^3]

V_c Discharge chamber control volume [m^3]

Greek symbols:

α Phase delay [rad], equal to $2\pi / m$

β Angle of swash plate [rad]

μ Absolute fluid viscosity [$N.sec/m^2$]

ω Angular velocity of the pump drive shaft [rad/s]

Chapter 1 Introduction

1.1 Background

Condition monitoring is an area that has seen substantial growth in the last few decades. As a simple definition, condition monitoring is an approach which can be used to gain information on the "health" of components or systems. Condition monitoring includes not only fault detection and fault diagnosis, but also fault analysis. The purpose for implementing condition monitoring in industry is to increase productivity, decrease maintenance costs and increase safety. Therefore, condition monitoring can be used not only for planning maintenance, but also for allowing the selection of the most efficient equipment to minimize operating costs. The final goal of a successful condition monitoring scheme is to detect the presence of faults before a catastrophic event or unscheduled shutdown occurs. Condition monitoring is a management tool which provides information about the likely future performance, which is most suitable when the failure mode is gradual and progressive.

Hydraulic systems are becoming more complex in design and in function. The reliability of these systems must be supported by efficient "maintenance regimes". There are three such regimes: breakdown maintenance (most expensive), time based maintenance, and condition based maintenance (least expensive) [1]. Choosing a maintenance regime depends on the system. If the systems do not require high reliability or if economics or safety is not the issue, the breakdown maintenance approach may be sufficient. However, for maximum reliability and safety, the condition based maintenance approach should be implemented. In general, most hydraulic systems do require high reliability and thus the latter condition monitoring approach is most desirable.

Condition based maintenance of a system can be very cost effective. Hibberd (1988) estimated that it would save about £100M to £150M per year to apply condition based maintenance of pumping systems alone in British industry [2]. Thus, the condition monitoring of a hydraulic system can bring benefits other than just reliability and improved safety.

Fluid power systems are widely used in industries such as aerospace, automotive, agriculture, and construction just to name a few. One of the most important

considerations in any fluid power system is the control of pressurized fluid. If the control components are not selected properly, the system will not work as required. Consider the hydraulic circuit shown schematically in Figure 1. This circuit shows three of the basic components which are usually found in hydraulic applications: pump, control valve and actuator. Due to component wear or failure, some system parameters may change causing abnormal behavior in each component or in the overall circuit itself. Therefore, if the accurate and reliable performance of the system is an objective, it is necessary to monitor the condition of the main components of the system. To do so, it is necessary to understand what kind of failures can exist in each component and how those failures affect both the component's performance and that of the complete system.

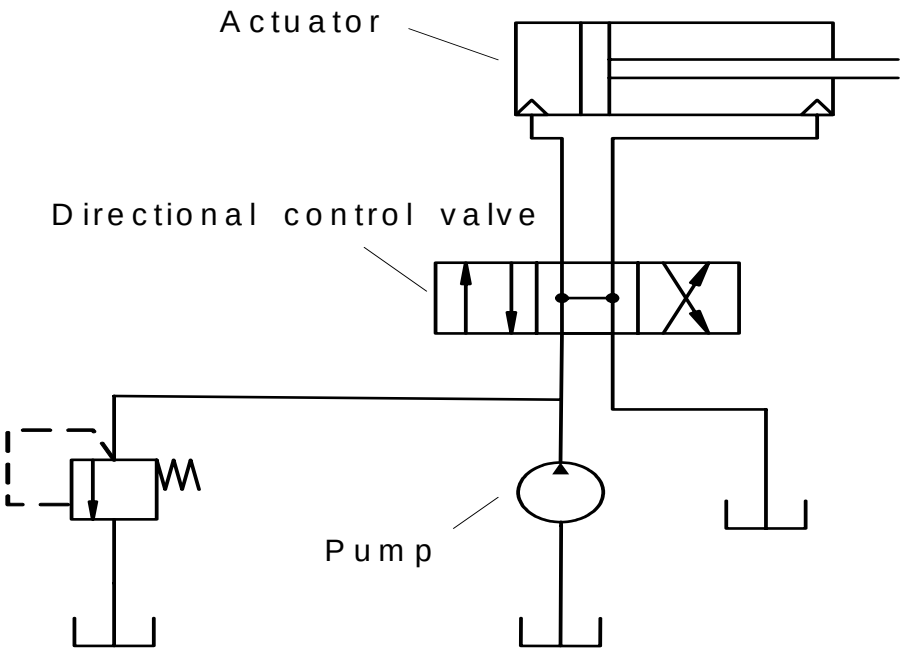

Figure1.1 A basic hydraulic circuit: pump, control valve and actuator

During the past few decades, a substantial amount of research has been done on the condition monitoring of hydraulic systems and components, mainly related to valves and actuators. Some of the more common techniques used for condition monitoring are: contamination control [3, 4], parameter or state estimation [5], spectral analysis [6], vibration analysis [7], acoustic emission [8], expert systems [1, 9], thermodynamic

measurement [10], extended Kalman filter (EKF) [5, 11], fuzzy logic [12], neural networks (NN) [1, 13, 14, 15, 16, 17] and support vector machine (SVM) [18]. Some of these techniques are “intrusive”; that is, they require the removal of a component part. Some are “off-line”, in that the analysis is done later or at some remote location. Some techniques are “on-line” in that the measurement is made in real time. A more detailed discussion of these areas and the work published on these topics is presented in the section on literature review.

Consider the circuit shown in Figure 1. As mentioned above, the main components are the pump, valve and actuator. Table 1 lists some of the more common faults which are experienced in these components and the effects that they have on the system performance.

Table 1.1 Typical components’ faults and their effects on circuit performance

Components	Faults	Effects
Actuator	1. Internal leakage (piston wear).	1. Poor positional accuracy, oil overheating, actuator drift.
Directional control valve	1. Internal leakage (spool and body). 2. Sticking (friction change).	1. Noise, inability to lock spool in the center position. 2. Noise, spool moves erratically.
Axial piston pump	1. Internal leakage (piston wear) 2. Wear of swash plate, bearing, slipper, driver shaft.	1. Pressure generation insufficient, flow drop off, noise. 2. Noise, overheating, vibration, increased torque and hence input power.

A great deal of the published research has focused on the application of condition monitoring techniques to one or several of the faults listed in Table 1. In most cases, verification tests on the components required physical failures which can be very costly, unsafe and in some cases, unreliable (a reasonable number of samples not being able to be collected for statistical significance). In order to reduce the cost, and to increase safety

and reliability, the components should not be damaged during these kinds of failures. Therefore, one approach that has been used is the introduction of “artificial faults” which simulate faults without damaging the components. Hindman et al [1] used “cross port calibrated orifices” to simulate internal leakage in the actuators and valves of an industrial backhoe loader. Bhojkar et al [19] used one of solenoids in a solenoid proportional valve to create an external force on the spool to mimic different friction characteristics on the valve spool. In addition, Le et al [13] and Crowther et al [14] introduced artificial friction at the actuators using a connecting cylinder whose damping was adjusted by cross port calibrated orifices.

1.2 Condition monitoring of hydraulic pumps

Many studies have been published during the past few decades on the topic of the condition monitoring of individual hydraulic components and of complete systems. Several techniques were used frequently in these studies. The following review will focus on the condition monitoring research and associated analyzing techniques as applied to hydraulic pumps which, as will be stated later, are the subject of this study.

Neill et al [8] used acoustic emission (AE) to detect incipient cavitation in centrifugal impeller pumps. The raw AE data from the AE sensors at three points were processed using root mean square (RMS). The results showed the AE can detect cavitation inception by non-intrusive means.

Yates [20] proposed that thermodynamic theory could be used to monitor pump performance. A monitoring system was used to measure various parameters, such as relative enthalpy change, suction pressure, discharge pressure, fluid temperature, and input power to the motor. The efficiencies of the pump and motor were calculated. Weddfelt et al [10] used a thermodynamic measurement method to monitor the condition of a fluid power system. The efficiencies of a pump, motor and fluid power transmission lines were calculated. The thermodynamic method was found to be dependent on measuring the quantities flow, pressure and temperature as compared to more traditional methods which use angular speed and torque in additional to flow rate, and pressure. The main drawback with a measurement system based on the thermodynamic properties was that it was very slow.

Cao [5] utilized the extended Kalman filter (EKF) to estimate parameters for the swash plate assembly and control piston in a load-sensing pump. In this research, the spring constant, damping coefficient and spring pretension in the swash plate assembly were estimated. The results indicated that the estimated values did agree quite well with their physical counterparts.

Lu et al [16] used neural networks (NN) to predict the wear in pistons in an axial piston pump. He simulated piston wear by machining clearances between the piston and sleeve. He used pump inlet pressure to detect changes in the performance of the pump. The sum of the inlet pressure variation (peak ripple of certain pistons) was used to train a neural network. The trained network was then tested by subjecting the network to a signal from a pump which was not used to train the network. He found that NNs could be used to detect increasing wear in the pistons. However, he found that if a network was tested with data that displayed faults larger than those used in the training, then a successful fault prediction was not possible. Conversely, he found that if the degree of wear was equal or less than that used in training, then the success rate was high. He concluded that this method had some limitations in reliably detecting faults. He also pointed out that the cost to replace the original piston by the machined pistons was very expensive, and introduced uncertainty in the experimental technique. He recommended that some other form of introducing the fault would be highly desirable.

In the most studies involving the condition monitoring of pumps, bearings were often the focus of the study and often involved vibration analysis. Luo and Smith [21] used demodulation analysis (one method to process the original vibration signal by filtering and rectifying) to classify the rolling-element bearing faults for earlier detection of bearing faults. Demodulation enhances repetitive signals which are caused by pulses emanating from damaged bearings. In the early stage, the signals for bearing flaws may go undetected among general machine noise. The use of the demodulation detection technique makes it possible to pinpoint not only the nature, but the location of bearing damage, such as inner race, outer race, rolling element, etc. This method could be use to classify early bearing faults in pumps.

Wang et al [22] classified bearing faults into six types. Six bearings with these faults were tested on a test-rig pump and vibration signals were collected under similar

conditions. All six sets of data were pre-processed. The input vectors were then formed by the time-domain RMS values plus the frequency-domain RMS values in each frequency band for all six sets of data. The bearing faults were classified successfully using neural network models. Wang concluded that the most relevant features of pre-processing the data for this problem were not only to save time, but also to achieve a high pattern classification success rate.

Domotor and Tepro [23] detected rolling bearing defects in a hot water circulating pump by frequency spectral analysis. They concluded that defects and cavitation are similar in appearance in the case of water pumps. Therefore, the vibration spectra must be analyzed carefully. In addition, they concluded that it is advisable to measure several parameters vibration, for example, acceleration, envelope acceleration and RMS velocity. Envelope acceleration usually can give an earlier alert signal than RMS velocity.

In contamination monitoring, ferrography is used widely. Ferrograhy is a monitoring method used to characterize wear debris recovered from the oil-wetted parts of an operating machine. The wear debris can be classified according to size, quantity, composition and morphology that give clues to the possible sources or regions of the wear debris. Ding et al [24] concluded that ferrography monitoring techniques are one of the most important and useful applications of ferrography, in terms of spectrometric oil analysis (SOA) and oil analysis.

Ukrainetz et al [25] used ferrography to study the wear particles generated in an axial piston pump that was operated under high temperature and high pressure. Two identical axial piston pumps in two independent, identical circuits were studied. However, the oil temperature in each circuit was controlled to be different (one at 50 ^{o}C, circuit No.1; the other at 100 ^{o} C, circuit No.2). The authors found that the oil in circuit No.2 became darker more quickly than that in circuit No.1. The cause of this discoloration was due to two sources: oxidation and wear. From the ferrograms, the number of particles in circuit No.2 was twice that of circuit No.1. Ukrainetz et al [26] also studied the wear of an axial piston pump operated under elevated fluid temperature and constant loading conditions. From their experiments, the components most susceptible to wear in the pump were the valve plate face, and the end of the relief groove. Although the authors did not use their study for condition monitoring, their

results did show where pumps are most susceptible in terms of wear under extreme variations in temperature.

Hunt [27] monitored the pressure at the inlet of coal high-pressure water ram pumps using a computer to plot the outlet flow and inlet pressure. Experiments were undertaken by gradually reducing the inlet pressure and permitting air to enter the inlet. From his pressure - flow plots, the results indicated that, at lower inlet pressures, especially when the temperature rises, or air enters the pump, the pump characteristics (for example, outlet flow) changed significantly. He also concluded that monitoring need not be complex; the simpler the approach, the more reliable it is. However, he concluded that what is most essential is that the "appropriate features" are monitored. Therefore, it is very important to carefully choose what parameter is to be tracked in condition monitoring.

Chen and Jiang [28] used wavelet analysis and fractal geometry to monitor the pressure signal of an axial plunger pump with seven plungers. One plunger “shoe-doffing” (a condition which occurs when the slipper becomes disconnected with the plunger) was employed to simulate the fault condition. From the pressure signal, it was noticed that, compared to the normal pressure signal, the pressure signal at the shoe-doffing state demonstrated a substantial “concave dip”. They concluded that the combination of wavelet analysis and fractal geometry was effective in condition monitoring of hydraulic pumps.

The literature reviewed to date has shown that little research has been reported which deals with introducing “artificial faults” into pumps. A possible reason for this is that, compared with valves and actuators, pumps have a much more complicated structure. For example, the variable displacement axial piston pump illustrated in Figure1.2 consists of a swash plate, barrel, valve plate, control piston, return spring, drive shaft, several pistons and bearings, etc. Each part of the pump is susceptible to wear and can be a cause of total failure if not detected early. To introduce faults directly by either running the pump to failure or by disassembling the pump to introduce a fault through part substitution, is very difficult compared to doing the same for a valve or actuator. Introducing artificial faults into the pump is equally difficult and remains a challenge for research.

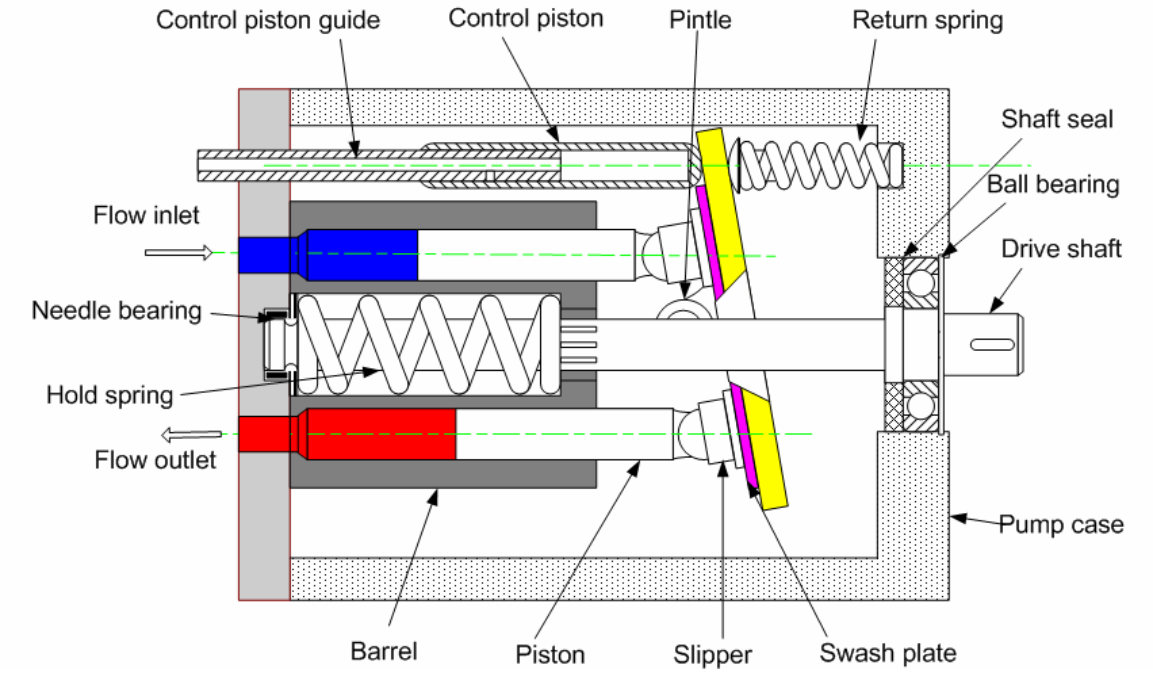

Figure 1.2 A variable displacement axial piston pump

1.3 Project objectives

In any hydraulic system, each component has a different function. If any individual component does not function properly, the overall system usually cannot work properly. (Note, an exception can be if the actuator is leaking, then the pump can deliver more flow to compensate). The pump is the heart of the hydraulic system and, as such, is indispensable for efficient circuit operation. In order to improve the reliability of hydraulic systems, it is necessary to continuously track the condition of pumps. The swash plate type variable displacement axial piston pump illustrated in Figure 1.2 is widely used because it is simple to control and easily adapted for energy saving systems and hence is the one that was used in this study.

It is known that leakage is a very useful indicator of wear between the various contact faces in hydraulic components such as valves and actuators. Le et al [13] and Crowther et al [14] monitored the condition of an actuator using leakage as an indicator. Others such as Hindman [1] introduced artificial leakage across a directional valve and actuator in a commercial loader backhoe as a means of simulating piston wear. Therefore,

leakage might be a logical parameter in a pump to be considered when monitoring the health of a hydraulic pump.

In pumps, wear between the various faces of components can occur in many parts of the unit. As a consequence, leakage can occur between the valve plate and barrel, the drive shaft and oil wiper, the control piston and piston guide, and the swash plate and slippers. In this study, wear (and hence leakage) between the pistons and cylinder bores in the barrel is considered. However, to introduce actual wear in the piston or cylinder bore can be very difficult and, as discussed by Lu [16], very expensive and unreliable. Hence, introducing piston wear or cylinder bore wear in an artificial manner would be of great benefit in evaluation various condition motioning techniques. Since leakage is a direct consequence of piston wear or cylinder bore wear, it is logical to conclude that varying the leakage in some prescribed manner can be used to "artificially" simulate wear. A prime concern, therefore, is to be able to understand the dynamic relationships between the wear and leakage and the affect it will have on the output flow or pressure waveform from the pump.

Piston wear and cylinder bore wear have similar cause and effect on leakage and subsequently on output flow and pressure waveforms from the pump. Therefore, to consider only one of them (piston wear or cylinder bore) is sufficient. To some extent, piston wear is easy to describe and to be understood and as such, is the focus of this study.

The objectives of this research were, therefore, as follows:

1. To understand in detail the cause and effect of piston wear on piston leakage and, subsequently, the output performance of the pump.
2. To develop methodologies for introducing artificial wear via leakage into the pump in accordance with Objective 1 and to determine their feasibility through simulation.
3. To implement the above methodologies in order to determine their success in artificially simulating wear in pistons in a variable displacement axial piston pump.

1.4 Thesis outline

This thesis is organized following the order of the research procedure. It is made up of six chapters.

Chapter 2. Description of the variable displacement axial piston pump: a variable displacement axial piston pump's structure and mechanism are presented. Failure modes and effects for pump components are discussed.

Chapter 3. Pump simulation: the piston wear which causes leakage is explained. The simulation results from a simplified model of an axial piston pump are presented. The change of flow ripple and pressure ripple from the pump outlet caused by a worn piston are illustrated.

Chapter 4. Methodology: the method of how to introduce artificial leakage into a pump is presented. The experimental test system is presented as well. In addition, one of the main components in the test rig, the pressure control servo valve, is described and the model of the servo valve is established.

Chapter 5. Experimental results: the experiment procedure is described. The experimental results are presented in tables and figures. A discussion on the repeatability of the experimental data is conducted.

Chapter 6. Conclusions and future work: the project objectives stated in Chapter 1 are revisited. Some conclusions are drawn and future work is recommended.

Chapter 2 Variable Displacement Axial Piston Pump

The inner construction and operation of a variable displacement axial piston pump are described in this chapter. Some of the more common faults and the effects that the faults have on the performance for each component in this pump are analyzed. The pump used in this study was a Vickers PVB 5 variable displacement axial piston pump but the discussion applies to all pumps of this type.

2.1 Introduction of variable axial piston pump

In every hydraulic circuit, the pump is an indispensable component. It is the pump that converts mechanical power into hydraulic power. Pumps can be classified by the direction of the output flow. A uni-direction pump is one in which the flow is in one direction, that is, the flow always is drawn in from the inlet suction port and delivered through the outlet, discharge port. However, in bi-direction pumps, the flow can change direction in several ways: changing the rotational direction of the drive shaft or using an "overcentre" swash plate. In a bi-direction pump, the outlet and inlet are interchangeable. In the overcenter type of pump, the flow is reversible without changing the rotational direction of the drive shaft. Instead, the angle of the swash plate (see Figure 1.2) can be varied from minus maximum, through zero, to plus maximum.

There are many kinds of pumps which are classified according to the different displacement elements: gear pump, piston pump, screw pump, vane pump, etc. Amongst them, the piston pump is widely used in industry because it possesses many advantages. Piston pumps can work over a wide range of pressures, are easy to control and are highly reliable. The displacement chambers of the piston pump are cylindrical surfaces, which mean that they can be manufactured with ease to a high degree of accuracy [29]. In addition, cylindrical surfaces require less complicated seals (usually, metal to metal seals). Small tolerances and precise sealing can result in smaller flow losses (commonly known as internal leakage). Therefore, piston pumps have high volumetric efficiencies.

According to the arrangement of the pistons with respect to the axis of the drive shaft, piston pumps are further sub-classified as axial piston or radial piston pumps.

- Axial piston pumps are those in which the axis of the pistons is parallel or at an angle less than 45 degree to the axis of the drive shaft.

- Radial piston pumps are those in which the axis of the pistons is perpendicular or at an angle greater than 45 degree to the axis of the drive shaft.

Axial piston pumps have a simple construction and are employed most commonly in hydraulic applications. Therefore, it is this type of pump that was considered in this study.

Axial piston pumps can be designed as fixed displacement or variable displacement systems. For fixed displacement pumps, the output flow is not adjustable. Some axial piston pumps can deliver different output flows by changing the angle of swash plate, and these are called variable displacement axial piston pumps. A cross section of such a pump is shown in Figure 2.1.

Variable displacement axial piston pumps convert mechanical power into hydraulic power by delivering different flows at different load pressures at the pump output. Variable displacement is accomplished by changing the swash plate angle about the pintle (see Figure 2.1). The main subcomponents of this kind of pump are the pistons, barrel, swash plate, bearings, drive shaft, valve plate, and the control piston.

Consider Figure 2.1. The drive shaft passes through a hole in the swash plate. One end of drive shaft is supported by a needle bearing in the valve plate. The other end of the drive shaft is supported by a deep groove ball bearing in the pump casing and connects to an electric motor through an appropriative coupling. The swash plate rotates about the pintle and is balanced by a control piston and a return spring. The angle of the swash plate can be controlled by the control piston that is modulated by some valve outside of the pump casing. The swash plate can be moved on a plate perpendicular to the axis of the drive shaft to obtain different displacements.

The barrel is attached directly to the drive shaft. As the drive shaft rotates, the barrel rotates. The pistons slide inside the barrel and the piston ends move along the swash plate on “slippers”. The pistons reciprocate inside the barrel holes (called barrel cylinders) due to the action of the piston ends (via the slippers) on the swash plate. This reciprocating action is responsible for the pumping capability of the unit.

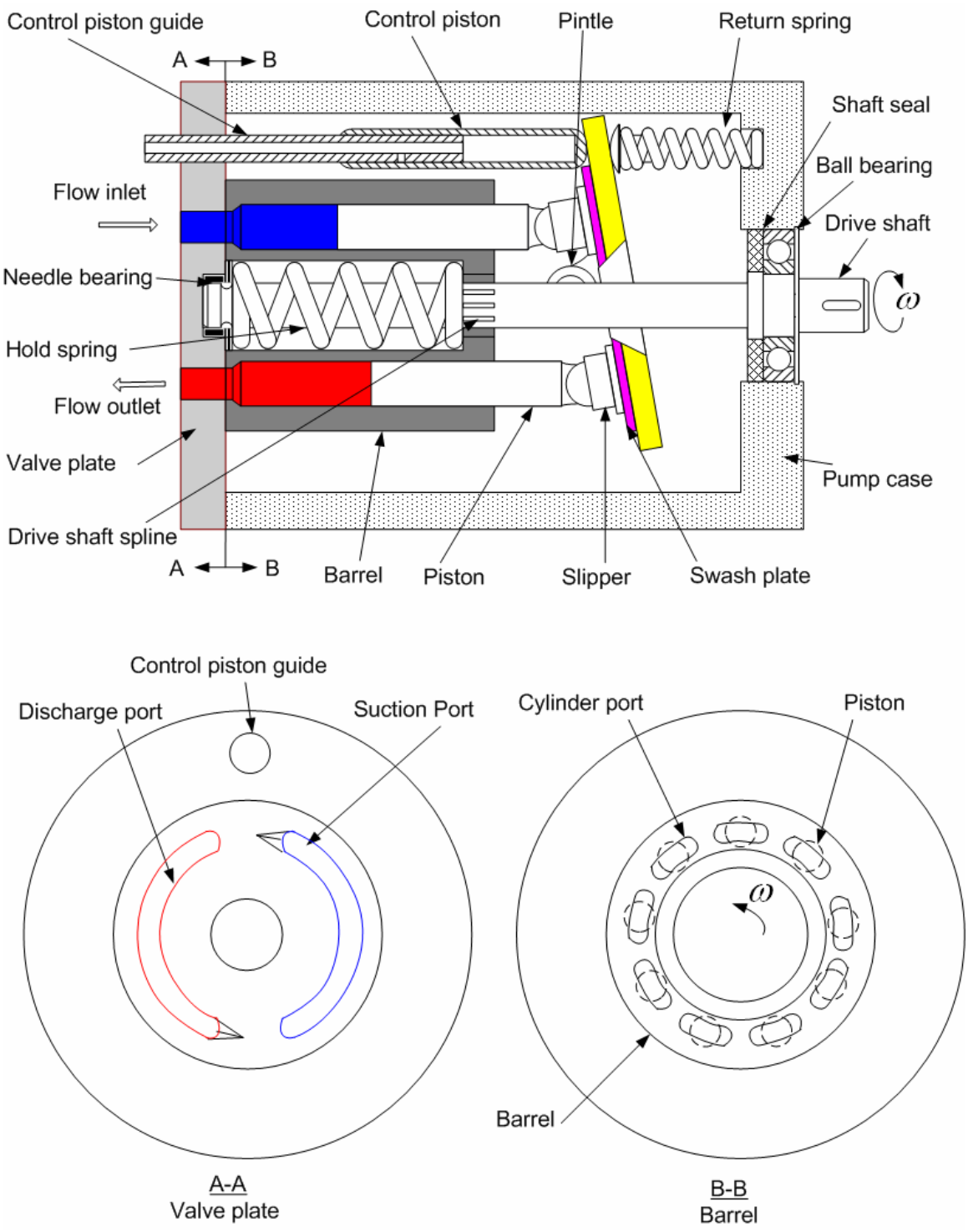

Figure 2.1 Variable displacement axial piston pump

The pump barrel is always held against the valve plate, via a spring that is inside the barrel. There are two “kidney shape” ports in the valve plate. One is at the suction

port connected to the pump inlet (see sections illustrated in Figure 2.1). The other is the discharge port connected to the pump outlet. The barrel also contains cylinder ports on the end that contacts the valve plate. The movement of the cylinder ports against the valve plate directs the fluid into or out of the cylinders. In this manner, fluid is drawn in through the suction port and discharged through the discharge port repeatedly as the barrel rotates.

In order to facilitate discussion, it is assumed that the pump operation begins at the suction port. Consider Figure 2.2. The red kidney ports are the high pressure ports and the blue ones, the suction ports. When a piston is at the very top, this condition is called "top dead centre" (TDC), (Figure 2.2a). When the barrel rotates (clockwise in Figure 2.2a to 2.2b), the piston in the barrel moves away from the valve plate (out of the page) creating a vacuum and thus fluid is forced into the chamber from the inlet line. The piston continues this outward motion in the barrel, until the piston reaches the bottom dead centre (BDC), Figure 2.2c. The arrows in the figures show the direction of the barrel rotation. At the BDC, the piston chamber is completely filled with fluid. Once the piston passes the BDC, the piston moves backwards towards the valve plate (into the page) and fluid is discharge through the outlet of the pump. The piston continues to discharge fluid, (Figure 2.2d) until it reaches the TDC again. This process defines one complete pumping cycle for one piston and is repeated every revolution.

In every pump, there are more than one piston and usually the number is an "odd" value [30]. For example, there are 9 pistons in the Vickers PVB5 pump. Each piston follows the above cycle but with a certain phase delay with respect to the other pistons in the barrel over one revolution. When the pump is running, half of the pistons are usually delivering fluid to the discharge kidney port. Therefore, the output flow appears to be continuous. In reality, each piston delivers flow in a sinusoidal fashion and the total flow is the sum of each individual piston flow over one cycle. This will be demonstrated in the following chapter.

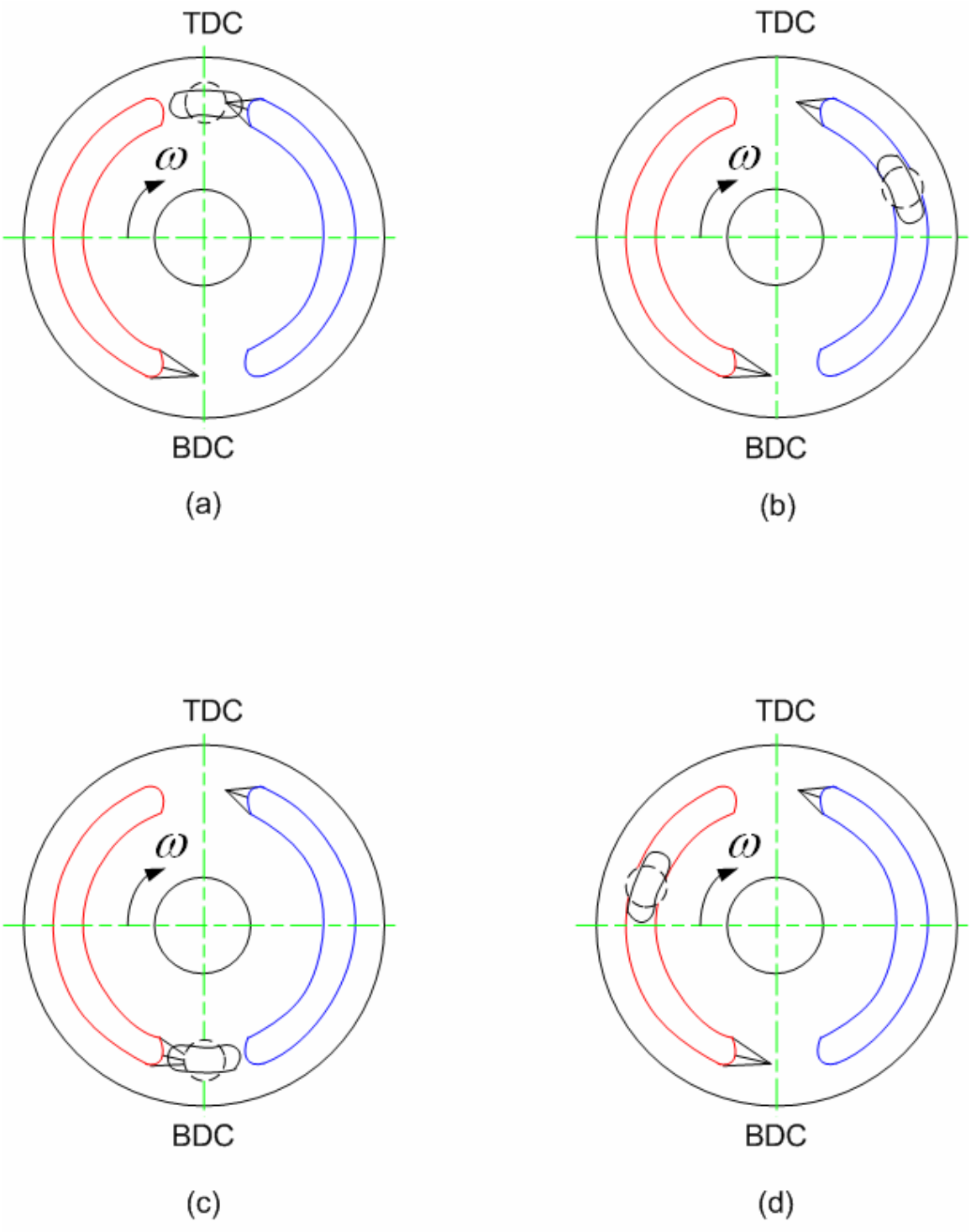

Figure 2.2 Pump pumping motion

In order to reduce the noise of pump and to make the output flow more even, there are specially designed relief notches on the valve plates, as shown in Figure 2.3.

The two “relief notches” have a “V” shape, which starts at zero depth near TDC or BDC and then reaches a maximum depth at the beginning of the kidney shape ports. The relief notches “expose” the cylinder chamber to the outlet or inlet ports in the valve plate in a gradual manner, which helps to facilitate a slower pressure gradient in the cylinder chamber. From a noise point of view, a very sharp pressure gradient can translate into a loud knocking sound in the pump and should be avoided.

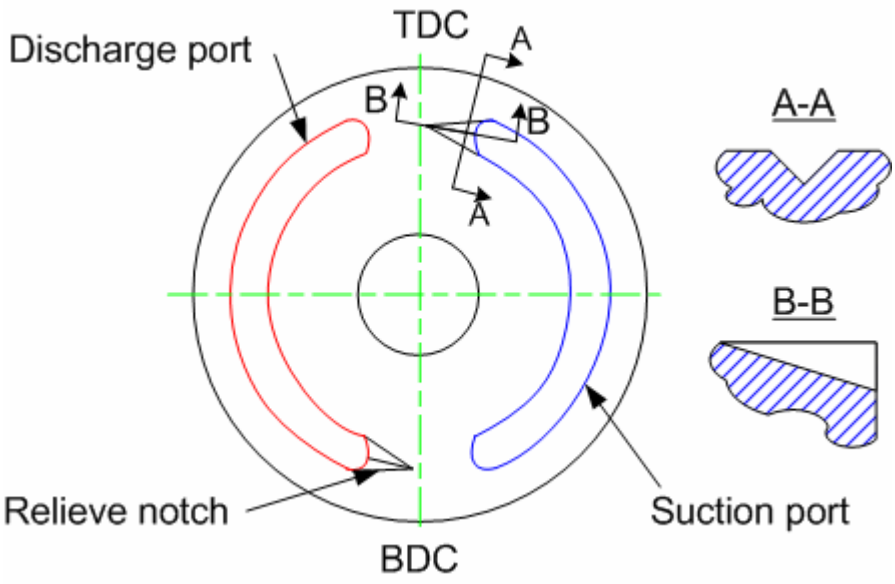

Figure 2.3 Relief notches in valve plate (Vickers PVB5)

Figure 2.4 shows a comparison of the transient pressure between a valve plate with relief notches and one without relief notches. From both of the figures, it is apparent that the relief notches force the transient pressure gradient to be more gradual than when there are no notches. In actual fact, the pressure overshoot for some “no notch” situations can be quite severe. Figure 2.4c provides the nomenclature for Figures 2.4 a and b.

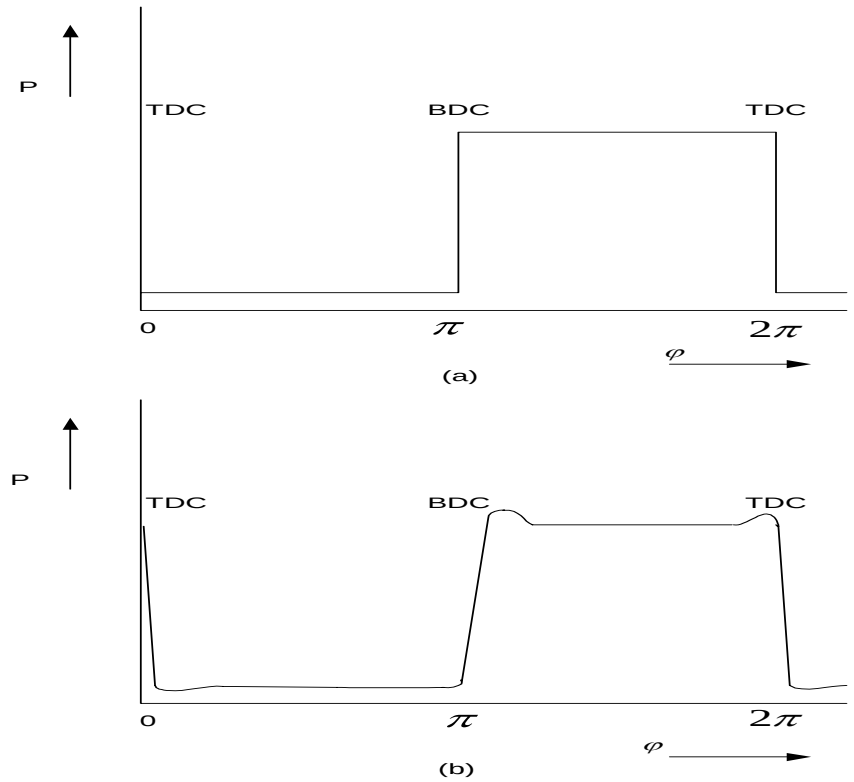

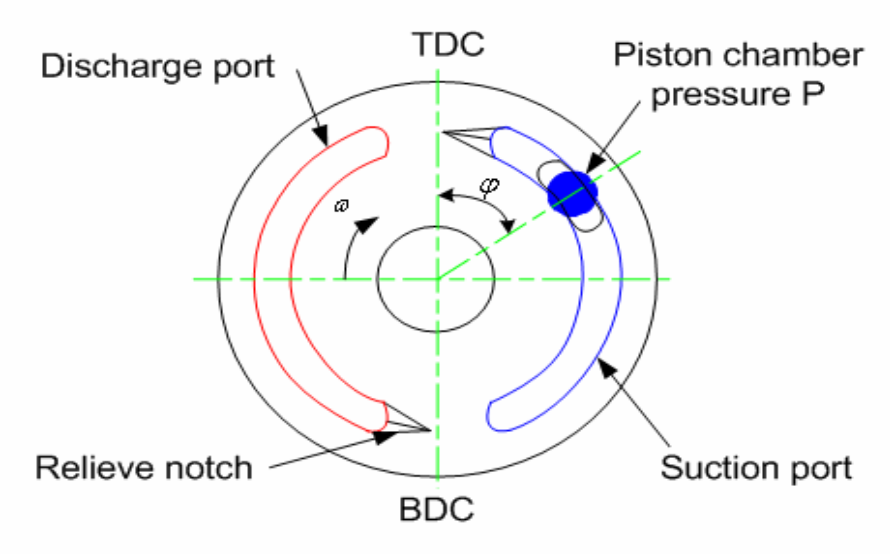

(c)

P: pressure, φ: cylinder angle on valve plate

Figure 2.4 Instantaneous cylinder chamber pressure

a. valve plate without relief notches

b. valve plate with relief notches

c. definition of P and φ

Pumps are flow sources, and not pressure sources. Pressure in the system is a consequence of the resistance to output flow. Therefore, the primary function of a controller on axial displacement pumps is to control the output flow by adjusting the angle of the swash plate. In Figure 2.1, the control piston and return spring are used to change the angle of the swash plate. A control piston slides along the piston guide which is a bored cylinder chamber in the pump case. When pressurized fluid is directed into the control piston guide chamber, the control piston moves away from the valve plate (the swash plate angle decreases) until it reaches a position where the torques acting on the swash plate are balanced. As the swash plate angle decreases, the displacement of the piston decreases and hence the output flow is reduced. When pressurized fluid is vented from the control piston guide chamber to the tank, the control piston moves towards the valve plate, which results in an increase in the swash plate angle, increasing the displacement of the pistons and hence an increase in the output flow. This, then, is how a variable displacement axial piston provides different flows.

2.2 Failure modes and effects for pump components

In this section, some faults that could occur during pump operation are documented. It is very important to know and understand all of the pump faults and their effects on the system performance. Knowing the causes and effects from the faults, it should be possible to obtain some understanding about what parameters could be best examined for condition monitoring purposes. The following table shows common failure modes (causes) and the effects for some of the critical pump components.

Table 2.1 Pump components' possible faults (causes) and effects

(Using the configuration of a Vickers Variable Displacement Axial Piston Pump PVB 5 as a basis)

Components	**Causes (Faults)**	**Effects**	**Pump outlet flow waveform**
1. Needle bearing	Wear or aged (Fatigue, spalling, friction increases)	1. Higher level of noise, 2. Near needle bearing oil temperature increases faster, 3. More torque needed to drive the pump, 4. Drive shaft vibrates, 5. Efficiency is lower.	Irregular waveform
2. Ball bearing	Wear or aged (Fatigue, spalling, friction increases)	1. Higher level of noise, 2. Oil temperature increases faster, 3. More torque needed to drive the barrel, 4. Drive shaft vibrates, 5. Efficiency is lower.	Irregular waveform
3. Barrel spline /drive shaft spline	Wear (fret wear, friction increase)	1. Higher level of noise, 2. Oil temperature increases faster, 3. More torque need to drive pump, 4. Barrel vibrates, 5. Efficiency is lower.	Irregular waveform
4. Barrel face (contact with valve plate)	Wear (friction increase)	1. Higher level of noise, 2. Oil temperature increases faster, 3. More leakage between the valve plate and barrel face and more external leakage, 4. More torque needed to drive pump, 5. Efficiency is lower.	Flow lower (more leakage between the valve plate and barrel face).

Components	Causes (Faults)	Effects	Pump outlet flow waveform
5. Valve Plate(inner face)	Wear (friction increase, especially at the relieve groove)	1. Higher level of noise, 2. Oil temperature increases faster, 3. More leakage between the valve plate and barrel face, 4. More torque need to drive pump, 5. Efficiency is lower.	Flow lower
6. Shaft seal	Wear (friction decrease)	1. Leakage along drive shaft.	No significant change
7. Piston	Wear (internal leakage increased)	1. Flow waveform has bigger ripple and flow drop off, 2. Bigger ripple at the pressure waveform, 3. Pressure generation insufficient, 4. Higher level of noise, 5. Oil temperature increases faster, 6. Suction vacuum not sufficient, 7. Efficiency is lower.	Regular frequency but big ripple,
8. Return spring	Spring aged (spring constant reduce)	1. Outlet pressure is not as designed, 2. Flow control is not accurate.	Normal, but the flow and pressure are different than that designed for certain position of control valve,

Components	Causes (Faults)	Effects	Pump outlet flow waveform
9. Control piston	Piston wear (leakage, viscous friction increase)	1. Outlet pressure is not as designed, 2. Flow control is not accurate, 3. Oil temperature increases.	Normal, but the flow and pressure are different than that designed for at certain position of control valve,
10. Pintle	Wear (friction increase)	1. Oil temperature near pintle increases faster, 2. Higher level of noise, 3. Swash plate assembly vibrates, 4. Irregular ripple at the flow and pressure waveform, 5. Efficiency lower.	1.Irregular wave form, 2.Max flow change irregular
11. Slipper	Pad face wear and upper face wear (friction increase)	1. Outlet pressure is not as designed, 2. Irregular ripple at the pressure waveform, 3. Oil temperature increases, 4. Higher level of noise, 5. Efficiency lower.	No significant change
12. Swash plate	Face wear (friction increase)	1. Oil temperature increases, 2. Higher level of noise, 3. More torque needed on drive shaft, 4. Efficiency is lower.	No significant change

From Table 2.1, some of the faults are visible, such as external leakage past seals, but others can only be recognized by measuring certain pump parameters, such as the output pressure or the output flow waveform. The fault that was chosen for this study, leakage in the pistons due to piston wear, will now be considered.

2.3 Choice of parameter to be studied: piston wear

There is contamination in the oil due to wear in the pistons and other sliding surfaces. In addition, pistons also can touch the cylinder bore and hence the movement of the pistons is not parallel to the bore axis. In other words, once a pump runs, the pistons automatically start to wear, which is a normal situation. This process is accelerated at high load pressures and high flow rates (swash plate angle is larger). A consequence of piston wear is that there will be an increase in leakage to the case drain; therefore, the output flow from the pump reduces. Thus, leakage to the pump case is a useful indicator of changing wear in the pump pistons. (Increased wear also affects the friction characteristics of the pistons, but this was not pursued in this study.)

Excessive leakage causes low volumetric efficiency of the pump and hence increased temperatures locally and can affect the performance of system. From Table 2.1, it is seem that piston wear affects the flow waveform from the pump output. Since pressure is related to flow, the pressure waveform will also be affected. Pressure is very easily measured by a pressure transducer (especially compared to the measurement of flow). Hence, pressure measurement was used in this study. In summary, it was decided that the parameter to be examined in this study would be wear (hence leakage) in the pistons and that pressure at the outlet of the pump would be used as a means of indirectly assessing the amount of wear. The next chapter considers how the pressure waveform changes as wear increases.

2.4 Summary

The principle and operating mechanism of a variable displacement axial piston pump have been described in this chapter. Some potential faults which can occur over the life time operation of the pump have been presented. In particular, leakage from piston wear has been identified as the parameter of interest in this study. In the next chapter, the change of flow waveform (and hence indirectly pressure) due to piston wear is demonstrated using a simplified mathematical model of the pump. In addition, the physical and mathematical concepts of leakage in the pistons are presented.

Chapter 3 Simulation

In Chapter 2, a variable displacement axial piston pump was described. In this chapter, simple mathematic models for the output flow and output pressure from the pump are presented. Of particular interest were the simulated flow and pressure waveforms from which some insight into how the waveform changes in the presence of pump faults (piston wear) can be obtained.

3.1 Relationships between piston leakage and piston wear

When the pump is in operation, the pistons are continuously pumping in a cyclic motion. In a “normal” pump, most of the pump flow is available to the system circuit; however, some fluid makes it way through the various internal passages into the case drain chamber and is defined as internal leakage. In this research, leakage past the sliding pistons was one of the internal leakages of interest because it is highly related to the condition of the pump. It is necessary, therefore, to understand the mechanism behind this leakage.

In the following development, a few assumptions are made. First, there is a load in the hydraulic circuit. Because piston leakage is related to pressure, if there is no load (or resistance) in the circuit, there is no pressure at the pump outlet. Second, for each piston, the pumping motion starts at TDC (see Figure 3.1) for each revolution. Once the piston moves into the suction port (the blue area in Figure 3.1 a), the piston leakage is very small due to the low pressure fluid in the piston chamber, and because at this position, the fluid pressure in the piston chamber is only slightly greater than the case drain chamber pressure.

When the piston moves to the discharge port (the red area, in Figure 3.1 b), the pressurized fluid in the piston chamber is much higher than that found in the case drain chamber. Therefore, the flow (leakage) at the higher pressure chamber is directed into the case drain chamber, where the pressure is close to atmosphere. This is the process of the leakage from the piston chamber to the case drain chamber, and is illustrated schematically in Figure 3.2. It is important to note that the leakage from the piston

chamber to the case drain chamber occurs only for one-half of the period of revolution and that the magnitude of the leakage flow varies during each one cycle.

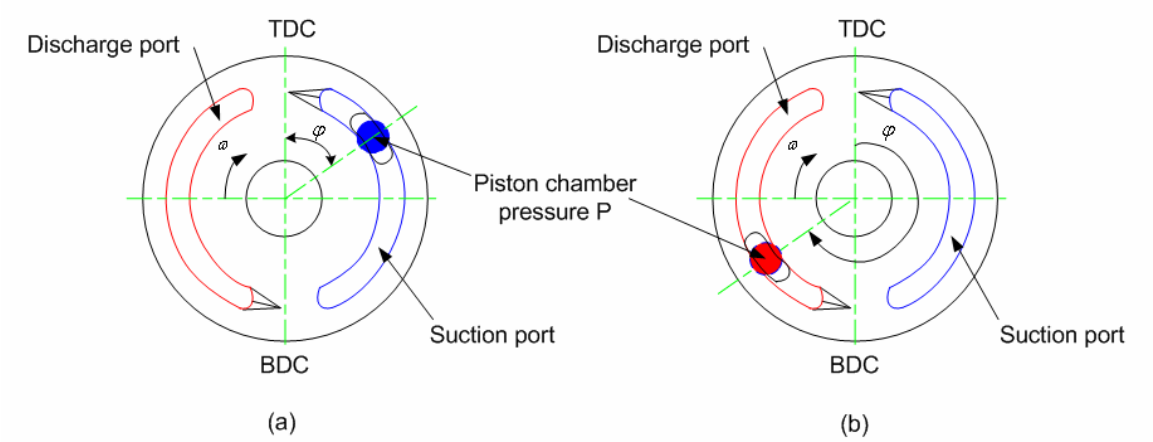

Figure 3.1 Pumping motion with leakage

The leakage passage is modeled as an annulus. It is further assumed that the leakage flow is laminar. As shown in Appendix A, the Reynolds number for this flow is 0.03, which confirms the assumption of laminar flow. Consider Figure 3.2. For simulation purposes, the eccentricity (denoted as "e" in Figure 3.2 a) is assumed zero. The flow through this orifice is given by Equation 3.1 [29].

$$Q_{lp} = \frac{\pi r h_g^3}{6 \mu L}(P_p - P_c) \tag{3.1}$$

where: Q_{lp} = Leakage from piston chamber to case chamber [m^3/s]

r = Radius of piston [m]

h_g = Gap (radial clearance) between piston and cylinder bore [m]

P_p = Piston chamber pressure [Pa]

P_c = Case drain chamber pressure [Pa]

μ = Absolute fluid viscosity [$N.sec/m^2$]

L = Length of leakage passage [m].

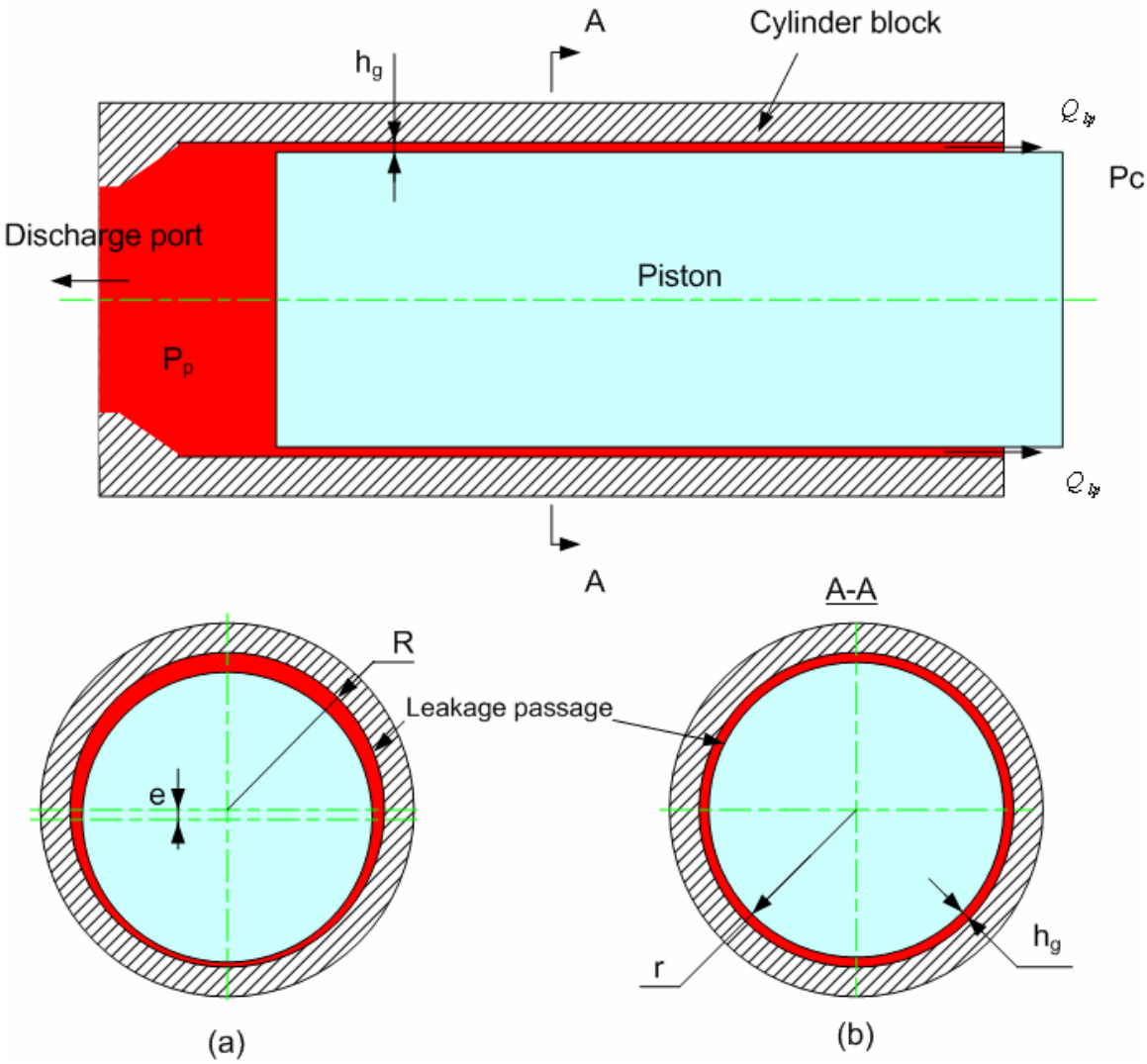

Figure 3.2 Piston leakage passage- Annular leakage path

a. the eccentricity is not zero

b. the eccentricity is zero

From Equation 3.1, and with reference to Figure 3.2, the more the piston wears, the greater is the parameter gap h_g between the piston and the cylinder bore. Hence, assuming the same loading and operating conditions, the leakage Q_{lp} increases. If the wear of the piston falls into some specified range, then the pump could be considered faulty. However, the increase in the leakage may be due to other reasons. For example, if, for the same loading conditions, the temperature increases in the system, the absolute fluid viscosity decreases, and therefore the leakage Q_{lp} increases. However, if the

operating conditions at which the leakage is obtained remain unchanged, it can be inferred with confidence that the increased piston leakage is a consequence of increased piston wear.

3.2 Simulation model

As derived in Appendix B, in an axial piston pump, each piston delivers flow in a sine wave pattern. The total flow from the pump outlet is the sum of all flows delivered by each piston, which is given by a simplified mathematical "kinematical" model [29] shown in Equation 3.2.

$$Q_k = \omega \frac{\pi d^2 R_p}{4} \tan \beta \sum_{k=0}^{m-1} \sin(\omega t - k\alpha), \tag{3.2}$$

where: Q_k = Pump kinematical flow (total pump flow from the pistons) [m^3/s]

ω = Angular velocity of drive shaft [rad/s]

d = Diameter of piston [m]

R_p = Piston pitch radius on barrel [m]

β = Angle of swash plate [rad]

m = Number of pistons

t = Time [sec]

k = 0, 1, 2, 3….. m-1

α = Phase delay [rad], equal to $2\pi / m$

Equation 3.2 only defines the kinematical factor of the pump. The output flow can be affected by other factors such as leakage between the valve plate and cylinder bore, leakage between the slipper and swash plate, and leakage between the cylinder bore and piston. For this simulation study, the first two leakages were neglected. Under dynamic conditions, the output flow of the pump can be further reduced due to the compressibility of the fluid. Considering these factors, the pump output flow and output pressure can be represented by the following equations, the derivation of which is provided in Appendix B:

$$\dot{P}_s = \frac{B}{V_c}(Q_p - Q_s) \tag{3.3}$$

$$Q_p = \sum_{n=1}^{m=9} Q_{pn} \tag{3.4}$$

$$Q_s = C_{d2} A_v \sqrt{\frac{2P_s}{\rho}} \tag{3.5}$$

$$Q_{pn} = C_{d1} A_{dn} \sqrt{\frac{2|P_{pn} - P_s|}{\rho}} \operatorname{sgn}(P_{pn} - P_s) \tag{3.6}$$

$$\dot{P}_{pn} = \frac{B}{V_0 - A_p S_{pn}}(Q_{kpn} - Q_{pn} - Q_{lpn}) \tag{3.7}$$

$$Q_{kpn} = \omega \frac{\pi d^2 R_p}{4} \tan\beta \cdot \sin(\omega t - (n-1)\alpha) \tag{3.8}$$

$$Q_{lpn} = \frac{\pi r h_g^{\ 3}}{6\mu L}(P_{pn} - P_c) \tag{3.9}$$

$$S_{pn} = R_p \tan\beta \cdot (1 - \cos(\omega t - (n-1)\alpha)) \tag{3.10}$$

where: A_{dn} = The discharge area for P_n piston port opening to the discharge chamber in valve plate [m^2]

A_p = The piston area [m^2]

A_v = The discharge orifice area of the needle valve [m^2]

α = Phase delay [rad], equal to $2\pi / m$

B = Bulk modulus [Pa]

β = Angle of swash plate [rad]

C_{d1} = Flow discharge coefficient of the discharge area for piston port opening to discharge chamber

C_{d2} = Discharge coefficient of needle valve orifice

d = Diameter of piston [m]

h_g = Gap (radial clearance) between piston and cylinder bore [m]

L = Length of leakage passage [m]

n = 1, 2, 3….. m (m = number of piston)

ρ = Flow density [kg/m^3]

P_c = Case drain chamber pressure [Pa]

P_{pn} = Instantaneous pressure in P_n piston chamber [Pa]

P_s = Pump output pressure (discharge chamber pressure) [Pa]

Q_{kpn} = Kinematical flow delivered by P_n piston [m^3/s]

Q_{lpn} = Internal leakage from P_n piston to case chamber [m^3/s]

Q_p = Flow from piston chamber to discharge chamber [m^3/s]

Q_{pn} = Flow from P_n piston chamber to discharge chamber [m^3/s]

Q_s = Pump output flow [m^3/s]

r = Radius of piston [m]

R_p = Piston pitch radius on barrel [m]

S_{pn} = Stroke for P_n piston [m]

t = Time [second]

μ = Absolute fluid viscosity [N.sec/m^2]

V_0 = Piston initial volume [m^3]

V_c = Discharge chamber control volume [m^3]

ω = Angular velocity of the pump drive shaft [rad/s]

Substituting the pump parameters listed in Appendix C into Equations 3.3 to 3.10, the pump output pressure P_s and the output flow Q_s can be solved. This is the model of the axial piston pump that was used in the simulation studies.

3.3 Simulation results

The simulation was undertaken using commercial software package, Matlab Simulink Version 7.01. The “Domand-Prince” solver with 2*10^{-7} second fixed step was employed in simulation. For each simulation, the simulation time was 0.1 second, or

about 3 cycles of the pump at a rotational speed of 1800 RPM. In developing the simulation, the following assumptions were made:

1.) The pump worked at constant temperature and constant swash plate angle.

2.) The flow losses due to slipper leakage and valve plate leakage were ignored.

3.) The fluid density and bulk modulus were constants.

4.) The pump rotational speed was constant.

5.) The load in this system was constant (the needle valve area was constant).

In the Vickers PVB5 axial piston pump, there are nine pistons (m = 9). The pump was driven by a 1800 RPM electrical motor. It should be noted that all figures in this chapter show two complete cycles of the simulated waveform.

The simulation result for the pump kinematical output flow based on Equation 3.2 is shown in Figure 3.3. In this figure, the nine "rectified" sine waves in the bottom plot represent the flow delivered by the nine pistons individually, with each piston showing an appropriate phase delay. The upper red line represents the kinematical total output flow, which is the sum of nine rectified sine waves. It is apparent that the kinematical total output flow is not a straight line, but has a small periodic "ripple" superimposed on the mean value.

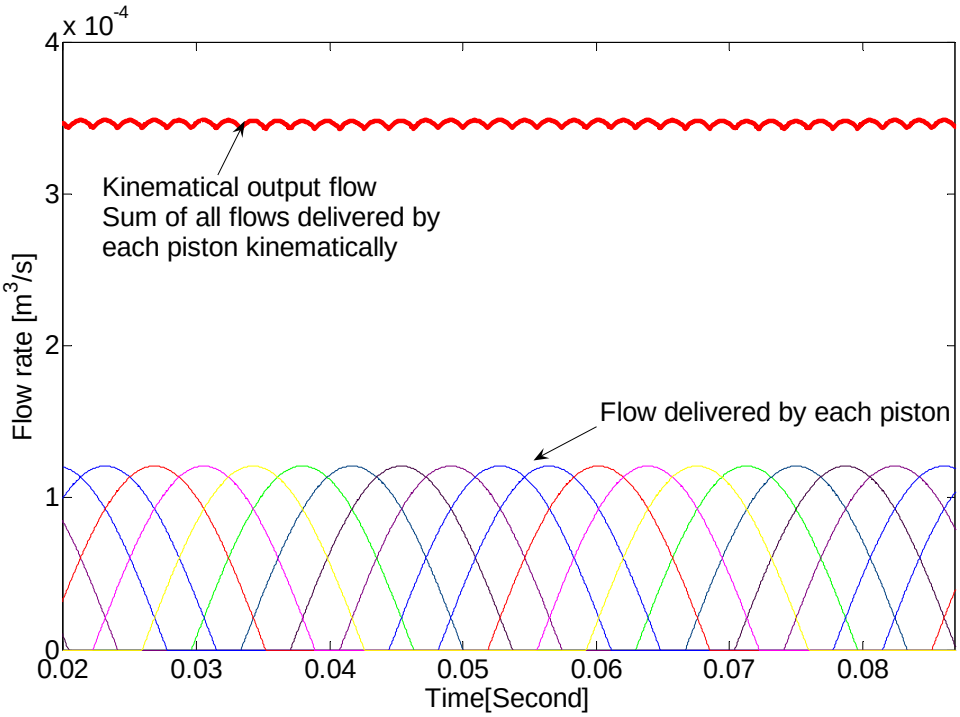

Figure 3.3 Pump kinematical output flow (simulated)

Based on Equations 3.3 to 3.10, the simulated pump output flow Q_s was determined (as opposed to the pump kinematical output flow, Equation 3.2, shown in Figure 3.3) and is shown in Figure 3.4. It is apparent that the simulated output flow waveform is different than the simulated pump kinematical output flow. As shown in Figure 3.4, the waveform demonstrated a large ripple, but between every second ripple, there is a deep gap. In contrast, the gap between every second ripple in Figure 3.3 has the same magnitude. A possible reason for this is as follows. In the pump model, a small "v" relief notch in the valve plate was included in the calculation of the piston flow into the discharge chamber. Once the piston moves to the relief notch from the low pressure region to the high pressure discharge region (see "S1" point in Figure B.5, Appendix B), the pressure in the relief notch is greater than the pressure in the piston chamber which at this point is at the inlet or suction pressure. During this very short transition period some fluid would be pushed back into the piston chamber (a negative flow) until the pressure in the relief notch is equal to the pressure in piston chamber. In one cycle, the pistons will move into the discharge chamber nine times; therefore, nine lower flow gaps appear in the flow profile.

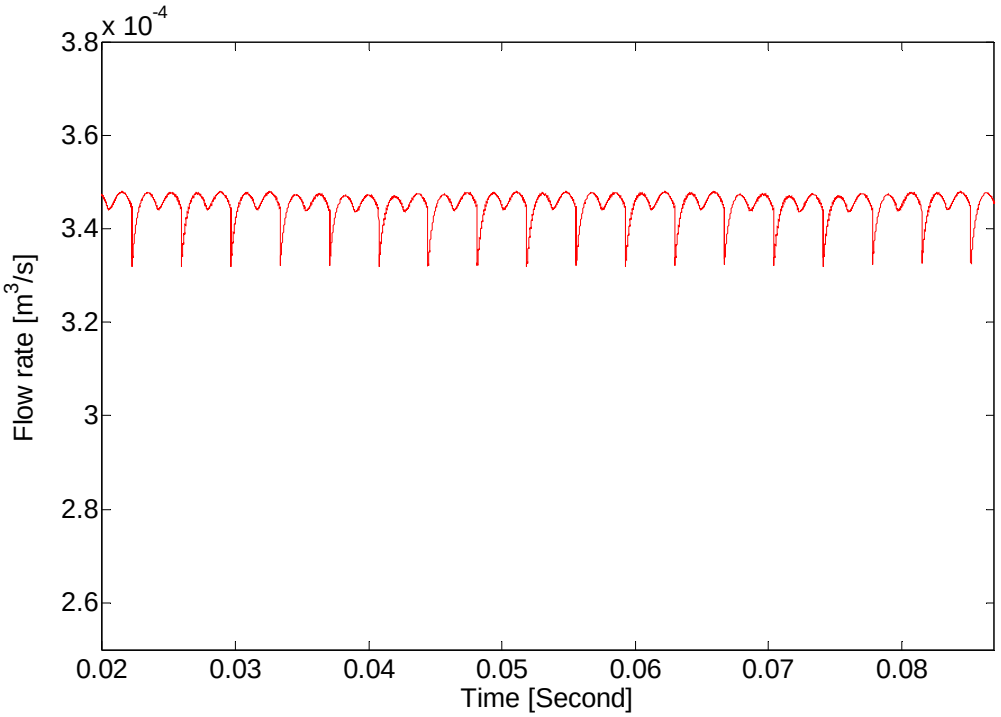

Figure 3.4 Pump output flow waveform (simulated)

It is to be noted that compared to the dynamic pressure, the dynamic flow is much more difficult to measure. For this reason, it was decided that the pressure wave form would be used for all comparisons since it is much more easily realized experimentally. In Figure 3.5, the simulated pump output pressure (assuming no leakage at this time) from the simulation is shown. It is noticed that the simulated pressure waveform is similar to the simulated output flow waveform. However, the ripples at pump pressure output were much more obvious than those of the flow output. In this study, the load employed in the system was an orifice load which could be adjusted. Pump output pressure P_s calculated from Equations 3.3 was based on an orifice load.

For comparison purposes, an experimental waveform of pump pressure ripple from a pump in shown in Figure 3.6. The actual measured pump output pressure does show similar trends to its simulated counterpart (see, Figure 3.5). The actual pump shows only nine dominant ripples but each ripple displays a few "tips". In the simulated pressure waveform, the tips are much smoother. There are a number of reasons for this. Firstly, the slipper leakage and the valve plate leakage were not included in the simulation model. The slipper leakage whose "dynamic waveform" is known to be a very complicated function of many parameters, has been shown to contribute to these "tips" in the ripple [31]. Secondly, in the simulation, the dynamics of the piston moving in and moving out of the discharge chamber have been simplified. It is believed, then, that these two factors would account, in part, for some of the differences in the waveforms.

For the purpose of the following feasibility study, it was concluded that the simulation model did show the same trends as its experimental counterpart, and that the model was sufficiently accurate to demonstrate the effects of leakage in one or more pistons.

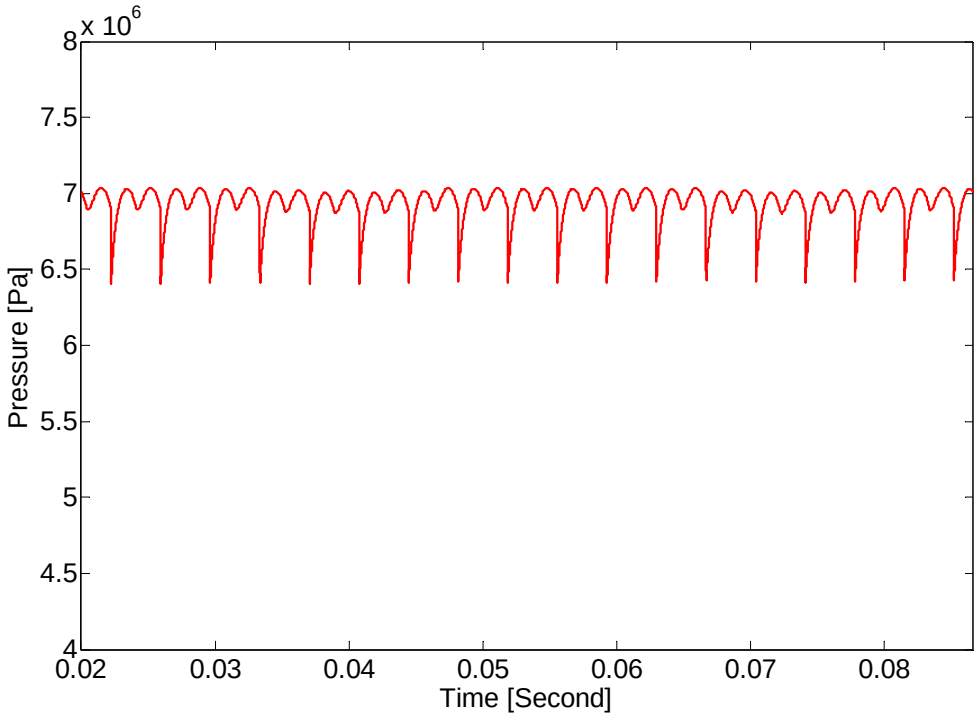

Figure 3.5 Pump output pressure waveform (simulated)

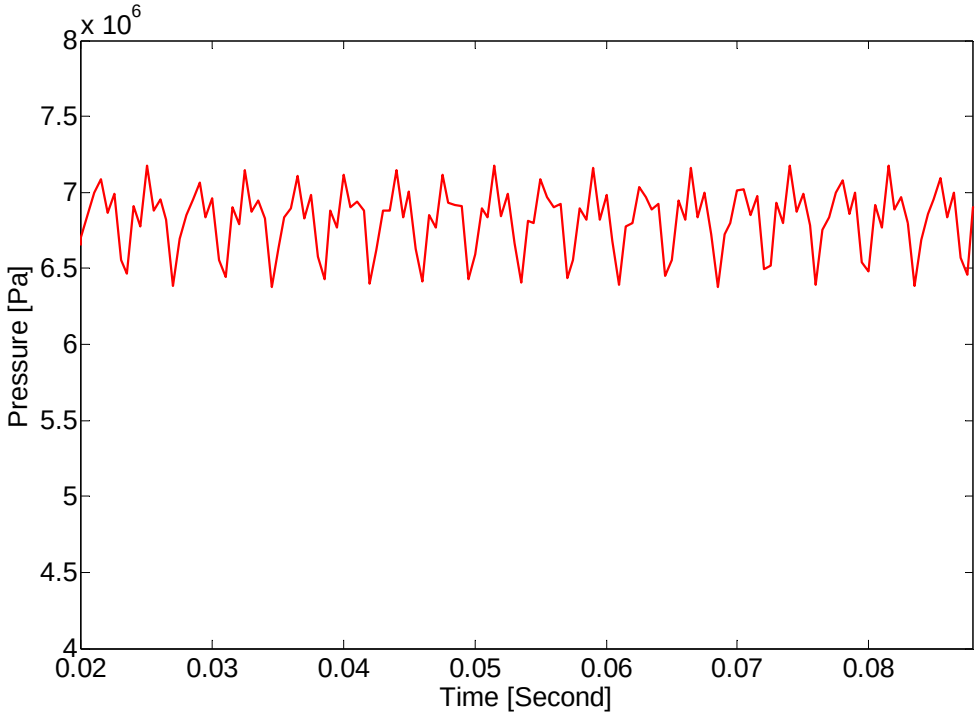

Figure 3.6 Pump output pressure waveform (experimental)

In normal pump operation, the piston wear would be gradual and the leakage would increase accordingly. Once the wear in one or more pistons reaches a critical range, the effect of reduced flow would become quite visible. In the first simulation study, it was assumed, that only one piston had significant wear. The simulation result for this condition is shown for the flow in Figure 3.7. Compared with the normal pump output flow, when the faulty piston is in its discharge part of the cycle, the overall output flow waveform shows a "concave dip" pattern. This concave shape forms because the faulty piston delivers less flow than the non faulty one, as shown in Figure 3.8, where the red line represents the normal piston flow and the blue line for the faulty piston flow. Overall, the pump with one faulty piston delivers less flow than a pump with no fault as would be expected.

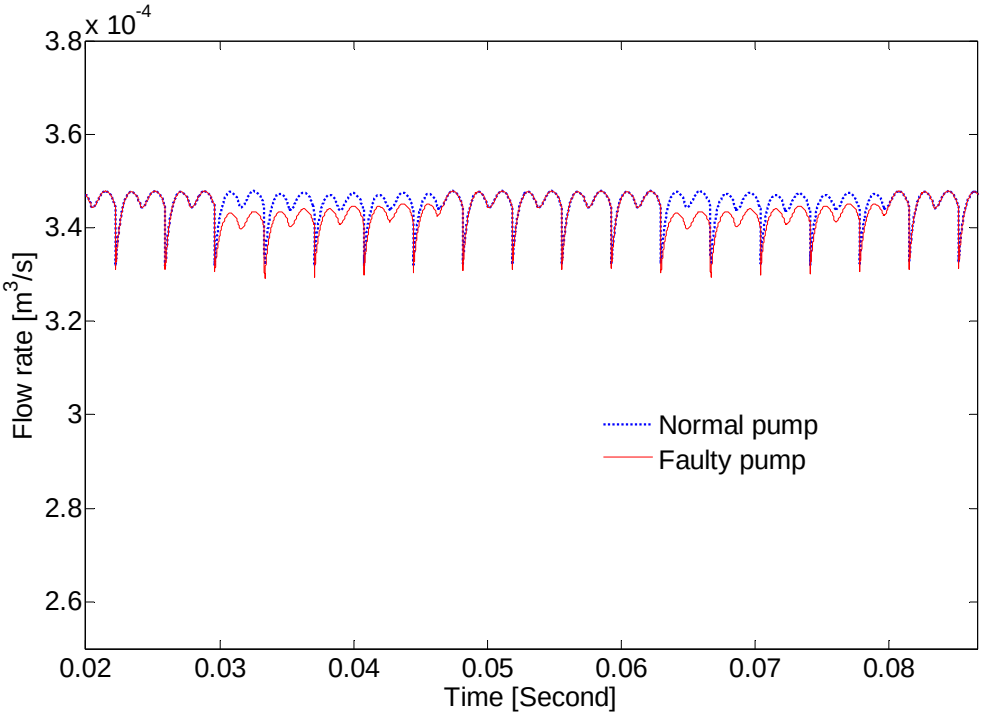

Figure 3.7 Comparison of normal and faulty pump flow waveform (simulated)

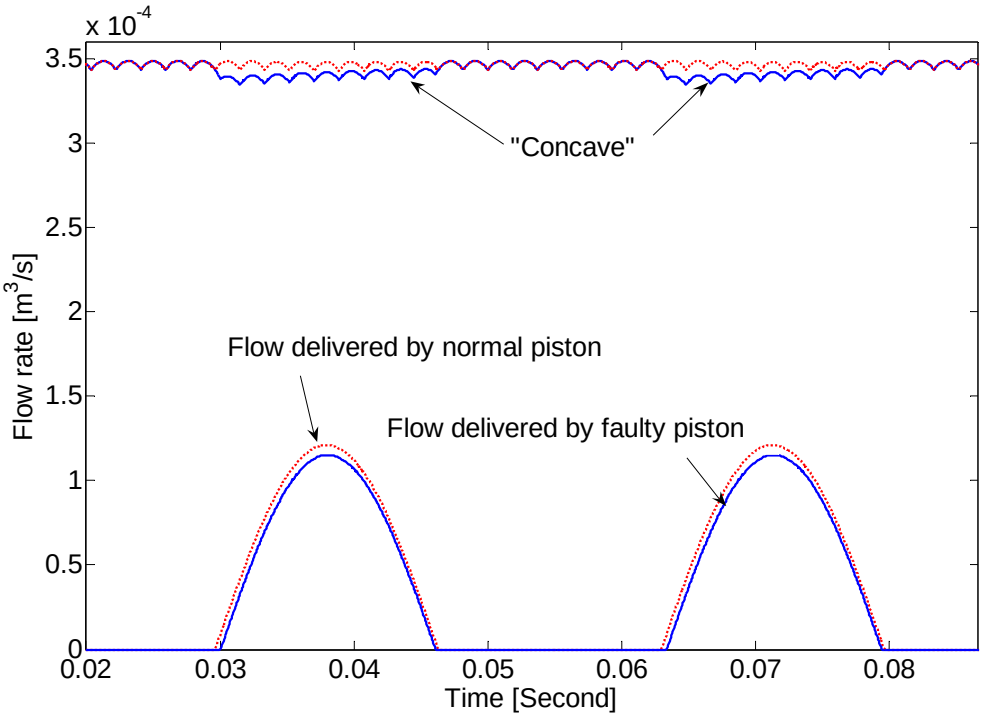

Figure 3.8 Piston delivered flow related to concave pattern (simulated)

It was of interest to determine how the outlet simulated pressure would change with changes in flow. In Figure 3.9, the "faulty" output pressure waveform shows the same concave pattern as the flow waveform at the same position. To demonstrate that, this does happen experimentally, an experimental pressure waveform for a faulty pump with one piston with a 60 microns gap was obtained and is shown in Figure 3.10, (where the green line is the experimental waveform.). Although the magnitude is different, the concave pattern is quite evident and the number of the affected ripples by the faulty piston is the same. So it was again concluded that the simulation could be used to study how changes in the pressure waveforms can be correlated to pump piston fault with some confidence.

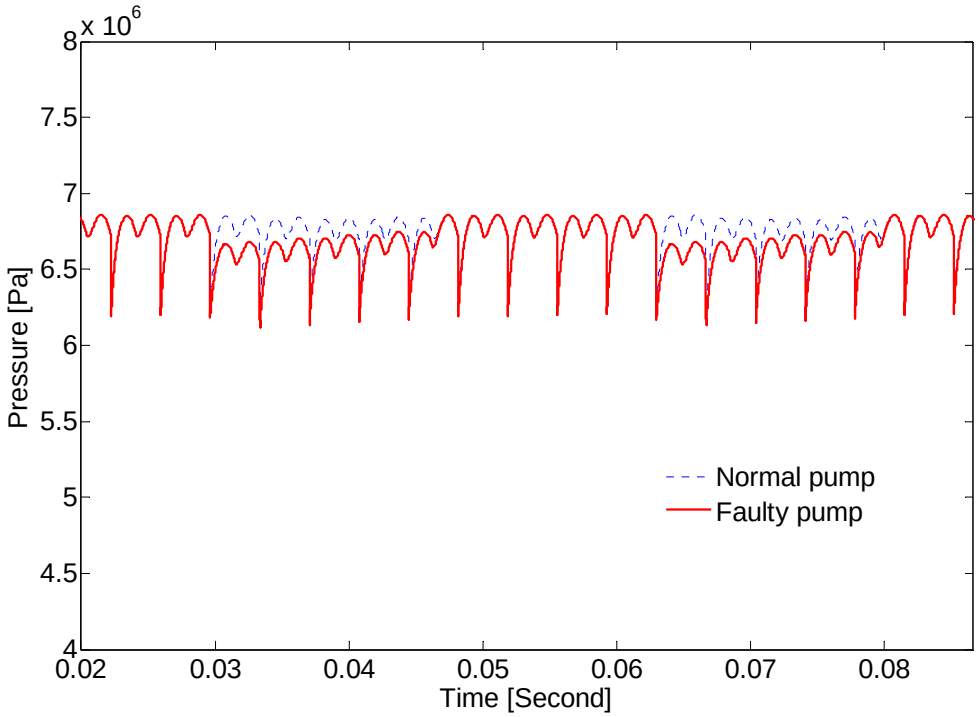

Figure 3.9 Comparison of normal pressure and faulty pump pressure waveforms (simulated)

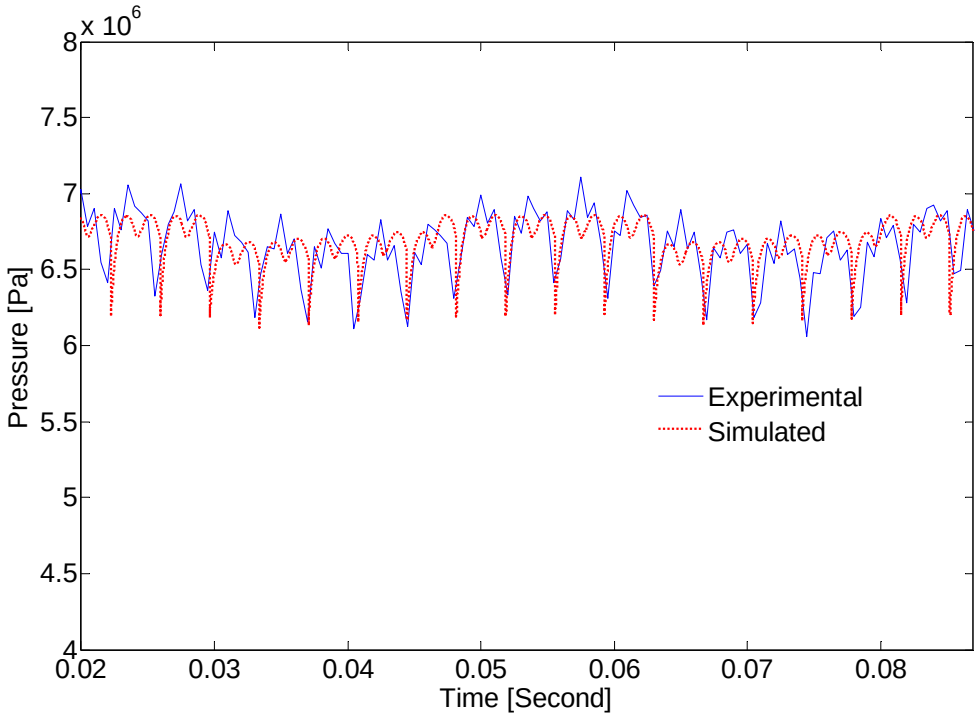

Figure 3.10 Faulty pressure ripples from simulation and experiment

Figure 3.11, shows how the simulated flow pattern changes as the diameter wears over a range of 30 to 90 microns gap. It is observed that the greater the gap between the piston and cylinder bore, the larger the total output flow deviates from the normal flow or the bigger the "concave". It is also noticeable that the concave patterns of output flow waveforms for pumps with only one worn piston are similar, except for the magnitudes are different. The pressure waveforms for one faulty piston, shown in Figure 3.12, have the same features as the flow waveform.

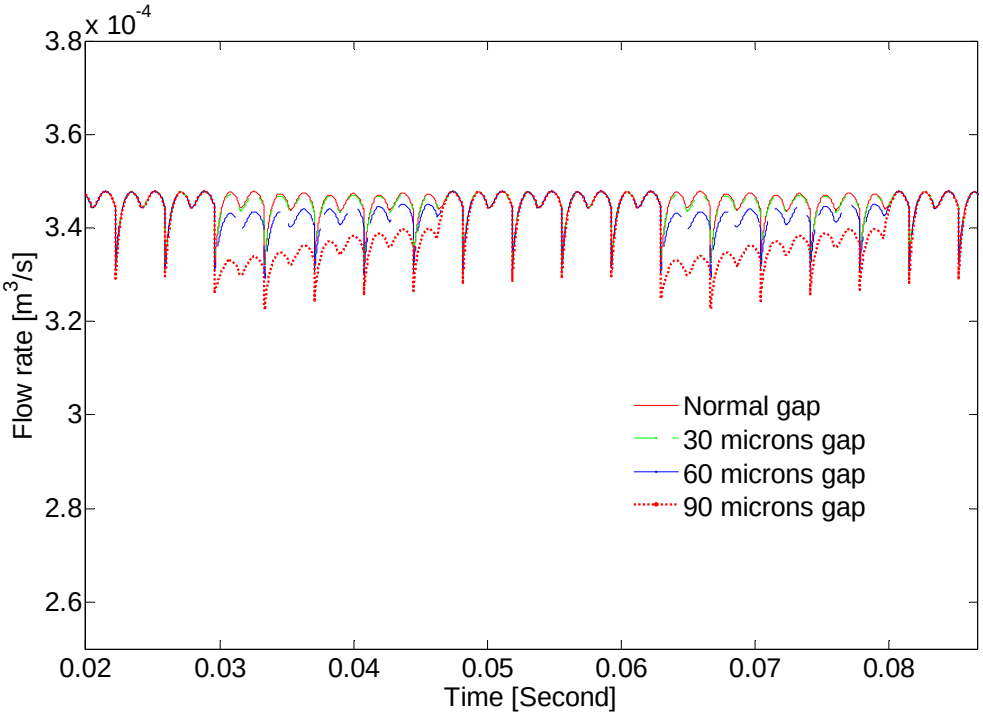

Figure 3.11 Comparison of pump flow ripples with different worn pistons (simulated)

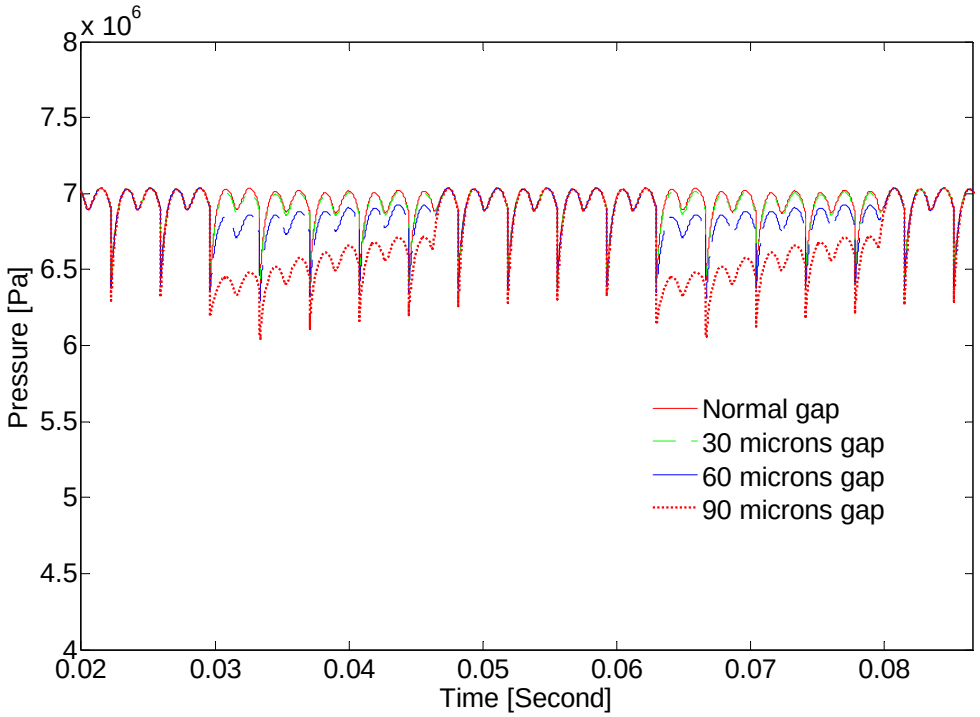

Figure 3.12 Comparison of pump pressure ripples with different worn pistons (simulated)

As mentioned, the pressure waveform, shown in Figure 3.12, demonstrates the same concave patterns as found in the flow ripple patterns. Compared with the "concave" pattern in the flow ripple, the percentage difference in the pressure concave pattern is larger than the flow percentage difference. Therefore, the pressure ripple could be a more effective way to detect faults in a pump. This, when combined with the fact that pressure is much easier to measure than flow, is further evidence that pressure might be a better and more practical indicator than flow for fault detection for pumps. Thus, this research concentrated on the change of the pressure waveform when the pump became faulty.

3.4 Summary

This chapter described the process and equations associated with the piston internal leakage. In addition, the models for pump output flow and pressure were presented. The simulation results for a normal pump and faulty pump with piston wear were presented. When one piston wears significantly, the simulated pump output

waveform shows a concave dip pattern. The output pressure wave has a similar concave pattern.

In the following chapter, the methodology of introducing artificial leakage to simulate the piston wear is presented. The test system is considered as well.

Chapter 4 Methodology

In Chapter 3 simulation results for a pump with one piston demonstrating some wear for the output flow waveform and the output pressure waveform were provided. The equations for the pump output flow and the output pressure were derived. In this chapter, a system employed to introduce artificial leakage to simulate the piston leakage from a worn piston is presented. This system consists of an axial piston pump, a pressure control servo valve, two needle valves and several transducers and sensors. The mechanism to create the hydraulically simulated leakage to mimic piston wear was accomplished using a pressure control servo valve and this component is discussed. In addition, the data acquisition system for the experiment is described.

4.1 Experimental methodology

One of the objectives of this study was to introduce artificial leakage to mimic piston leakage in one of the pistons in a pump. As described in Chapter 3, in one revolution, if piston leakage exists, it starts at the point BDC where the piston just starts to discharge fluid into the outlet and ends at the point TDC where the piston stops discharging fluid into the outlet, (see Figure 3.1). Usually, the pump is driven at a high rotational speed, for example, 1800 RPM in this study. For this case, the worn piston will pass 30 times through the point TDC in one second, which means that the piston leakage from the worn piston will commence and stop at a frequency of 30 Hz.

To introduce artificial piston leakage, a single line and controlling valve were connected from the discharge chamber (the outlet of the pump) to the case drain or tank (the pressure in the case chamber is usually the same as the tank pressure which is close to atmospheric conditions), as illustrated in Figure 4.1. The valve was used to control the period and magnitude of the introduced artificial leakage. Therefore, the valve had to meet two basic requirements: a high frequency response and an adjustable flow.

In Figure 4.1, the red solid line represents the actual piston leakage. From the Chapter 3 simulations, the pressure in the discharge chamber was found to be nearly the same as the pressure in the piston chamber. The fluid in the discharge chamber was connected to the fluid in the piston chamber, when the piston was adjacent to the discharge chamber. Therefore, in Figure 4.1 the dotted red line can be considered as

representative of the artificial leakage. If a valve was attached to this dotted red line path, then as the valve closes and opens, this action, if timed correctly, would simulate the piston leakage as it stops and starts to the case chamber when the pump is in operation. The challenge here was to accurately reproduce the starting and stopping of the simulated piston leakage at such a high frequency.

Normally, typical on-off valves cannot satisfy such a high frequency response criteria. A valve proposed by Cui [32] can open and close at high frequencies, but this valve was not designed to regulate flow directly. When used in a pulse width or frequency mode, this may be possible but this valve was not tested in this mode. A similar 2D valve was proposed by Ruan et al [33]. It could modulate flow in a proportional manner at a very high frequency, but it is not commercially available.

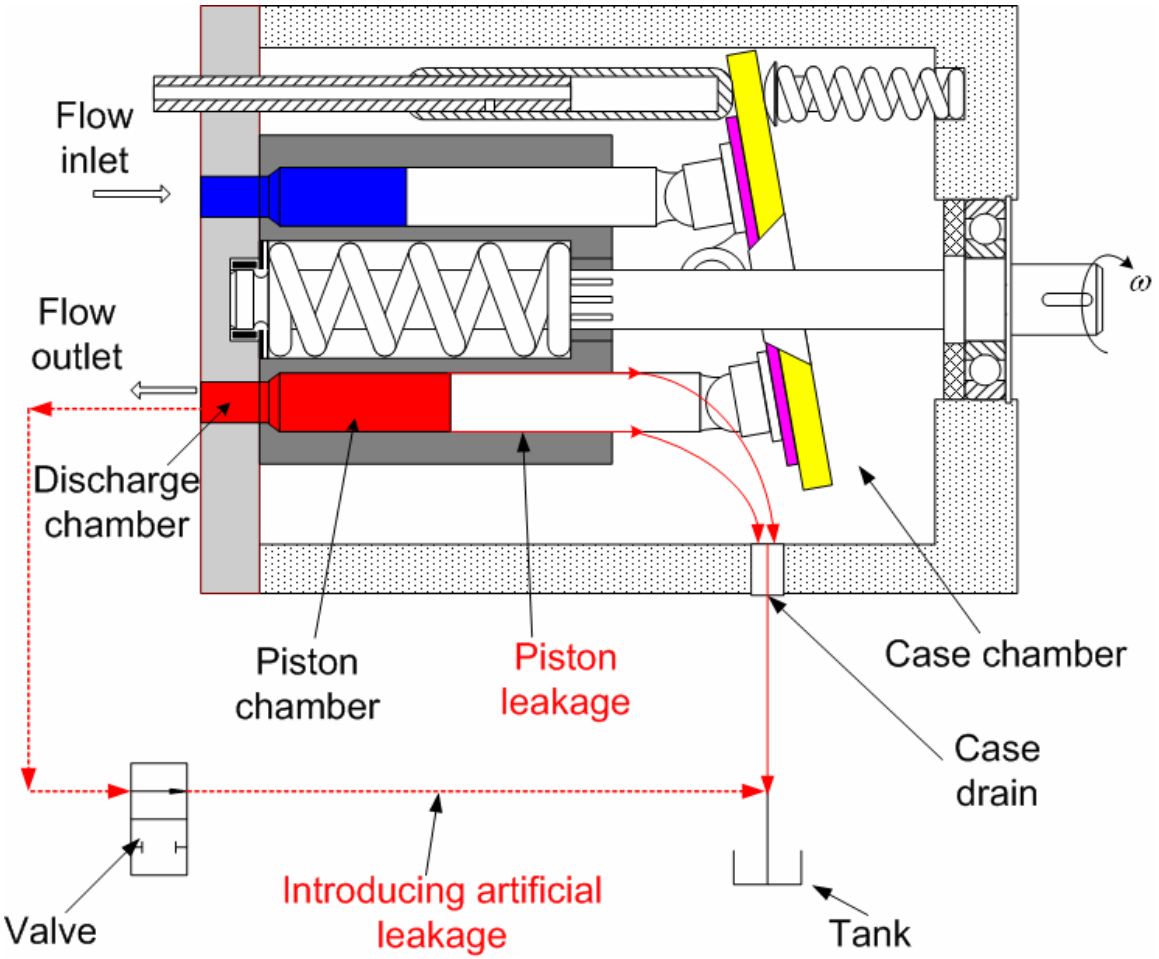

Figure 4.1 Schematic of introducing artificial piston leakage for pump

An alternative approach is to use a pressure control servo valve. A pressure control servo valve can satisfy the two specified requirements, high frequency response and proportional flow. For this reason, such a valve was used in this study. This was possible because the required flow rate through the valve was very small which accommodated the operation of the pressure valve.

Consider Figure 4.1 The line with the pressure control servo valve connects the outlet of the pump to the tank. When the servo valve is operated, some fluid is diverted from the load line to the tank according to the desired rate and amount. A pressure control servo valve usually controls pressure but since the flow and the pressure are related via the orifice equation (essentially a high impedance device) the flow can be regulated by changing the input to the pressure servo valve. By varying the frequency, the timing and the waveform shape of the input signal to the servo valve, the frequency, the timing and the shape of the simulated leakage flow can be achieved. It is in this manner that the artificial leakage simulating one or more worn pistons was attempted.

4.2 Experimental test system

4.2.1 Test circuit system

A schematic of the test system used is shown in Figure 4.2. This system consisted of a variable displacement axial piston pump (in this study, the angle of swash plate was fixed.), a pressure control servo valve, a temperature sensor, a pressure transducer, a flow transducer, a diaphragm differential pressure transducer, three needle valves, one pick-up magnetic sensor, several amplifiers and a data acquisition system. A photograph of the test system is shown in Figure 4.3.

As shown in Figure 4.2, the line with the pressure control valve (component 18 in Figure 4.2,) was connected to the outlet of the pump and tank. Theoretically, the fluid from the outlet of the pump is directed to the tank once the pressure control servo valve is opened and blocked when the valve is closed (no artificial leakage is introduced into the system). Practically, however, in the valve used in this study, there was a small steady state (quiescent) flow through the valve even when the input of the servo valve was zero. This steady state flow will be discussed later in this chapter.

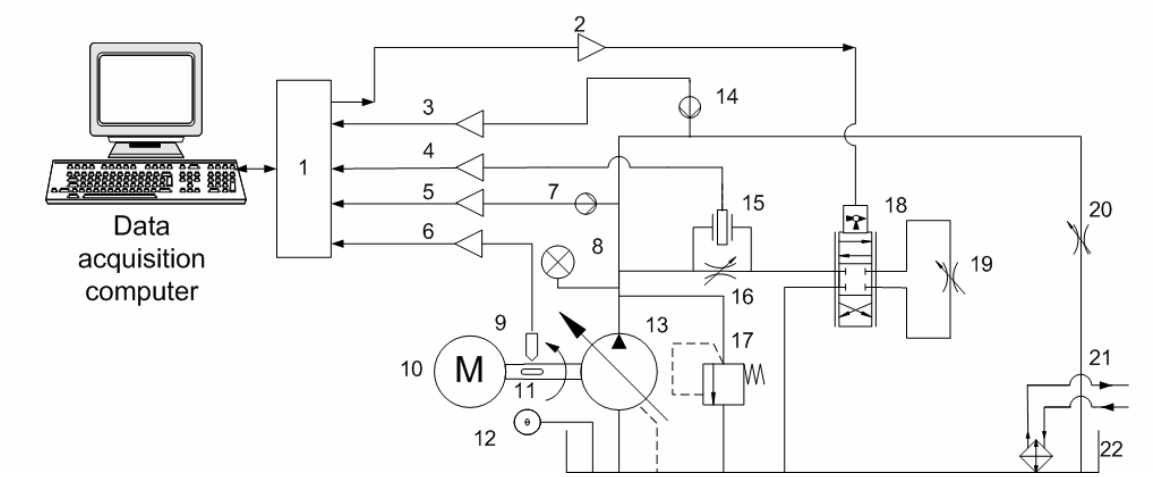

1. DAQ I/O box
2. Amplifier of pressure control servo valve
3. Amplifier of flow transducer
4. Amplifier of diaphragm transducer
5. Amplifier of pressure transducer
6. Amplifier of magnetic pick-up sensor
7. Pressure transducer
8. Pressure gauge
9. Magnetic pick-up sensor
10. Prime mover
11. Drive shaft key
12. Thermometer
13. Axial piston pump
14. Flow transducer
15. Diaphragm differential pressure transducer
16. Needle valve
17. Relief valve
18. Pressure control valve
19. Needle valve
20. Needle valve
21. Heat exchanger
22. Tank

Figure 4.2 Schematic of the experimental setup

The magnetic pick up sensor, component 9 in Figure 4.2, picked up the signal from the key (component 11 in Figure 4.2) on the drive shaft. The signal was used to trigger the electronic circuitry to open the pressure control servo valve. This timing sequence was the first and most important condition that had to be satisfied in the experimental system. As will be shown in the next chapter, this condition imposed constraints on simulating the actual waveform of the pressure (flow) concave dip.

For each revolution, the key on the drive shaft passed once by the magnetic pick up sensor. Hence, the servo valve was opened once each revolution. It should be noted that once the appropriate piston in which wear was simulated, moves into the discharge chamber, the pressure control servo valve must open at same time. That means that the simulated worn piston moving in the discharge chamber must be synchronous to the pressure control servo valve opening. In addition, the simulated worn piston moving out of the discharge chamber had to be synchronous to the pressure control servo valve closing. In this manner, the timing guaranteed that the introduced artificial leakage would be from a specific piston and would have the same period and phase as the real worn piston leakage.

In the following section, the functions of some components listed in Figure 4.2 are addressed. First, the needle valve, component 16 in Figure 4.2, was used to set the differential pressure in order to measure indirectly the introduced artificial leakage (using the diaphragm type differential pressure transducer). Because the artificial leakage was so small, available flow transducers could not measure the small flow rates reliably. A second needle valve, component 19 in Figure 4.2, was used to reduce the steady state leakage flow through pressure control valve. To some extent, this needle valve, component 19, was used to adjust the valve's speed of response.

A third valve, component 20 in Figure 4.2, was used to simulate a resistive type load in this test, which allowed the load pressure to be adjusted. Because the load flow was much larger than the leakage flows, the load pressure was constant (variations less than 2.4%). When the test system was operating, the temperature of oil was maintained almost constant by the heat exchanger, component 21 in Figure 4.2, at $26.5 \pm 1.0\ ^{0}C$ for each run.

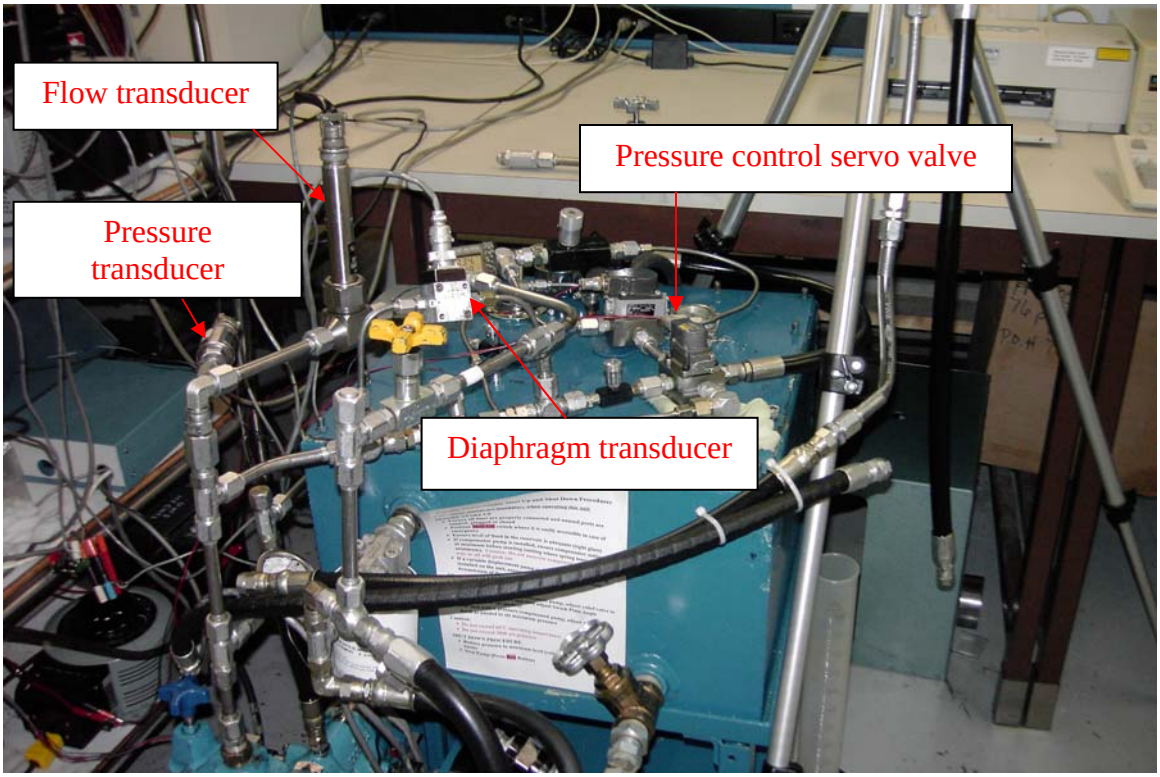

Figure 4.3 Photograph of the experimental system

4.2.2 Data acquisition system

The data for this experiment were acquired using the Matlab Realtime Workshop© software to connect an I/O connector board, component 1 in Figure 4.2, using the data acquisition board (NI PCI-6036E) in the PC motherboard. The sampling frequency for the data collection was 2000 Hz. Calibration information for the sensors and transducers is provided in Appendix D.

4.2.3 Pressure control servo valve

4.2.3.1 Pressure control servo valve inner structure and mechanism

In this study, a high frequency response pressure control servo valve, Moog model 15 010 series 112, was employed. The inner structure of this pressure control servo valve is shown in Figure 4.4.a. With reference to this figure, when DC current passes through the coils, the magnetic field so produced acts on the armature. The armature "tilts" a small amount. The flapper joined to the armature moves off centre in the flexure tube. The flow from each nozzle encounters a different resistance. This means that the

flow through the nozzles will be different and hence, the pressures P_A and P_B will be different. Therefore, a differential pressure across both sides of the spool is established, and the spool will move to the side where the pressure is lower, (see Figure 4.4a). The greater the current to the coil, the greater is the differential pressure across the spool, and hence the more the spool moves. However, as shown in Figure 4.4a, the load pressure ΔP_{12} is fed back via the two pilot lines shown to create an opposing force ($\Delta P_{12} A_S$). When this feedback force equals the applied differential force $\Delta P_{AB}\ A_A$, the spool stops as the forces are equal. This is stated mathematically as:

$$\Delta P_{AB} \cdot A_A = \Delta P_{12} \cdot A_S \tag{4.1}$$

where: ΔP_{AB} = The differential pressure of spool [Pa]

ΔP_{12} = The differential pressure of stud shaft [Pa]

A_A = The spool driving area [m^2]

A_S = The spool feedback end area [m^2].

The force which moves the spool is mainly a function of the differential pressure ΔP_{AB} on the spool; however, if the supply pressure is low, the ability of the valve to generate this differential pressure is decreased substantially and hence these types of valves do not work very well at very low pressures. Therefore, in this experimental system, the system pressure was always set to be greater than $5.5*10^6$Pa. Figure 4.4.b shows the null position for the valve spool. Theoretically, there is no flow through the valve when the spool is at the null position.

The cutoff frequency for pressure control servo valves is usually very high. For the specific Moog pressure control servo valve used in this study, the blocked port frequency response can reach up to 200 Hz [34]. It was felt that since the desired opening and closing frequency of the valve would be 30Hz, a valve cutoff frequency of 200 Hz would be adequate for this study.

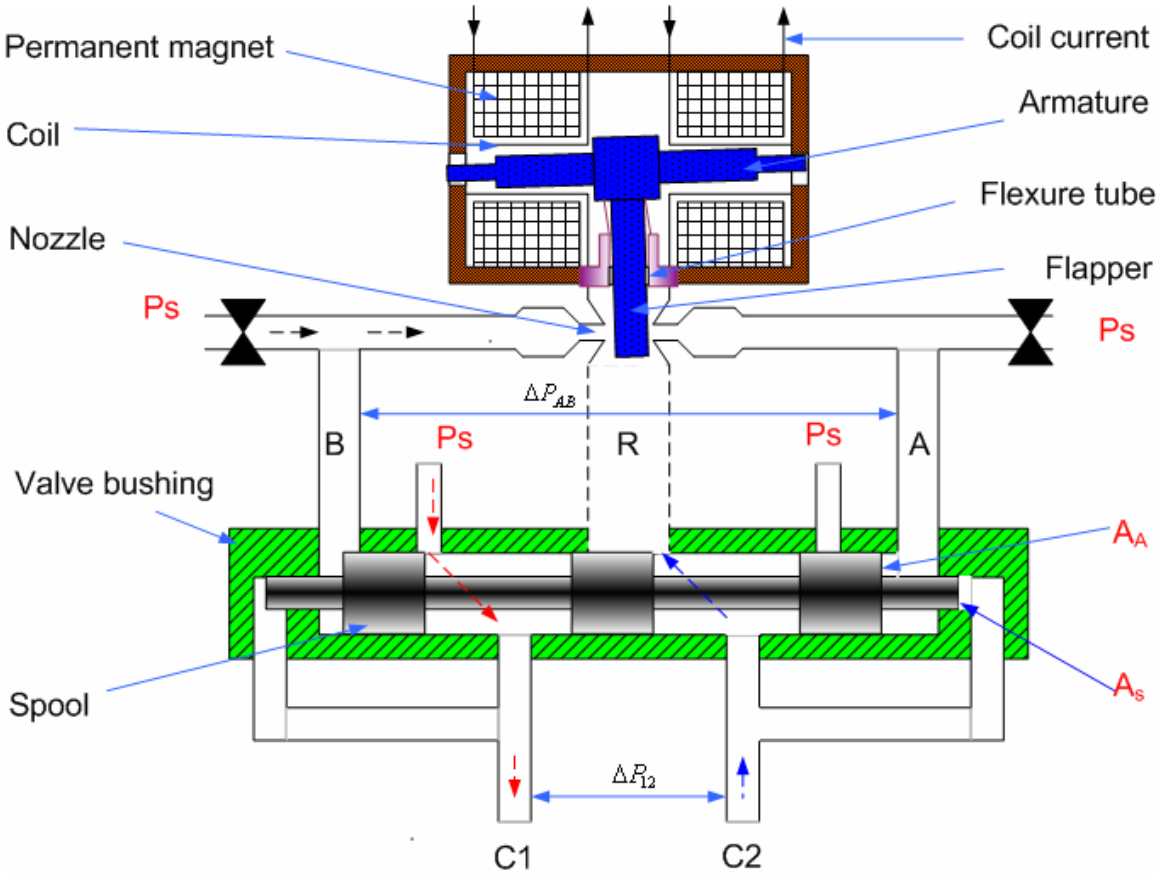

(a)

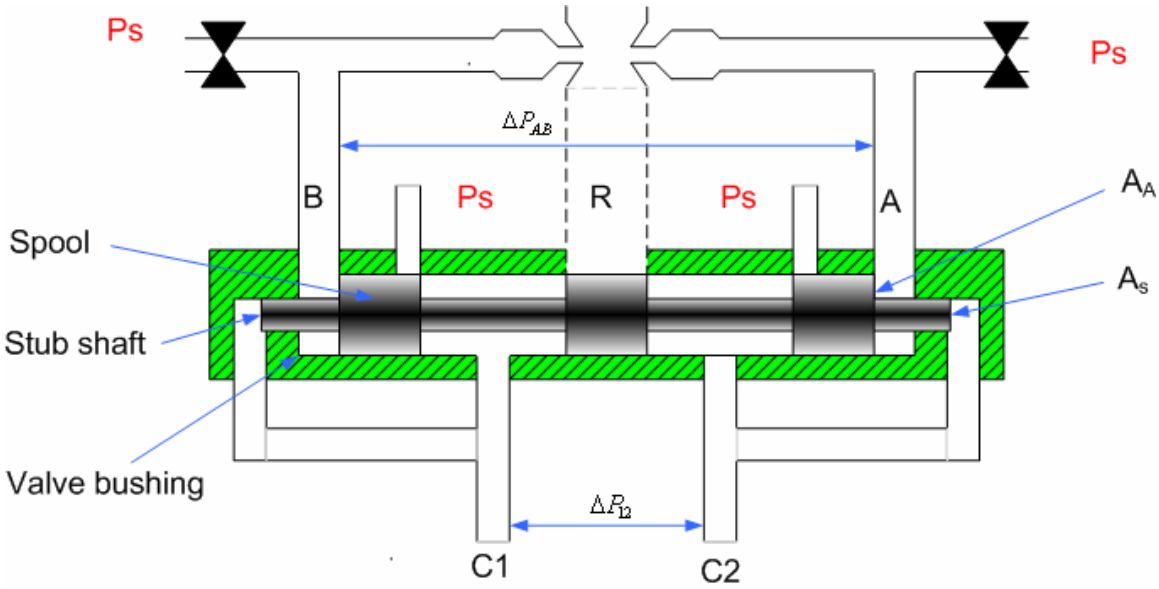

(b)

Figure 4.4 Inner structure of the pressure control valve

4.2.3.2 Pressure control servo valve steady state flow

When the test system was in operation, it was observed that there was a small steady state (quiescent) flow through the pressure control valve even if the input of the valve was zero. The steady state flow was unavoidable due to the structure of the valve and the lack of a load on the ports of the servo valve. Because there was no spring force on the spool, when the current was removed from the valve, it was possible for the spool to be at the non-null position. When the spool is not in the exact null position, a "transient flow force" can exist in this valve which acts in a direction so as open the spool [35]. This problem becomes more severe when the down stream lines of the valve are shorted (i.e., there is no load). Under these conditions, the spool could be open fully with most of the flow from the pump passing through this valve. This would be the case here since the original intent was to have the down stream sides of the valve connected to the tank. The solution was to ensure that there was a "load" across the servo valve ports and this was accomplished using a needle valve (component 19 in Figure 4.2).

This had an additional positive effect on the response of the valve. The smaller the needle valve orifice area, the greater the differential pressure, and hence the larger the differential force ΔP_{AB} on the spool. This resulted in a faster response of the valve. This effect was verified using a model of control servo valve (derived in Appendix F). The smaller the needle valve orifice area, the smaller the spool orifice loading K_{PQ2}. Hence the time constant of this system was smaller, which translated into a faster response.

Some initial feasibility studies were carried out in designing a feedback controller system using the error between the desired flow and the measured flow through the servo valve. This proved to be a very difficult task; indeed, the output flow responses were inferior to the open loop results. Thus, it was decided that the approach here would be to "calibrate" the magnitude of the input signal to ensure that the magnitudes of the output pressure ripple (since pressure was used for comparisons) and timing of the ripple from the pressure servo valve matched the actual faulty piston pump pressure waveform and the starting and closing points. It was believed that the results so produced by this open loop system would be a worst case scenario and that a more sophisticated controller could

be used to drive the pressure servo valve once the initial concept had been shown to be feasible. Time constraints prevented this from being attempted in this study.

4.3 Method to measure leakage

4.3.1 Average leakage from the worn piston (real leakage)

In order to measure the average leakage from the worn piston, measuring the case drain from the pump was one possibility. Case drain leakage was measured using a very simple method. While the pump was in operation, the case drain flow was collected into a graduated cylinder over a specified period. The oil temperature remained the same during these tests which was an important factor since the piston leakage was laminar and hence temperature dependent. The average of several tests at the same pressure and temperature was evaluated and this represented the “normal” average leakage flow, Lcnp. At normal conditions, the clearance of each piston was between 4 to 7 microns. If the operation conditions did not change, and an increase in the average case drain leakage was noted over time, then it could be concluded that the piston was experiencing wear. It should be noted that this assumed that all other types of internal leakage did not change. This is reasonable because the tests were conducted over a very short time span and the leakage was induced using different diameters of pistons.

In the leakage experiments, specially machined pistons with 30, and 60 microns clearances were placed in the pump. The case drain leakages from the pump with the worn pistons were measured. For the same operation conditions, the difference, Lp, between the case drain leakage of the worn piston pump, Lcwp, and the case drain leakage, Lcnp of the normal pump represented the total average leakage from the worn piston, that is:

$$Lp = Lcwp - Lcnp \tag{4.2}$$

It should be noted that the total average leakage was only used to as a guide to design the experiment. The dynamic leakage was the parameter used in this study.

4.3.2 Introducing artificial leakage using the pressure servo valve

For testing of the normal pump, the input signal to the pressure control servo valve was set to zero, and the needle valve (component 19 in Figure 4.2) for the servo valve was adjusted to a convenient opening, (approximately one sixth of a turn). This

then represented a condition of zero artificial leakage. In the experimental system, the total flow (artificial flow leakage, defined as Fal) through the pressure servo valve consisted of two parts: the steady state (zero input to the servo valve) flow, Fss, (quiescent flow), and the introduced additional artificial leakage Fial. The difference between the artificial flow leakage Fal (the actual flow through the servo valve) and the steady state flow Fss (the valve condition with zero input) represented the total introduced additional artificial leakage, Fial as seen by the pump:

$$Fial = Fal - Fss \tag{4.3}$$

For example, if the objective was to simulate an average leakage flow (introduced additional artificial leakage Fial) of 10 ml/s, and the steady state leakage Fss was 5 ml/s, then an average artificial flow leakage Fal of 15 ml/s would be needed. The relationship between of Fial, Fal and Fss is illustrated in Figure 4.5.

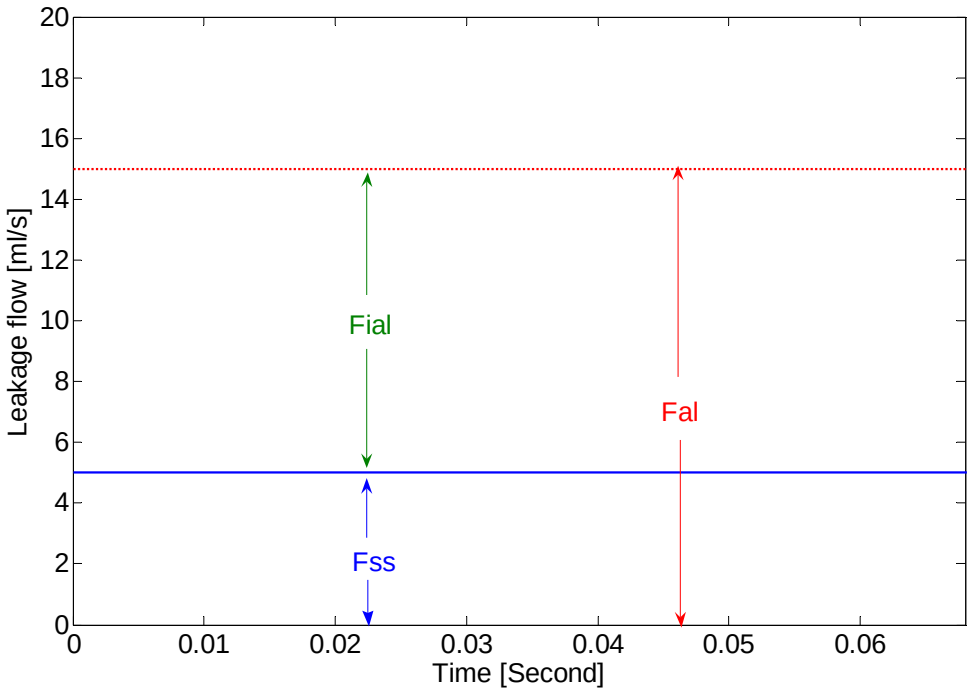

Figure 4.5 Relationships of Fss, Fial and Fal

As a first step a computer was used to collect all data from the system for a normal pump. By applying to the servo valve a predetermined, calibrated signal, a desired introduced additional artificial leakage could be introduced into the pump. The flows Fss

and Fal were measured by the diaphragm differential pressure transducer, component 15 in Figure 4.2

The flow through the pressure control servo valve as derived in Appendix F, was obtained as follows;

$$i_c = K_a V_c \tag{4.4}$$

$$\Delta P_{12} = \frac{9.608}{5.700 * 10^{-3} s + 1} i_c$$

(4.5)

$$Q_{nv} = C_d A_{nv} \sqrt{\frac{2}{\rho} \Delta P_{12}} \tag{4.6}$$

where i_c = Current through the coil [A],

V_c = Voltage across the coil of the torque motor, input voltage [V],

K_a = Gain of the servo valve amplifier [A/V],

Q_{nv} = Flow through the needle valve, or flow through control valve [m^3/s]

C_d = Discharge coefficient of needle valve orifice (component 19 in Figure 4.2)

A_{nv} = Orifice area of needle valve (component 19 in Figure 4.2) [m^2]

ρ = Density of oil [kg/m^3]

ΔP_{12} = Differential pressure across needle valve (component 19 in Figure 4.2) [Pa]

From Equations 4.4 to 4.6, with all parameters known, the flow through the pressure control servo valve, Q_{nv}, could be solved mathematically. It must be emphasized that these equations were used initially to assist in the “design” or “calibration” of the input signal to the valve. The actual input signal design was then refined using trail and error methods.

4.4 Pressure control servo valve response

The flow through the pressure control servo valve in response to the desired input signal is illustrated in Figure 4.6.This figures shows that the flow waveform through the pressure servo valve (red solid line) has approximately 0.01 second delay compared to the input signal (represented by the blue dot sinusoidal wave). In addition, it took longer

to close, compared to the opening time. This is reflected in Figure 4.6 as a smaller slope during valve closing than valve opening. This is due to the limitation of this particular pressure control servo valve. As discussed earlier, once the appropriate piston in which wear was simulated, moved into the discharge chamber, the pressure control servo valve must open at the same time. This meant that simulated worn piston moving in the discharge chamber had to be synchronous with the pressure control servo valve opening. In addition, the simulated worn piston moving out of the discharge chamber had to be synchronous with the pressure control servo valve closing. It is clear that the waveform did not follow the desired input in an acceptable fashion. Because of the slight delay in the opening of the servo valve and the asymmetric transient response of the valve, the use of traditional closed loop controllers was not successful in improving this response. This represented a challenge to the design of the leakage simulator given the desired high frequency of the waveform.

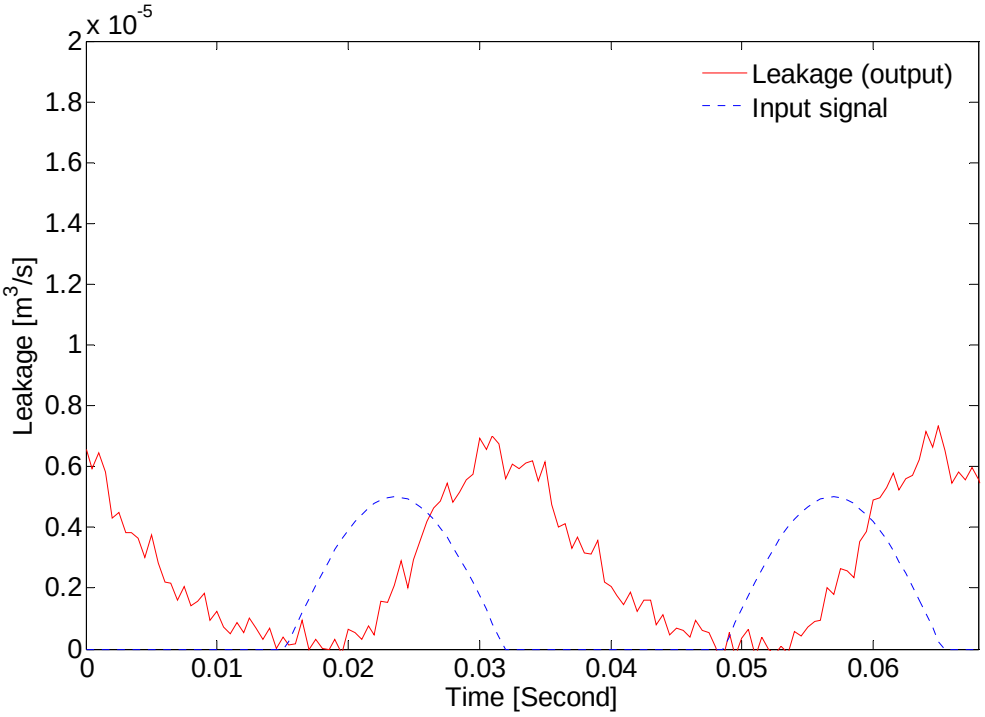

Figure 4.6 Pressure control servo valve flow response for the given input signal

During the experiments, the amplitude of the input signal to the servo valve was adjusted (calibrated) to force the output pressure waveform magnitude to correspond to

the actual desired magnitude. The servo valve was calibrated to produce the correct magnitude for various desired conditions of artificial leakage. In addition, the opening and closing times of the servo valve were forced to correspond to the actual experimental traces of the pumps with actual faults. This required adjusting by a trial and error approach, the shape and timing of the input signal to force the output flow to approach the desired leakage waveform. This actual approach is described in the next chapter.

4.5 Test conditions and procedure

In order to make the test results comparable, all the experimental tests followed the same operating conditions and procedures. These are summarized as follows:

- The oil temperature of tank was kept at $26.5 \pm 1.0\ ^{0}C$ during each test by using a heat exchanger.
- For safety purposes, the pressure of the relief valve (component 17 in Figure 4.2) was set to 20.7 MPa.
- All tests were repeated four times to check for repeatability. The results so presented in this thesis are the average value from four experiments carried out at the same conditions at different times.
- For each test, the system load was held constant; that is, the needle valve orifice (component 20 in Figure 4.2) was not changed.
- The pump swash plate angle was fixed.
- All transducers were re-calibrated before each set of tests.
- The needle valve orifice (component 19 in Figure 4.2) was set at the same position.
- The computer began to collect data after the system ran for 10 seconds to allow starting transients to die down.

The experimental results are presented in detail in the next chapter.

4.6 Summary

In this chapter, the methodology used to introduce artificial leakage to simulate piston wear for the pump was presented. The experimental systems, including the test systems, and the data acquisition system, were explained. One of the main components of

the experimental systems, a pressure control servo valve, was discussed. In the next chapter, the experimental results are presented and are followed by some discussion.

Chapter 5 Experimental Results

In Chapter 4, the experimental hydraulic circuits, the data acquisition system and the test procedure were described. In addition, a model of the pressure control servo valve was derived. In this chapter, the experimental results of artificially introducing leakage faults into a hydraulic circuit are presented followed by discussions pertaining to the system performance.

5.1 Experimental data repeatability

In any experimental study, it is imperative that the results are repeatable within an acceptable margin. This provides confidence when interpreting the results and drawing conclusions. In all the experiments, several data sets for the same type of tests were collected for the same operating conditions (such as fluid temperature, pressure, same inputs to the pressure control servo valve, same operating scheme, etc.). For most of the studies, the operating pressure was approximately 6.60 MPa and fluid temperature 26.5 ^{0}C.

Figure 5.1 illustrates the data repeatability for the pressure ripples (as an example). Four data sets were collected at different times for the same operating condition of 26.5 ^{0}C and in this case, 6.60 MPa. It can be observed that visually, the pressure ripples were very similar from test to test. All four data sets show similar trends, time period and magnitude. Variation between the traces is very small. However, to quantify what the actually variation was, the values of each data sets' minimum, maximum, mean, and standard deviation were evaluated and are presented in Table 5.1. The minimum and maximum were found by examining all the data within one set (2000 points) and recording the maximum and minimum values. The mean was the average value of the 2000 data points for each set from which the standard deviation and range of all the data points were calculated. With reference to this table, it is observed that the values of five performance indicators, minimum, maximum, mean, standard deviation, and range, for these four data sets are very close, all varying within 0.79%. These indicators would indicate that the data repeatability was acceptable.

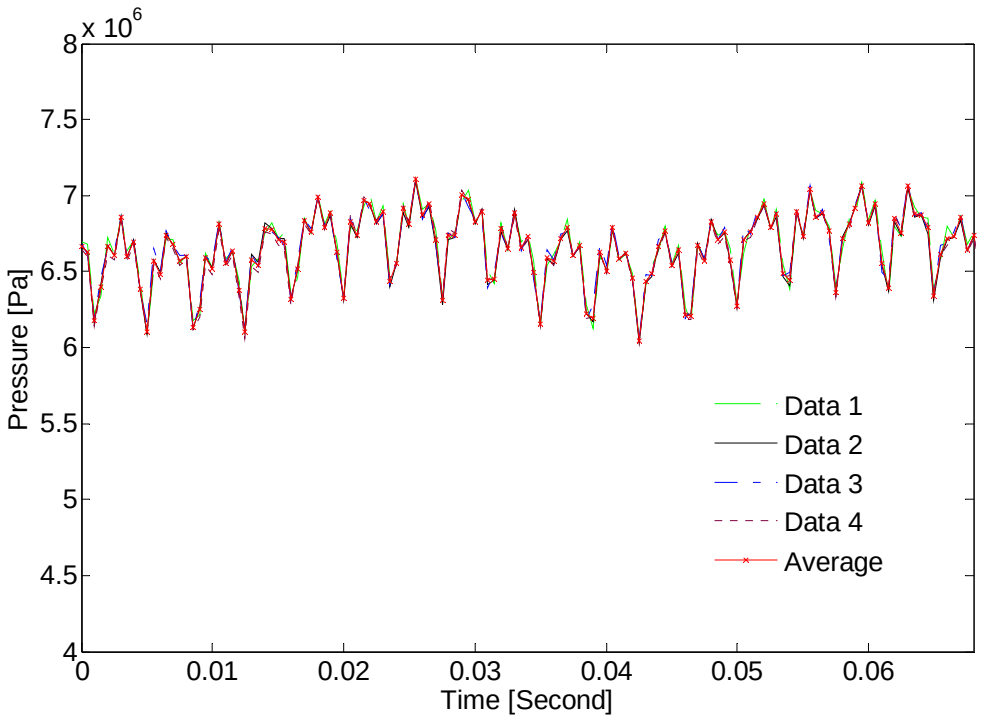

Figure 5.1 Pressure ripple repeatability (experimental)

Table 5.1 Comparison indicators of four data sets

Comparison item	Data 1	Data 2	Data 3	Data 4	Mean	% Variation
Min (MPa)	6.03	6.03	6.04	6.02	6.04	0.49
Max (MPa)	7.14	7.12	7.12	7.12	7.11	0.42
Mean (MPa)	6.66	6.64	6.65	6.64	6.68	0.30
Standard Deviation (MPa)	0.23	0.23	0.23	0.23	0.23	0.79

Although the repeatability was good, there was still a small variation between the four data sets. Therefore, the average value at any time t of these four sets was used rather than individual sets and was assumed to be a sufficient representation of the experimental data for that operating situation. The average value of these six sets was calculated and was almost same as the average value of four sets. Subsequently, all experiment data waveforms presented in this work represent the average of the four data sets collected in the same manner and at same operating situations.

5.2 Pressure ripples from the normal pump

5.2.1 Pressure ripples

It was necessary to know what the physical pressure ripple from a "normal" pump looked like (in Chapter 3, the theoretical ripples were shown). The normal pump waveforms were those to which the base information was to be compared. The pump would have some break-in wear but would not demonstrate any substantial faults. In Figure 5.2, the pressure ripple of the normal pump is shown. The pressure ripple was obtained at a system pressure of 6.82 MPa and temperature 26.5 ^{0}C. Referring to Figure 5.2, there are nine large periodic ripples for one revolution of the pump. The pressure ripple waveform appears complex but the basic waveform is made up of a fixed periodic signal and, "almost uniform" magnitude ripples.

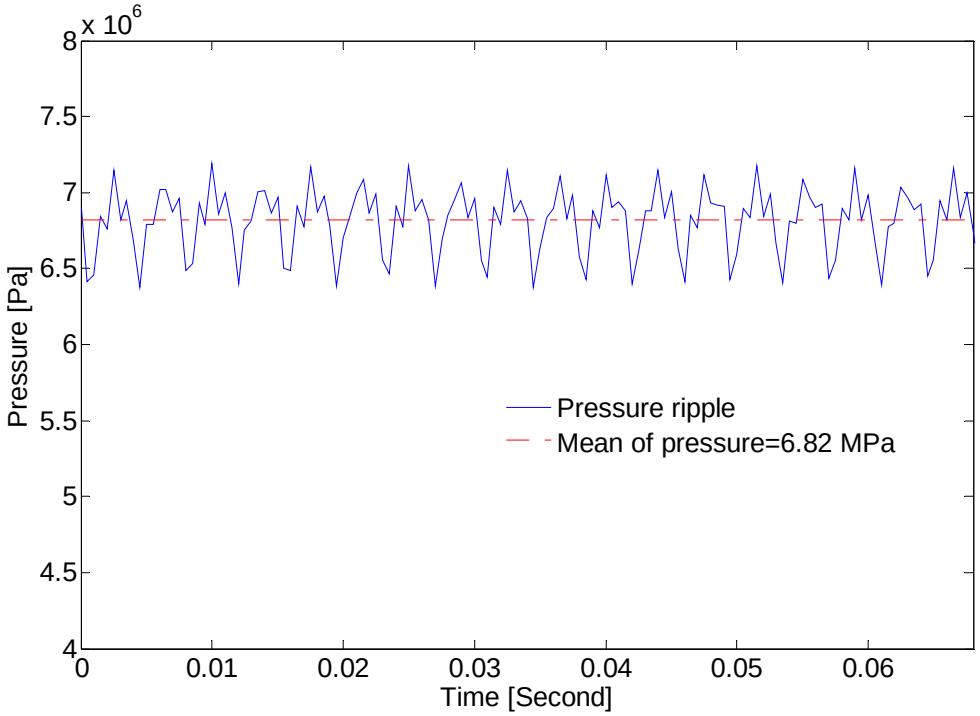

Figure 5.2 Pressure ripple for the normal pump (experimental)

In this time domain waveform in Figure 5.2, it is often very difficult to extract information from complex time domain waveforms such as that displayed by the pressure ripple. However, extracting frequency information can readily be accommodated using the "power spectral density" to process the pressure ripple. An explanation of the concept

behind power spectral density analysis is provided in Appendix G. The power spectral density of the pressure ripple from the normal pump is illustrated in Figure 5.3.

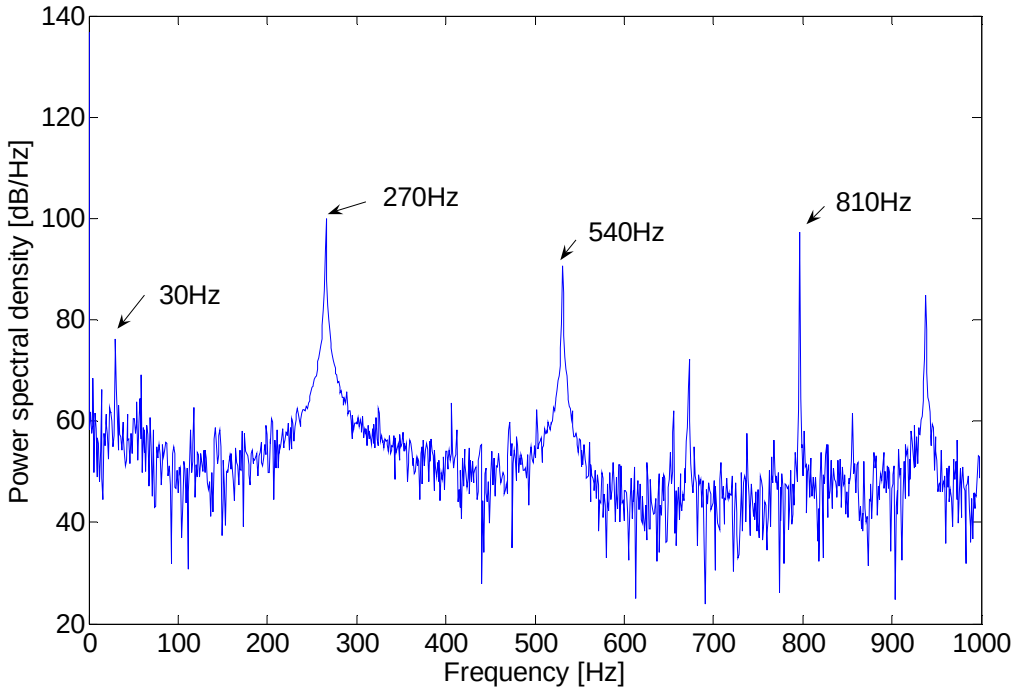

Figure 5.3 Power spectral density of normal pump pressure ripple

It can be observed from Figure 5.3, that there are several significant frequencies which demonstrate a higher density value. The frequency which shows the highest peak is 270 Hz. This frequency can be readily explained because there are nine pistons in the pump; at a pump rotational speed of 1800 RPM (30 revolutions per second), in one second, the pistons passed by the discharge chamber 270 (9 times 30) times.

The other frequencies can be explained as:

- 30 Hz, the rotational speed of the pump (electrical motor drive speed)
- 540 Hz, the second harmonic of the rotational speed of the pump pistons
- 810 Hz, the third harmonic of the rotational speed of the pump pistons

Thus, the power spectral density can be used to effectively explain the pump performance (in this case, the complex time domain waveform) very well.

5.2.2 Pressure ripples changes with temperature

Although a variable displacement pump was used in this study, during the experiments, the angle of the swash plate in the pump was fixed. Hence, the theoretical flow from the pump was constant if the operating conditions of the pump did not change. From a practical point of view, the internal leakage, including piston leakage, slipper leakage and valve plate leakage, changed with temperature and/or pressure. Hence, the output flow from the pump also changed with the temperature and/or the pressure.

The temperature and the pressure affect the leakage considerably. Referring to the piston leakage Equation 3.1, as the temperature increases, the fluid viscosity decreases. If the other operating conditions are kept constant, then leakage will increase, (see Figure 5.4). Referring to Figure 5.4, it can be seen that the temperature affects the leakage substantially. For example, the mean of the pump output flow at 26.5 ^{0}C was 3.48*10^{-4} m^3/s, but at 38.0 ^{0}C it was 3.37*10^{-4} m^3/s. This was due to change in viscosity at different temperatures.

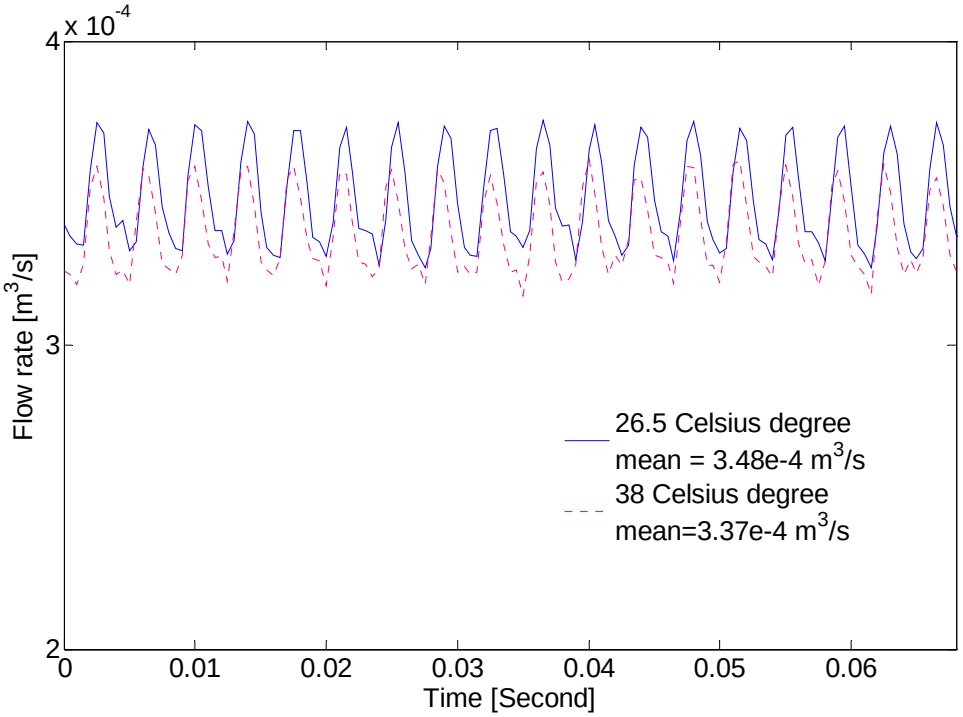

Figure 5.4 Comparison of the pump output flow at 26.5 ^{0}C and 38.0 ^{0}C (experimental)

In this study, the pressure waveform was used for comparison purposes; therefore, it was very important to observe how the pressure changes with temperature. The experimentally measured change in pressure for two temperatures is shown in Figure 5.5. It is observed that the mean value of the pressure at 26.5 ^{0}C, the blue solid line, is 6.76 MPa. However, the pressure dropped to 6.49 MPa at 38.0 ^{0}C. Thus temperature does affect the pressure values significantly.

In summary, it was very important that the temperature and the pressure during all the tests were well defined and controlled.

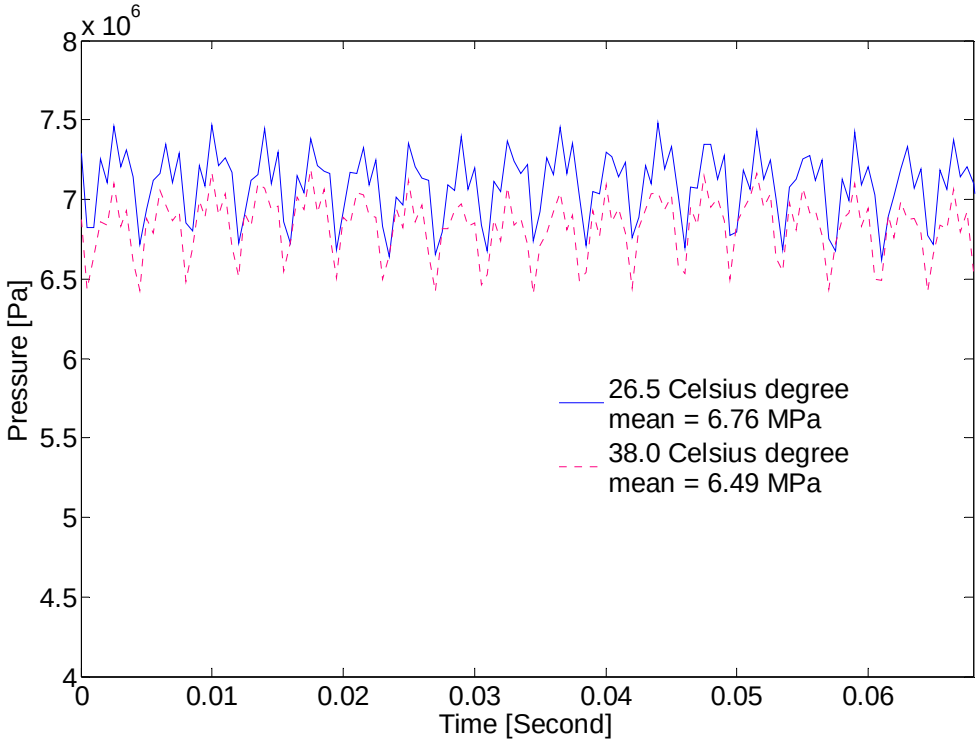

Figure 5.5 Comparison of the pump output pressure at 26.5 ^{0}C and 38.0 ^{0}C (experimental)

5.2.3 Output flow relationship with pressure

Because of the dependence of the leakage on the pressure, it was not surprising that for this "fixed" displacement axial piston pump, the output flow changed with the operating pressure. The output flows of the normal pump under a system pressure of approximately 7 MPa and approximately 21 MPa at 26.5 ^{0}C are illustrated in Figure 5.6. Some interesting observations arose from Figure 5.6.

First, it was observed that the pump flow at 7 MPa was larger than that at 21 MPa. When the system pressure increased, the pressure difference, ΔP (discharge chamber pressure minus case drain chamber pressure) also increased; consequently, if the other parameters were held constant, the leakage increased. Thus, the pump flow decreased as expected.

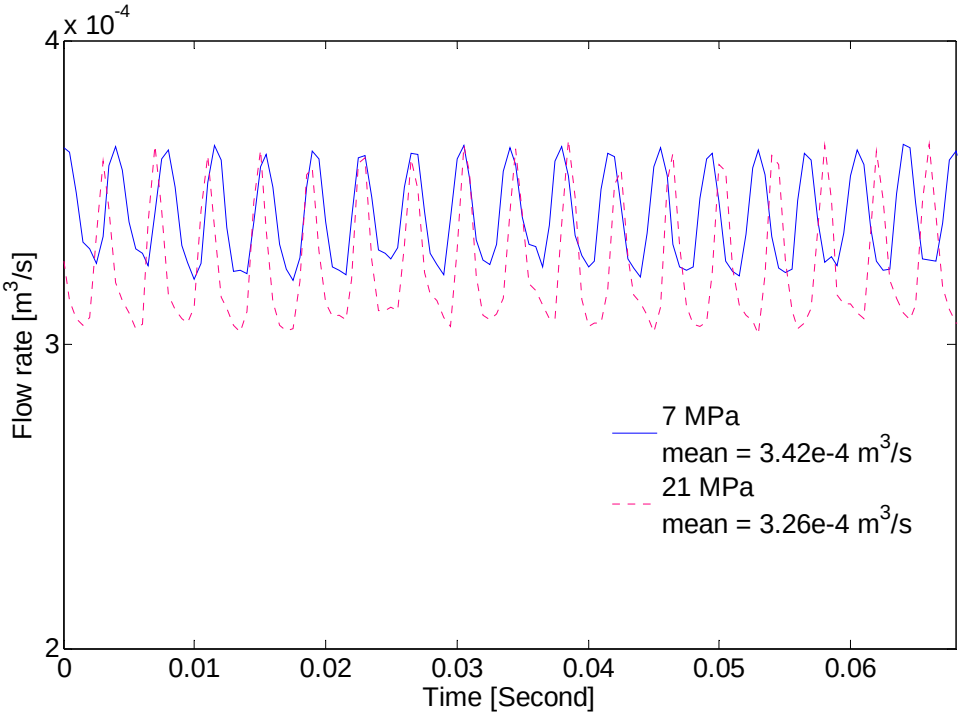

Figure 5.6 Comparison of pump output flow between 7 MPa and 21 MPa at 30.0 ^{0}C (experimental)

It was also observed that the period of revolution made up of nine ripples was not identical at 7 MPa and 21 MPa. The period of the 21 MPa was 0.0005 seconds longer than that of the 7 MPa, which was 0.034 second. The reason for this was that the increased pressure translated to an increased load on the driving electric motor which resulted in a slightly reduced speed.

A third observation was that the amplitude variation of the output flow, the difference between the ripple's peak and the lower trough over one revolution at 21 MPa was larger than the 7 MPa. This was attributed to the inner structure of the pump. During the pump operation, when the piston just moves to connect with the discharge chamber,

(high pressure conditions), some fluid in the discharge chamber is passed back into the piston chamber (where the pressure is low) through the relief notch which pre-opens to the discharge chamber. When the system pressure is 21 MPa, more fluid in the discharge chamber will be pushed into the piston chamber than that at 7 MPa. Therefore, at that point, the minimum value of flow at 21 MPa is less than that at 7 MPa. In addition, all fluid (including the fluid pushed from discharge chamber) in the piston chamber would eventually be pushed out to circuit, which means the mean of the output flow should be same at any pressure if the leakage is small. Hence, the flow variation in high pressure would be bigger than that at low pressures but the mean would be the same.

5.3 Pressure ripples from the experimental faulty pump

In this research, the experimental "faulty" pump contained one "worn" piston (in actuality, it was a machined piston) with different radial clearances. During the experiments, several machined pistons with radial clearances of 30 microns or 60 microns were fitted into the pump to replace a normal piston. The pressure ripple of the faulty pump with one 60-micron-clearance piston is illustrated in Figure 5.7. There were still nine ripples in one revolution, but the mean value 6.65 MPa was less than the mean of the normal pump 6.82 MPa, which was illustrated in Figure 5.2. This was as expected because since the leakage in the faulty piston increased, the average flow from the pump to the load decrease which in turn resulted in a slight drop in the average pressure.

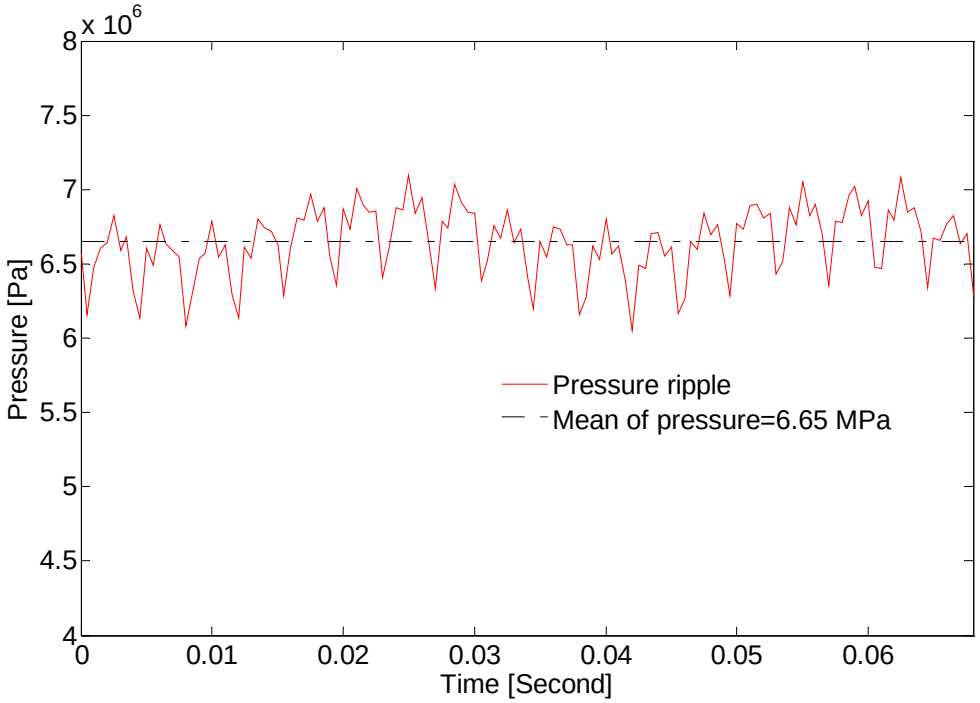

Figure 5.7 Pressure ripple of the faulty pump (experimental)

The power spectral density of the experimental faulty pump pressure ripple waveform is illustrated in Figure 5.8. It is noticed that the 30 Hz frequency component is very significant in this figure. This frequency is the fundamental frequency of rotation of the electric motor, and theoretically, should not be dominant at all. The reason that it is will be addressed in the following section.

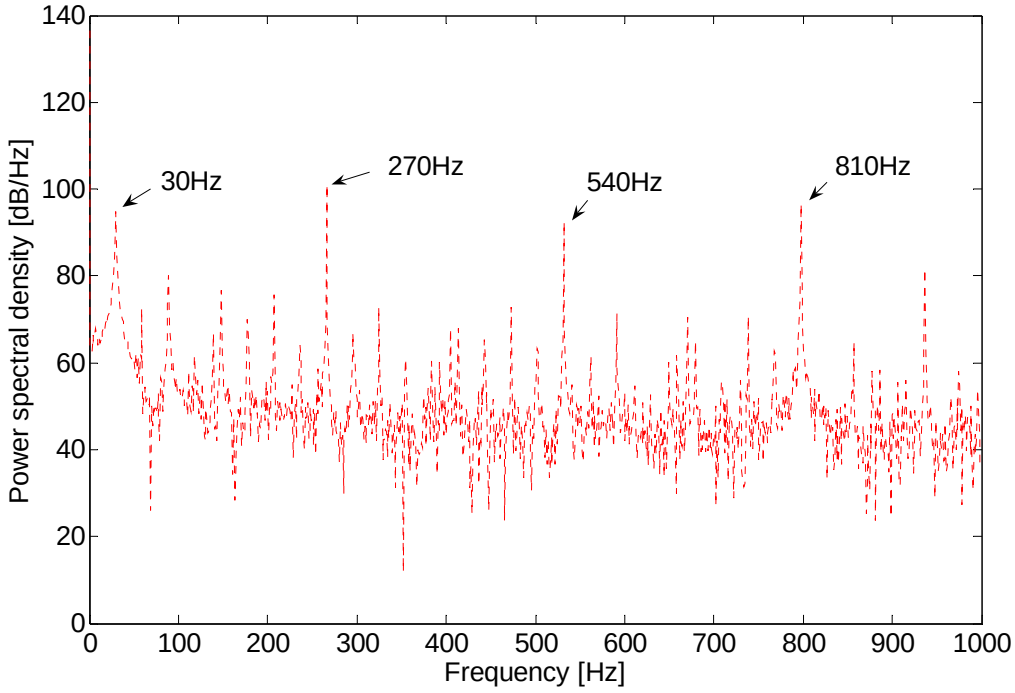

Figure 5.8 Experimental faulty pump power spectral density

The pressure ripples of the experimental normal pump and the faulty pump are shown in Figure 5.9. In this figure, the red solid line represents the normal pump and the dotted blue line the faulty pump. In each pump revolution, the faulty pump pressure was observed to be lower than the pressure of the normal pump at the same point which was about half way through the revolution; at all the other points the pressure ripple was almost same. This can be explained by the fact that the worn piston only affected the pressure ripple for the half revolution when the piston was in the discharge port. Because of the increased clearances between the piston and its sleeve, the leakage from the worn piston was much higher than that from the other single pistons. This increase in leakage resulted in a reduced output flow which in turn reduced the output pressure over this particular time frame.

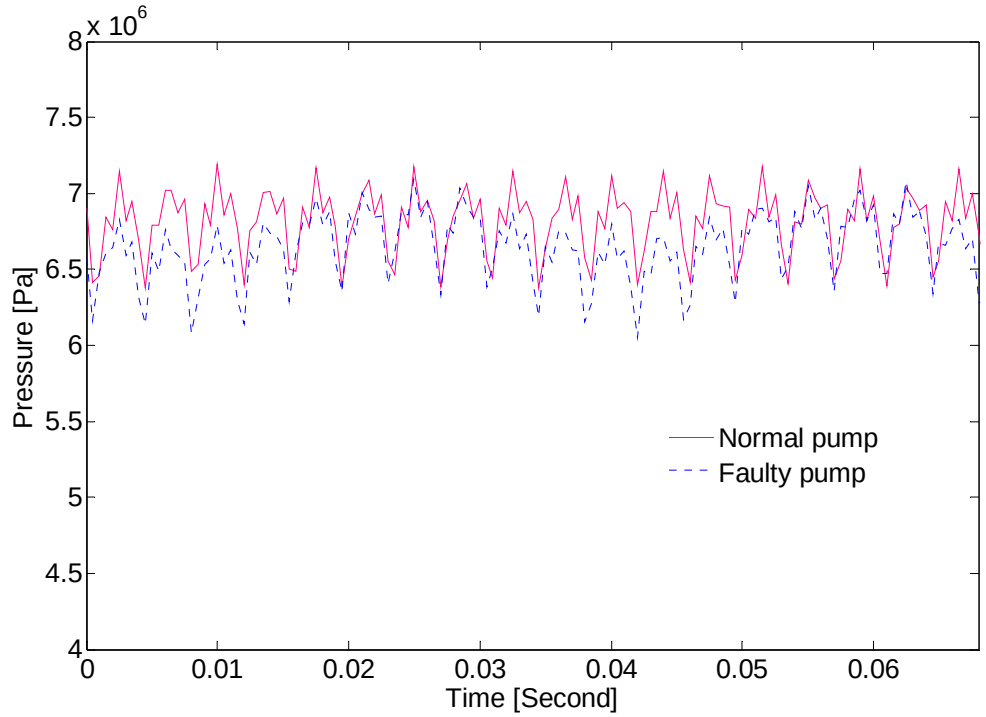

Figure 5.9 Pressure ripple comparison between normal pump and faulty pump (experimental)

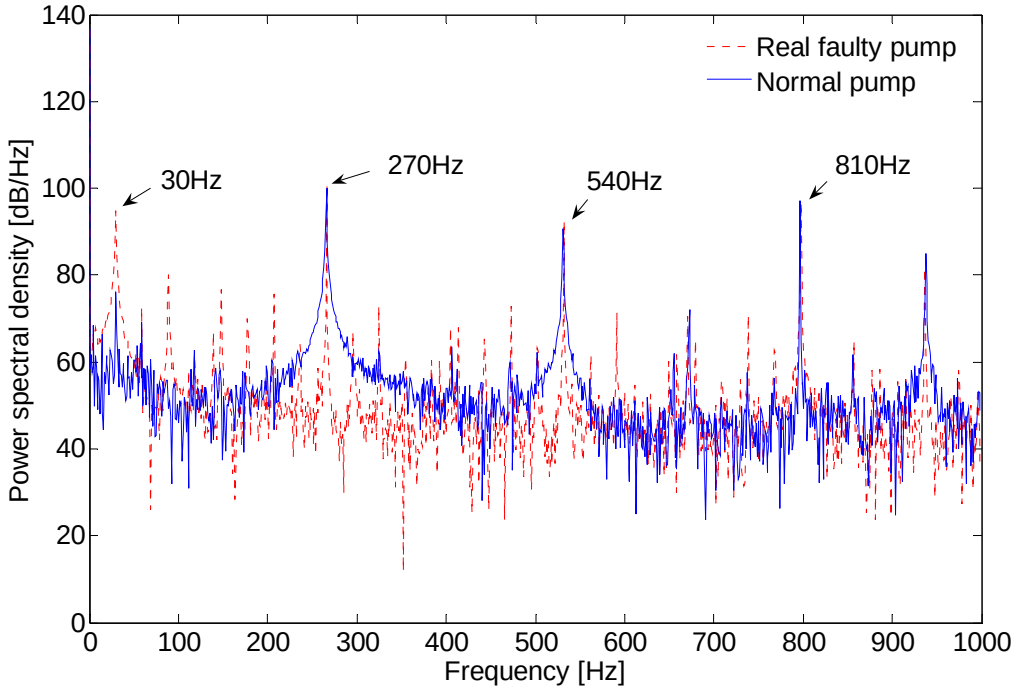

Figure 5.10 Power spectral density comparisons of normal pump and faulty pump pressure

The power spectral density of these two pressure ripples is illustrated in Figure 5.10. It is observed that both pumps displayed similar dominant power densities at 270 Hz, 540 Hz and 810 Hz. The one exception was at 30 Hz. In the faulty pump, the peak magnitude at 30 Hz was 95 dB, compared to that of the normal pump at 75 dB. That means the 30 Hz frequency was more significant in the faulty pump than in the normal pump. It was believed that because the worn piston encountered a high pressure port 30 times in one cycle (1800 RPM), the "slack" due to the piston's increased clearances created an "impulse" to the barrel which in turn was detected as a pressure spike at this frequency.

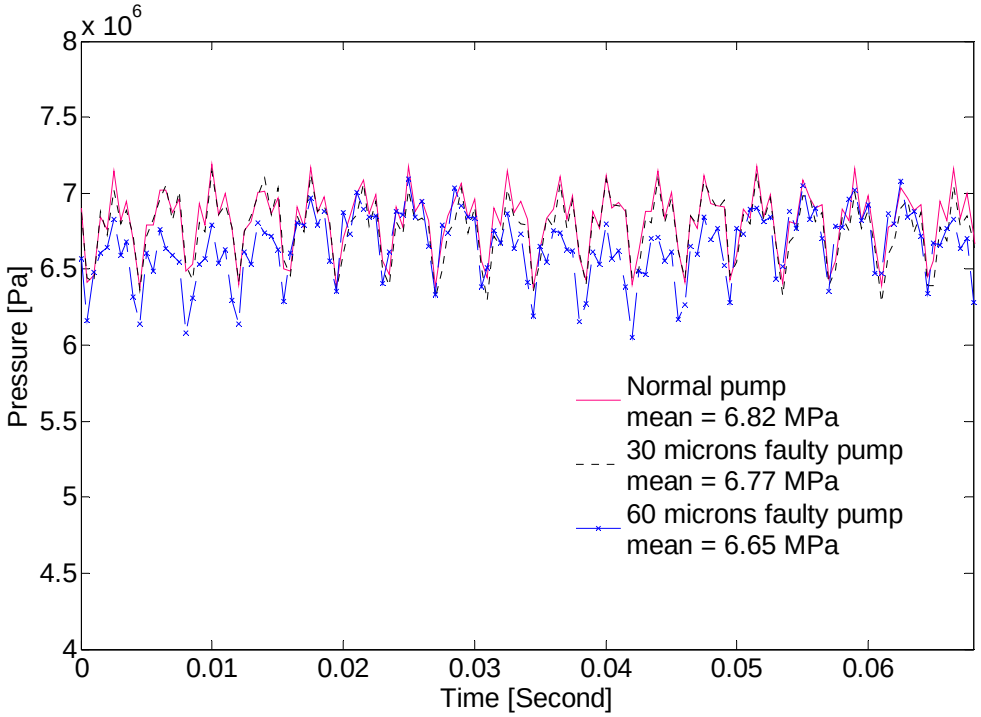

Figure 5.11 Pressure comparison of normal and real faulty pumps (experimental)

It was of interest to compare the power spectral density for the same pump but with worn pistons of different clearances. The actual waveforms for the three conditions are shown in Figure 5.11. The power spectral densities of the normal pump and the faulty pump are presented in Figure 5.12. Although difficult to see on the superimposed trace, it is noticed that the power spectral density function is similar but at 30 Hz, a difference exists. The faulty pump with 60 microns clearance had a larger power density of 95

dB/Hz, than the 85 dB/Hz power density of the pump with the 30 micron clearance piston. In comparison, the normal pump showed the smallest value at 75 dB/Hz.

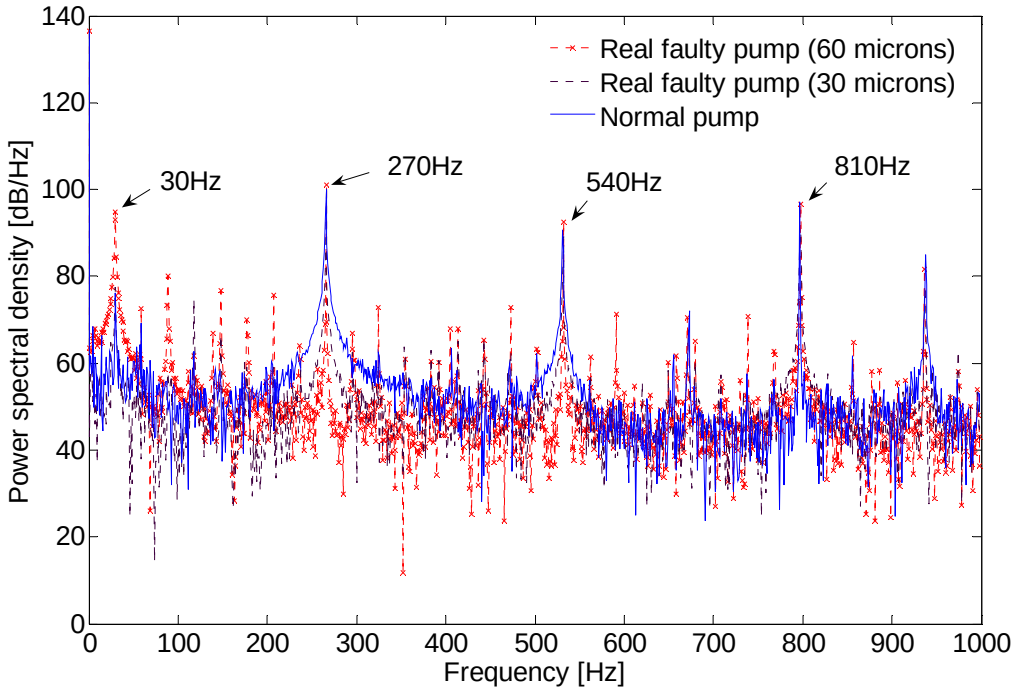

Figure 5.12 Comparison of normal pump and faulty pump power spectral density

5.4 Ripples from the artificial leakage faulty pump

5.4.1 Artificial leakage

As addressed in Chapter 4, there existed a steady state "quiescent" flow (defined as Fss) which passed through the pressure control servo valve even when the valve had zero input. This steady state flow through the valve is shown in Figure 5.13, as a black dotted line. This quiescent flow was not really a constant value, but an average steady state value with a small ripple superimposed on it. This ripple was a consequence of the normal pump output flow ripple.

In order to introduce the additional artificial leakage via this servo valve, a programmed signal from the computer (via Matlab Realtime Workshop®) was applied to the pressure control servo valve. As discussed in Chapter 4, the shape of this signal was designed by trial and error procedure to produce the desired simulated dynamic leakage in the pump.

In Figure 5.13, the green line represents the introduced additional artificial leakage (defined as Fial in Section 4.3.2), which was the subtraction of the artificial leakage waveform (the red line in Figure 5.13, defined as Fal in Section 4.3.2) and the steady state waveform (the black dot line in Figure 5.13, defined as Fss in Section 4.3.2). The introduced additional artificial leakage (green line in Figure 5.14), demonstrates the approximate same opening and closing times as the theoretical piston leakage (red dash line) shown in Figure 5.14. In addition, the average magnitude of the introduced additional artificial leakage and the theoretical piston leakage is very close as well. The theoretical piston leakage was based on a calculation from Equation 3.1.

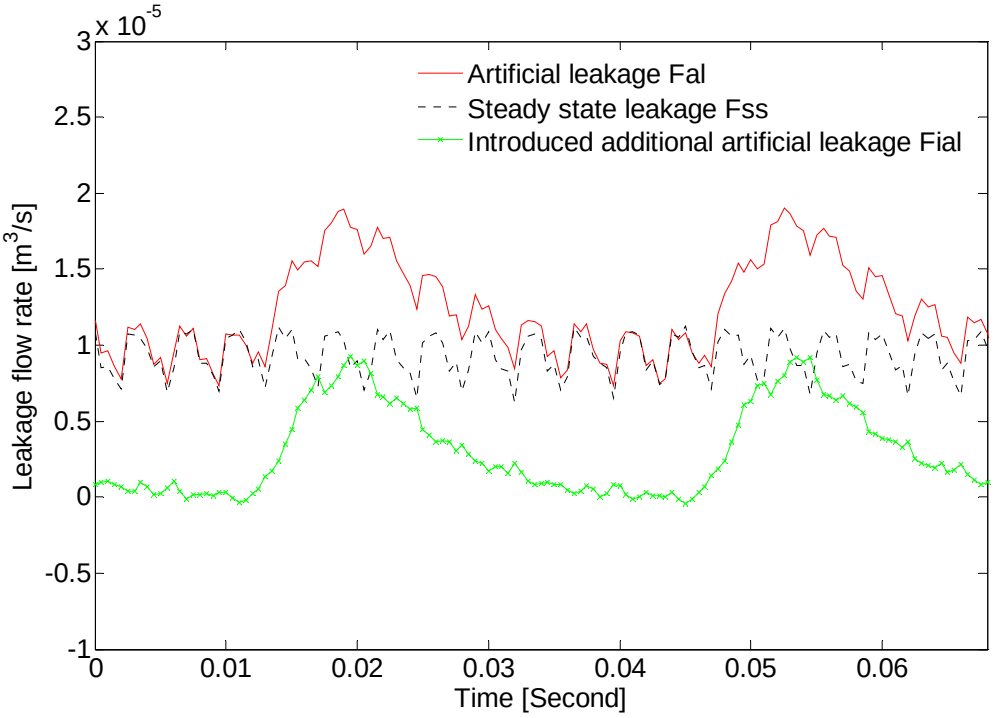

Figure 5.13 Introduced artificial leakage (experimental)

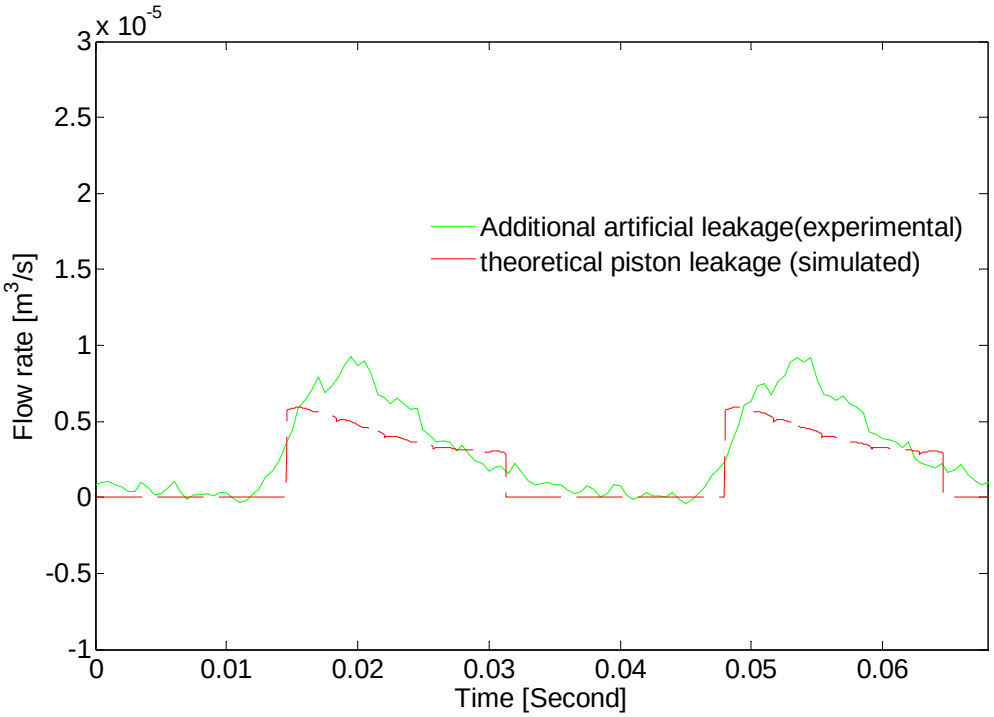

Figure 5.14 Comparison of the additional artificial leakage and simulated theoretical piston leakage

It is seen in Figure 5.14 that the introduced additional artificial leakage occurred only over one-half of the pump revolution. This waveform therefore mimicked the waveform that the actual leakage in a worn piston would have. Different calibrated inputs to the pressure control servo valve produced different additional artificial leakages. The inputs were based on a trial and error procedure which is summarized as follows:

1. The opening and closing times of the valve were adjusted to best approximate the basic waveform shape.
2. The pressure ripple magnitude was adjusted to be approximately the same on the average to a specified known faulty piston, such as at 60 microns or 30 microns.
3. The normalized data (to be discussed) were used to analyze the data and then to fine tune the timing and amplitude to closely approximate the normalized data of the known faulty pump.

The input signal to pressure control servo valve for the additional artificial leakage in Figure 5.14 is illustrated in Figure 5.15. Consider Figure 5.15; the width of the

input signal was changed to obtain different valve activation time (the period in which the valve was opened); in addition, changing the amplitude of the pulse signal illustrated in Figure 5.15 resulted in a change in the magnitude of the introduced additional artificial leakage. Figure 5.16 illustrates the artificial leakage waveforms related to the different magnitude inputs to the pressure control servo valve.

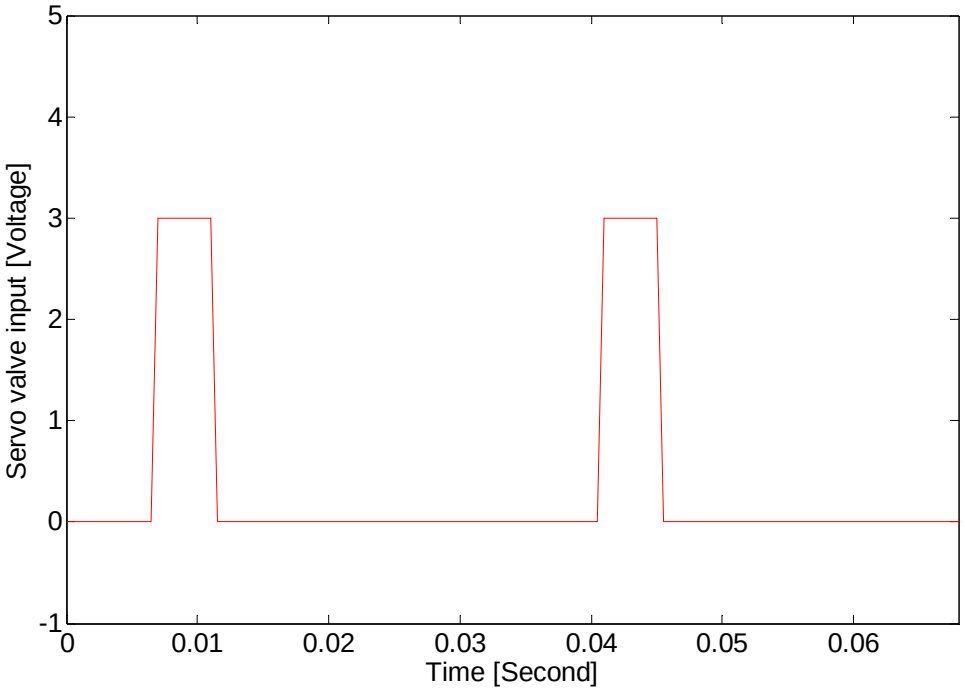

Figure 5.15 Servo valve input signal

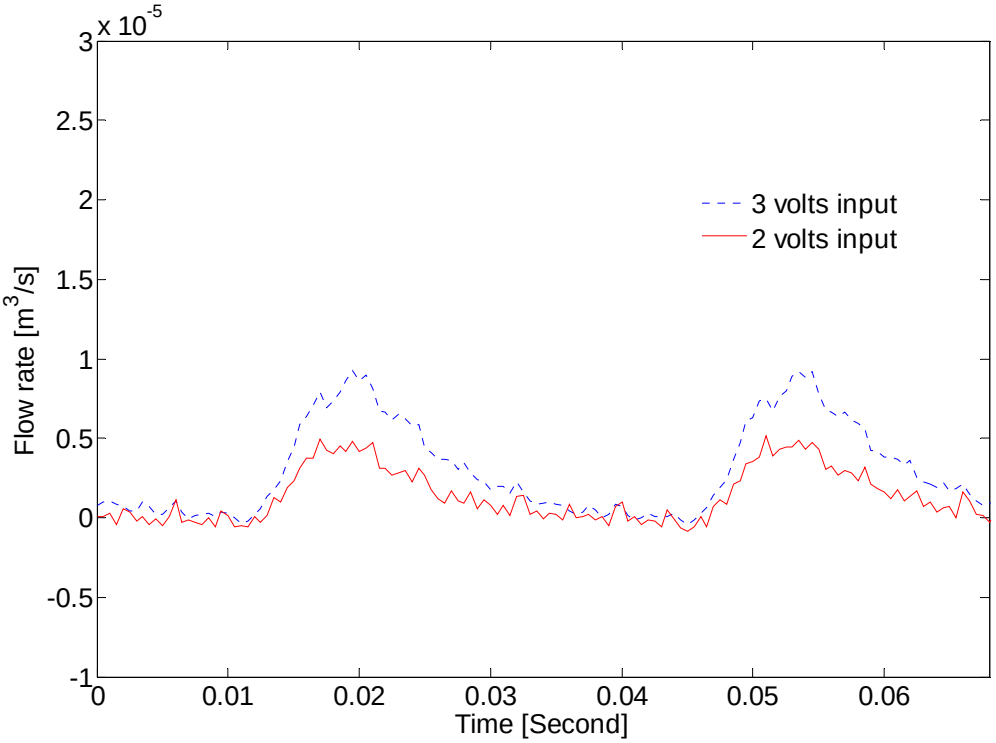

Figure 5.16 Introduced additional artificial leakages from different valve inputs (experimental)

5.4.2 Pressure ripple from the artificial faulty pump

The pressure ripple at the pump outlet as a consequence of the introduced additional artificial piston leakage discussed in Section 5.4.1 is shown in Figure 5.17. It is observed that compared to the normal pressure ripple, the artificial fault pressure ripple was concave over one cycle showing the same trend as the actual pump did with one faulty piston (see Figures 5.9 and 5.17).

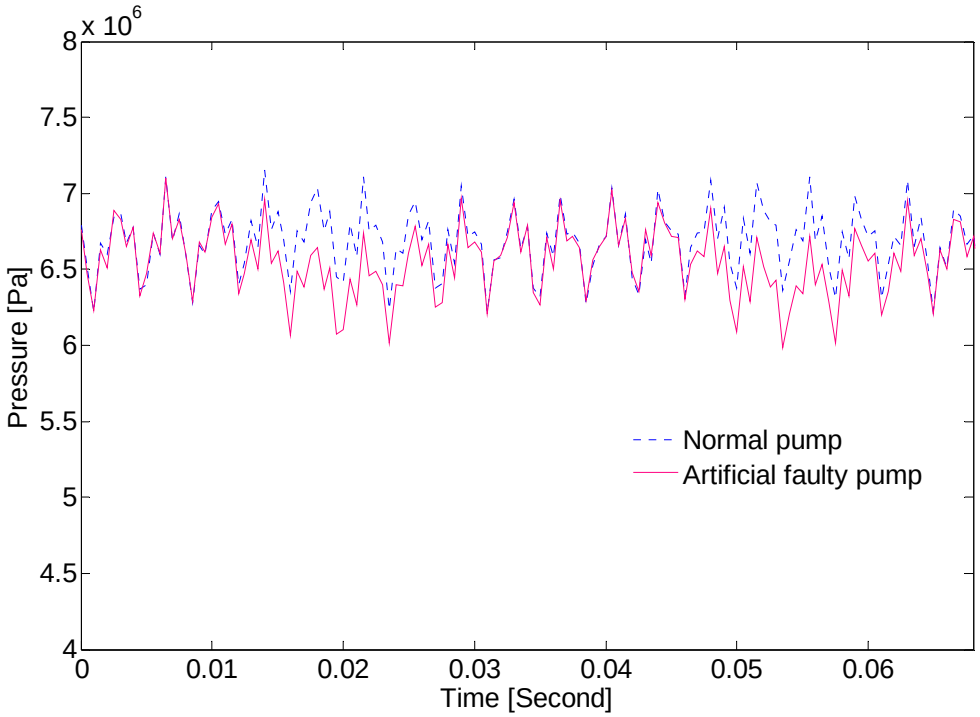

Figure 5.17 Pressure ripple from artificial faulty pump (experimental)

The power spectral density of the pressure ripple shown in Figure 5.17 is illustrated in Figure 5.18. Consider Figure 5.18; shows that all the dominant frequencies, (30 Hz, 270 Hz, 540 Hz and 810 Hz) found in the 60 microns faulty pump also appeared in Figure 5.8.

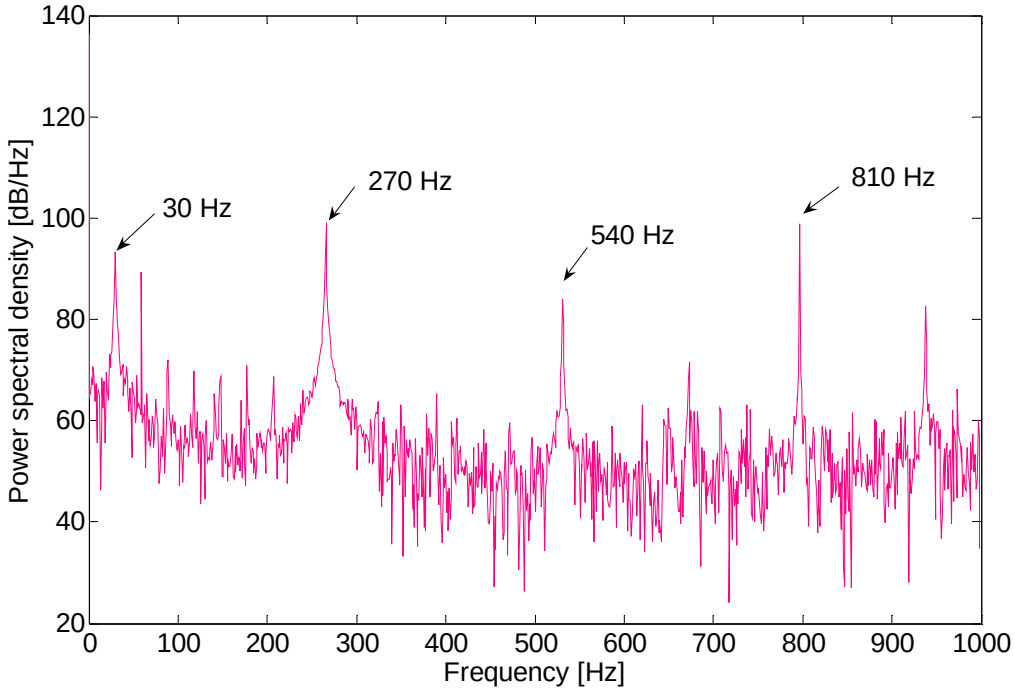

Figure 5.18 Power spectral density of the pressure ripple from the artificial faulty pump

Figure 5.19 and Figure 5.20 show the pressure ripples from several simulated artificial faulty pumps (Figure 5.20 is a detail of one part of Figure 5.19). It is observed that as the input to the servo valve increased, the more the pressure waveform deviated from the normal waveform.

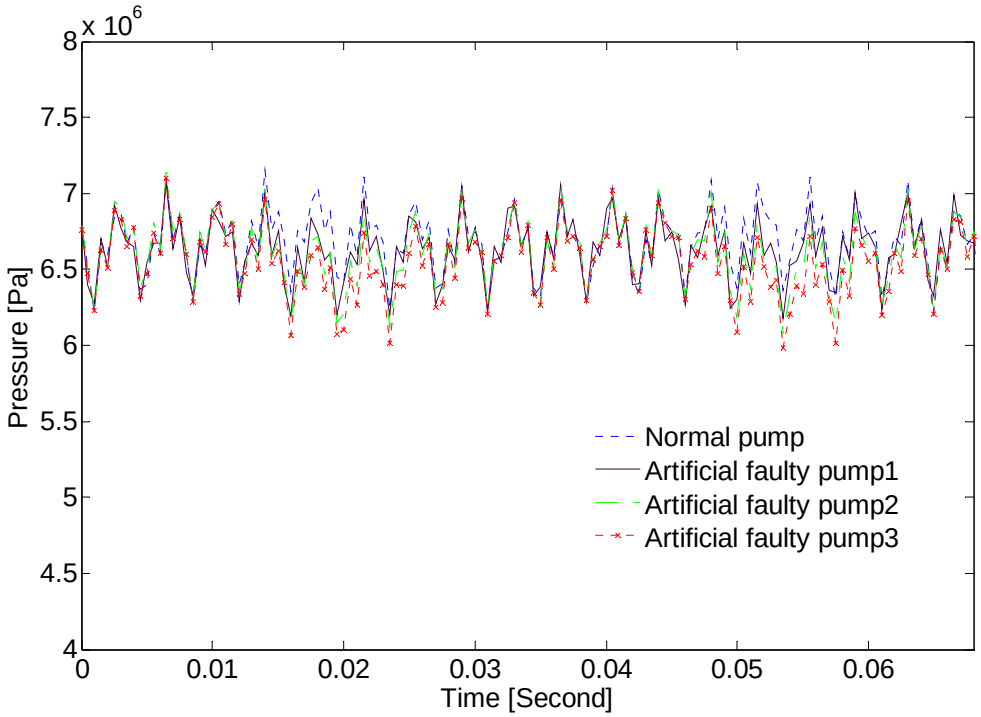

Figure 5.19 Pressure ripples from different artificial faulty pumps (experimental)

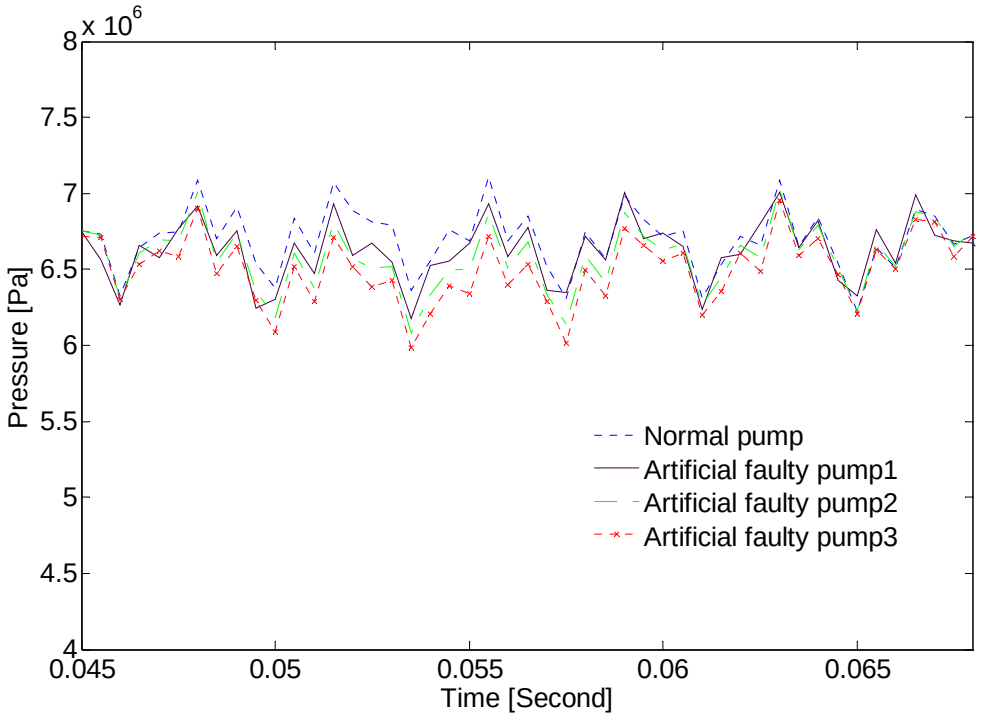

Figure 5.20 Pressure ripples from different artificial faulty pumps (detailed, experimental)

5.5 Comparison of the normal pump and faulty (artificial) pump pressure waveforms

At 7 MPa pressure and 26.5 ^{0}C temperature, with an appropriate input into the pressure control servo valve, the waveforms of the pump pressure and leakage through the pressure control servo valve were measured. In Figure 5.21 the pressure ripple with one worn piston at 60 microns is shown. These results indicate that the measured pressure waveforms had one concave dip in each cycle and the concave form repeated every revolution.

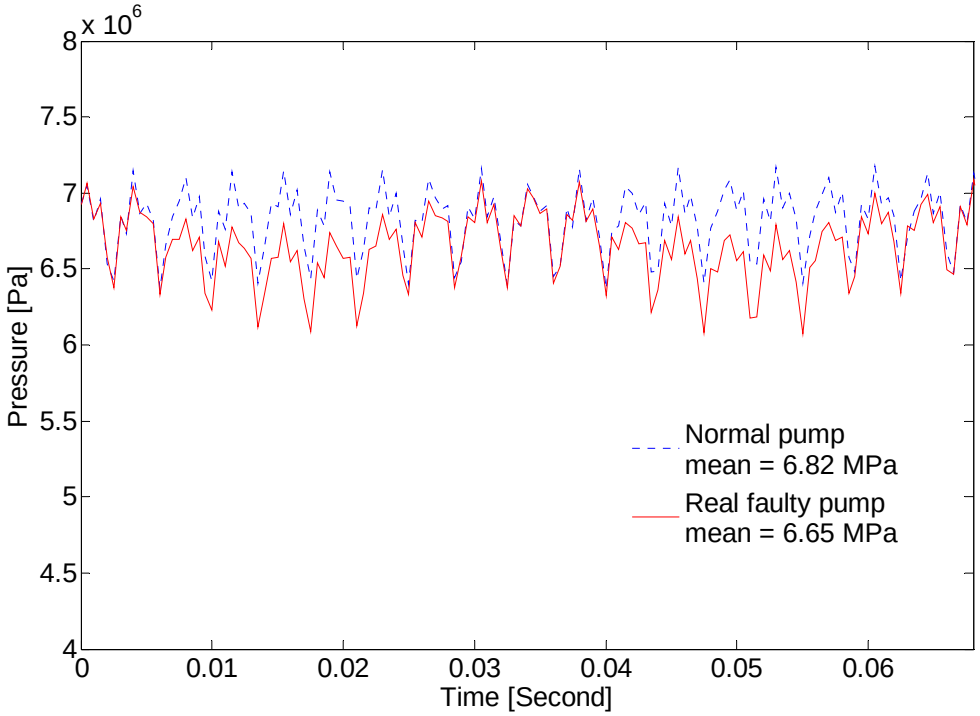

Figure 5.21 Comparison of the experimental pressure waveforms for the pump with a real fault (not artificially created) and a normal pump

The experiment was conducted using a constant (fixed between tests) steady state pressure. In order to facilitate comparison of the measured pressure waveform with that when leakage was artificially introduced, a technique to "normalize" the difference between the pump with a faulty piston (actual or artificially created) and with no faults was introduced. The normalization process is presented in Appendix H. In Figure 5.22, the normalized data of the pressure ripple illustrated in Figure 5.21 are shown for two

revolutions. From Figure 5.22 the basic shape of the normalized data consists of two peaks and two troughs. The magnitude of the peak is approximately 0.05 (5%); physically, this means the pressure of the pump was reduce 5% at this point of the cycle in the presence of one worn piston with 60 microns radial clearance. The time between the peaks was 0.034 seconds, which reflected the period of one revolution.

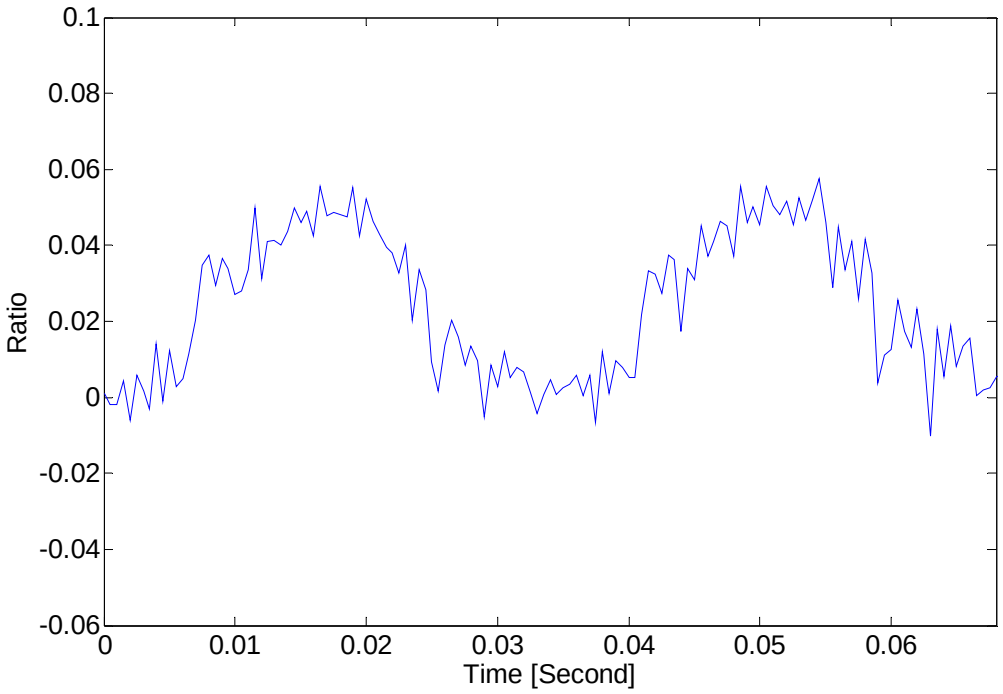

Figure 5.22 Normalized data of a pump with a real fault (60 microns) with respect to the normal pump

Consider now, the artificial faulty pump pressure ripple. The non-normalized form of the data is shown in Figure 5.23 and the normalized representation in Figure 5.24. Comparing Figure 5.23 to 5.21, it is observed that the artificial faulty pump also had a concave form in each cycle. In Figure 5.23, the normalized data show the same shape as in Figure 5.21. Further it can be seen that the peak normalized pressure is also 0.05 (5%), with a period of 0.034 seconds.

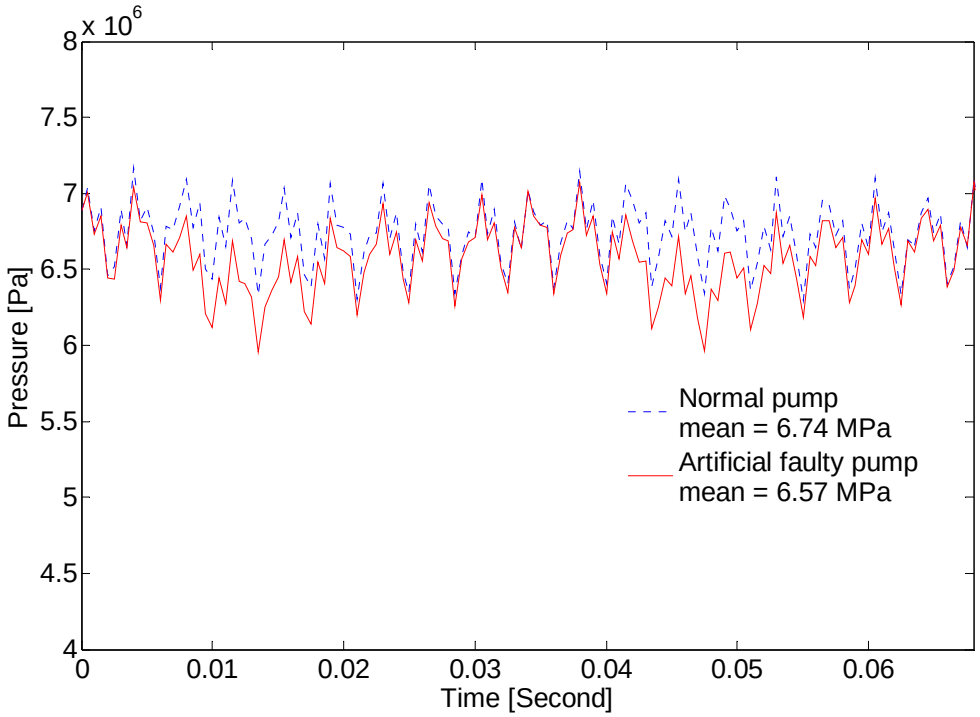

Figure 5.23 Comparison of the artificial faulty pressure and the normal pressure waveforms (experimental)

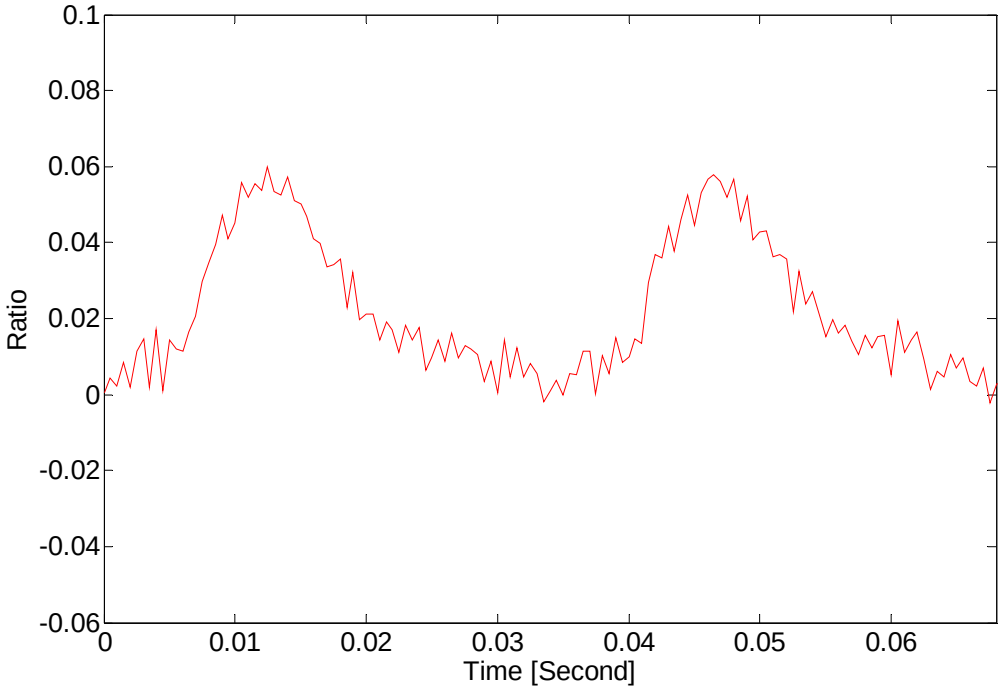

Figure 5.24 Normalized pressure data of artificial faulty pump

The pressure ripples of the actual and simulated faulty pumps are superimposed in Figure 5.25. The agreement appears to be very close. To provide a better comparison, the normalized pressure data is plotted in Figure 5.26.

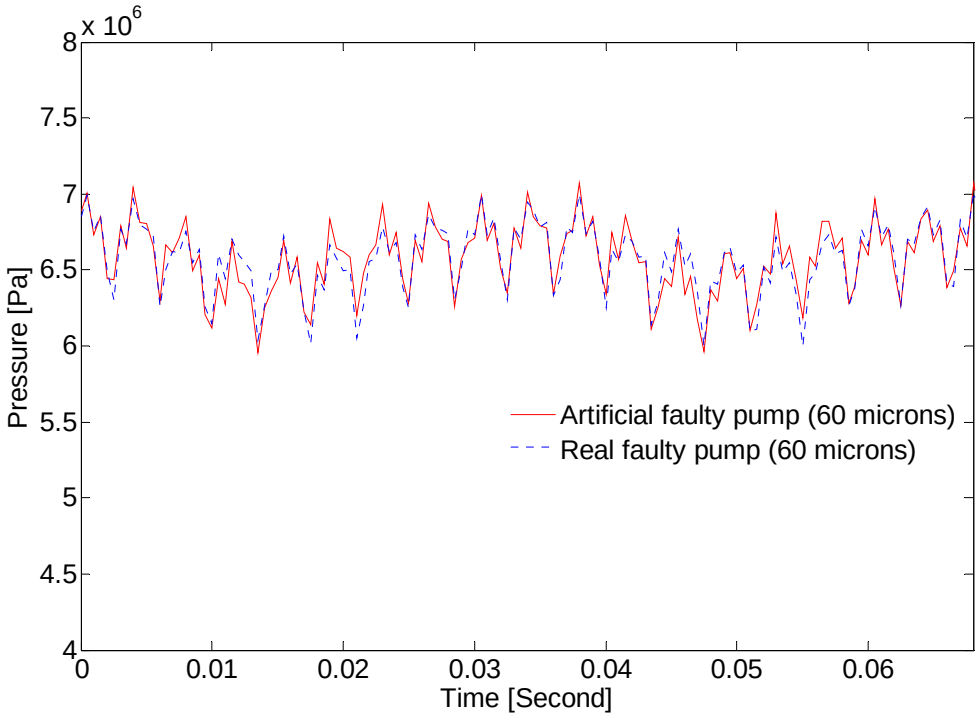

Figure 5.25 Comparison of pressure ripple between normal pump and faulty pump pressure waveforms (experimental)

Consider Figure 5.26; the actual shape of the two normalized curves, although very similar, did display some differences which need to be explained. It is observed that the slope of the artificial faulty pressure waveform was sharper than that of the real faulty pressure waveform. As mentioned in Chapter 4, the reason for this is that the pressure control servo valve required some time to close due to the limitation of the pressure control servo valve, which was much longer than the period of the time to open this valve. This characteristic was illustrated in Figure 4.6 of Chapter 4. The most important characteristic of the concave dip waveform was the synchronization of the point where the piston encountered and left the high pressure port in both the simulated and physical systems. Thus the input waveform had to be skewed slightly to ensure that the valve did indeed, completely close at the correct point. This precluded the use of classical closed

loop feedback. Indeed, as discussed earlier, the point at which the valve had to be closed was adjusted by trial and error until the opening and closing times were approximately reproduced. Thus, the artificial faulty pressure waveform could not be reproduced exactly as the desired waveform. However, the traces do indicate that the two pressure ripples demonstrate similar trends in shape and magnitude which then implies that the artificial faulty pump displays similar characteristics to the actual faulty pump for these conditions.

It should be noted that a nonlinear closed loop controller might be designed to achieve all three desired traits (waveform shape, magnitude and timing) but the design of such as controller was considered to be beyond the scope of this particular study.

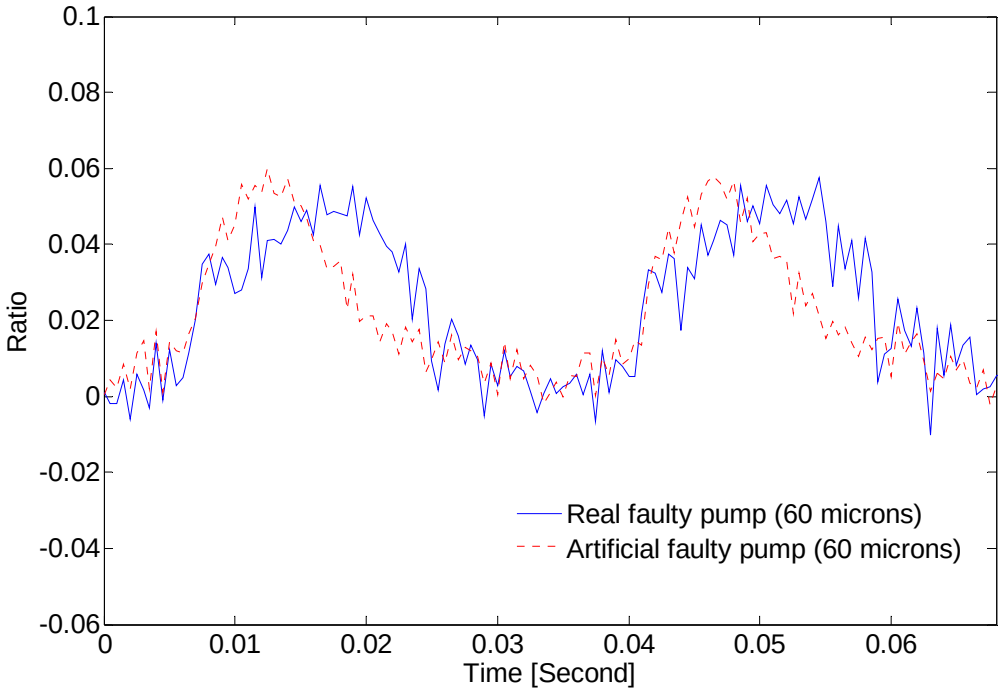

Figure 5.26 Comparison of normalization data of real fault and artificial fault pressure (60 microns)

It was of interest to observe how well smaller leakage conditions could be simulated by the fault simulator. A 30 microns worn piston was introduced into the pump. In Figure 5.27, the comparison of the pressure ripple waveform from the normal pump and that with a 30 microns clearance faulty piston is presented. The normalized data are presented in Figure 5.28. From Figure 5.27, it is apparent that in each cycle,

there is one concave dip in the waveform. It can also be observed that the amount of the concave dip for the 30 microns clearance fault was much less than that for 60 microns clearance fault. The mean value for the former was 6.77 MPa, and 6.65 MPa for the latter).

It is important to mention again that during the experiments using the 30 and 60 micron worn pistons, the amplitude of the input signal to the servo valve was adjusted to ensure that the magnitude of the pressure waveform for the fault simulator was the same as that using 30 micron and 60 micron faulty pumps.

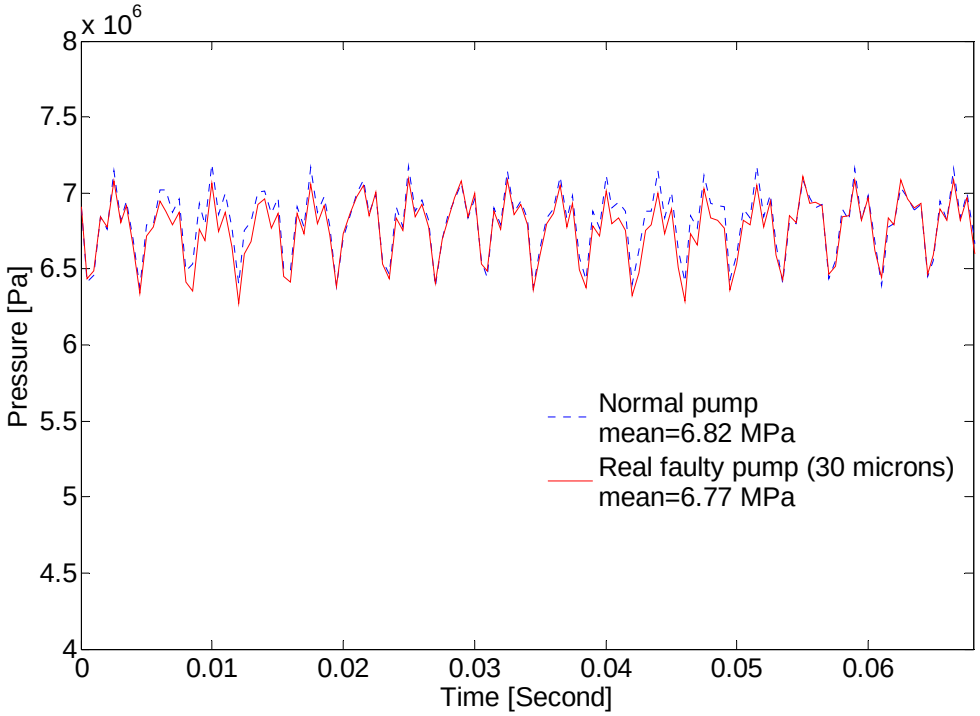

Figure 5.27 Pressure ripple waveform comparison of a normal and real faulty pump (30 microns) (experimental)

From Figure 5.28, it is observed that the magnitude of the peak was approximately, 0.02, which is much less than 0.05, the normalized data for the 60 microns faulty pump. In order to facilitate the comparison of the normalized data, the best line (red dot line) for this normalized data is shown in Figure 5.28.

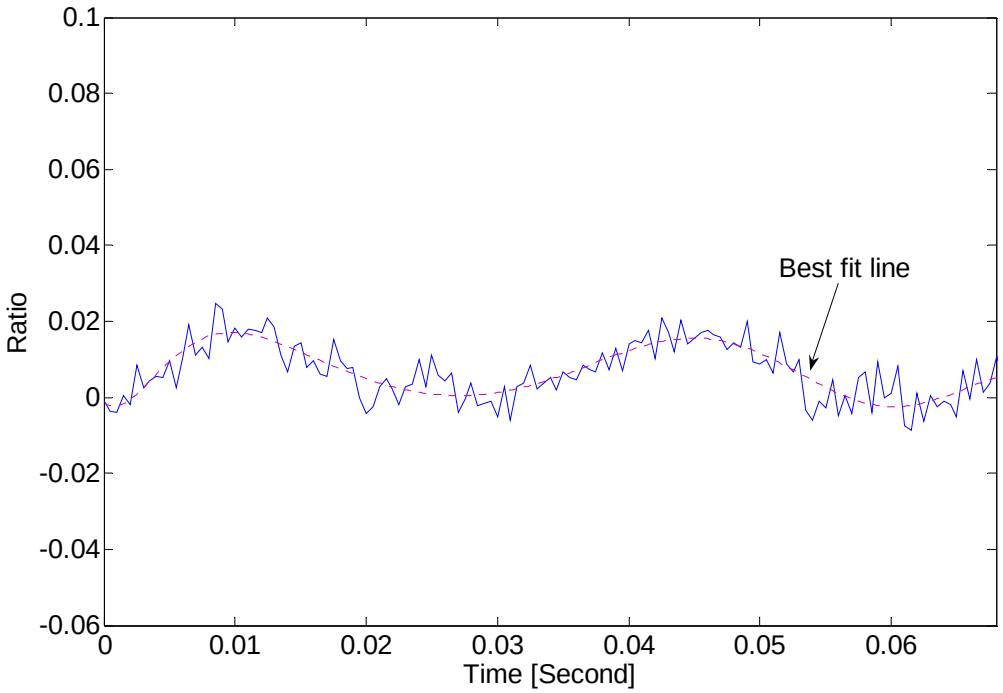

Figure 5.28 Normalized data of the real faulty pump (30 microns)

The artificial fault pressure ripple is shown in Figure 5.29 with the normalized data presented in Figure 5.30. As in Figure 5.27, the concave dip in Figure 5.29 is again apparent and as would be expected, is smaller than that of the 60 micron case. It is observed that the best line in Figure 5.30 is very similar to the best line in Figure 5.28.

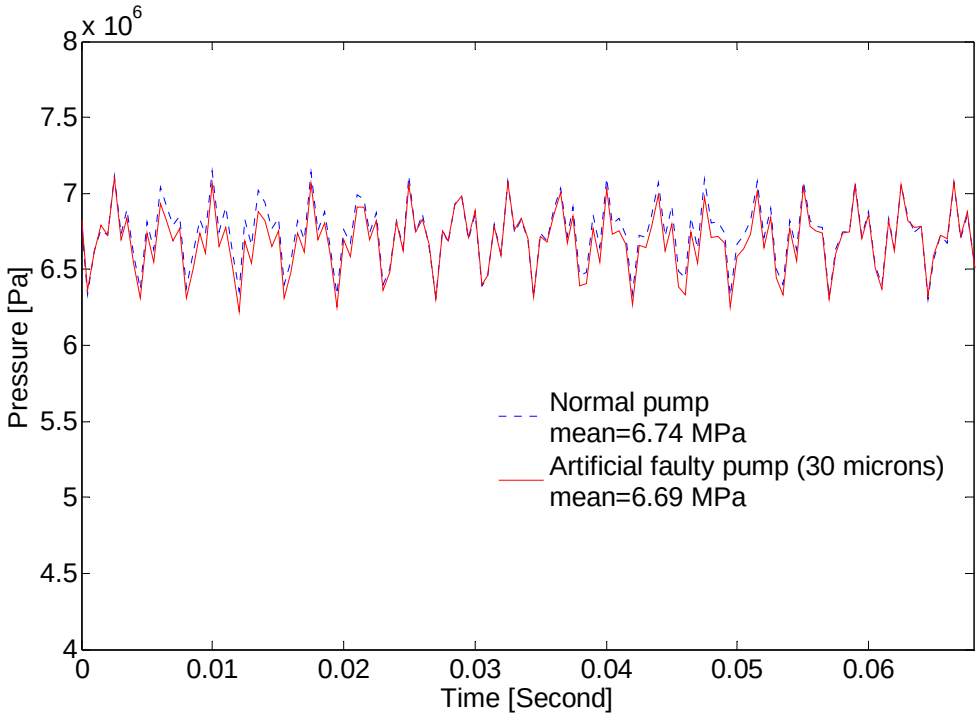

Figure 5.29 Pressure comparison of a normal and artificial faulty pump (30microns)

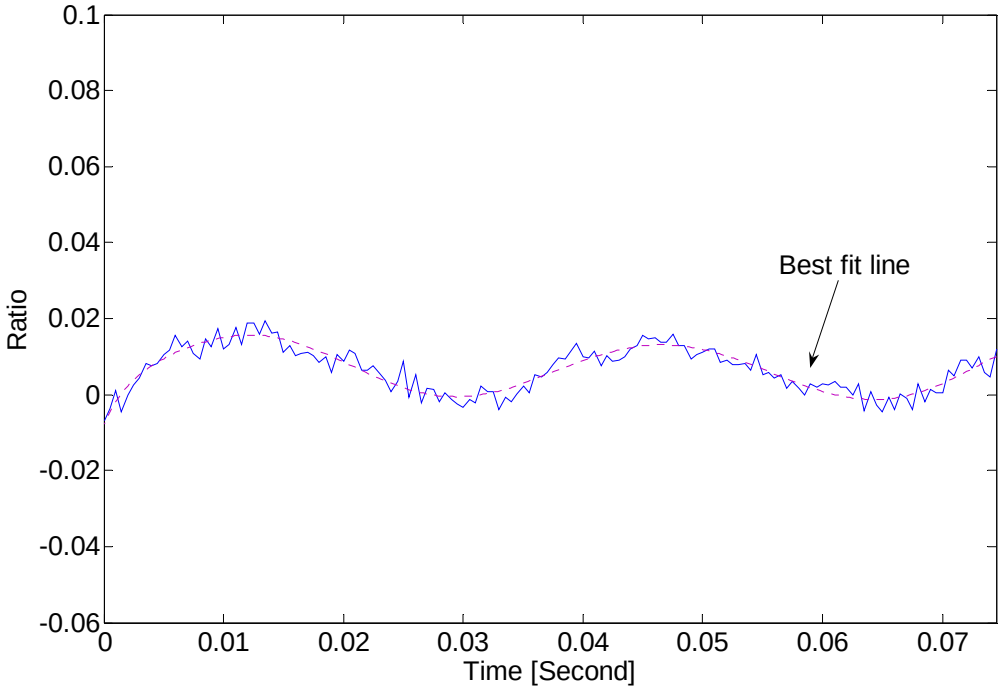

Figure 5.30 Normalized data of artificial faulty pump (30 microns)

A direct comparison of the normalization data for both the real faulty pump and artificial faulty pump is shown in Figure 5.31. These two traces display the same trends and peak values and are very close to each other for the full cycle. It is noticed that the real faulty pump has more "noise" in its trace than that found in the artificial faulty pressure trace. The asymmetric waveform for the artificial fault due to the different opening and closing times of the servo valve is also evident in the figure.

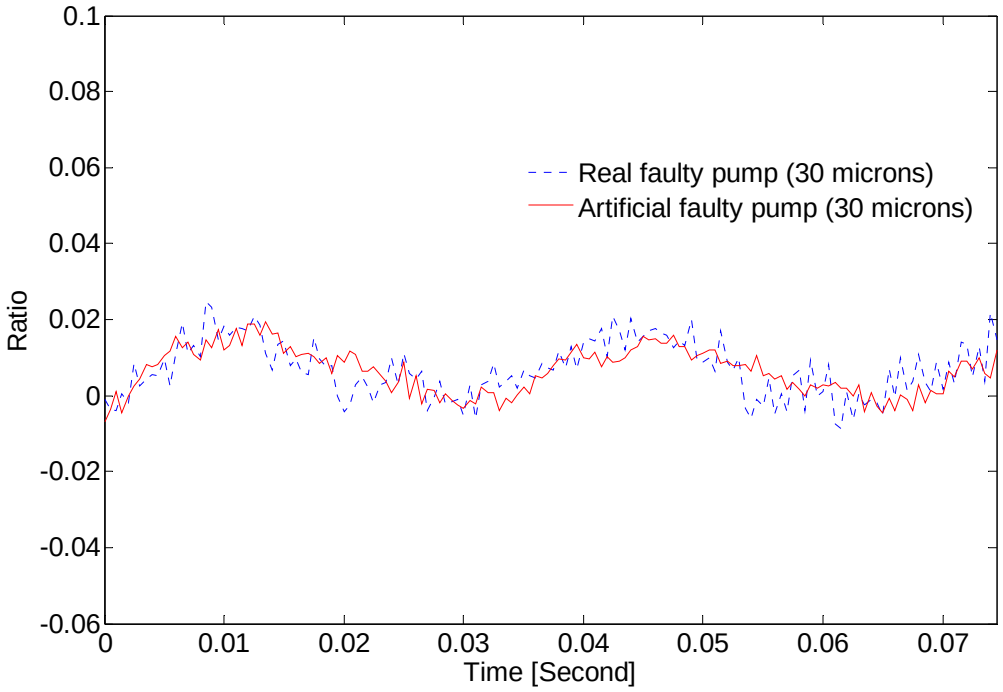

Figure 5.31 Comparison of the normalized data of the real faulty and the artificial faulty pump pressure waveform (30 microns)

A visual comparison of the real faulty pressure ripple waveform with the 30 microns worn piston and the artificial faulty pressure ripple is illustrated in Figure 5.32. It is noticed that two traces matched exceptionally well.

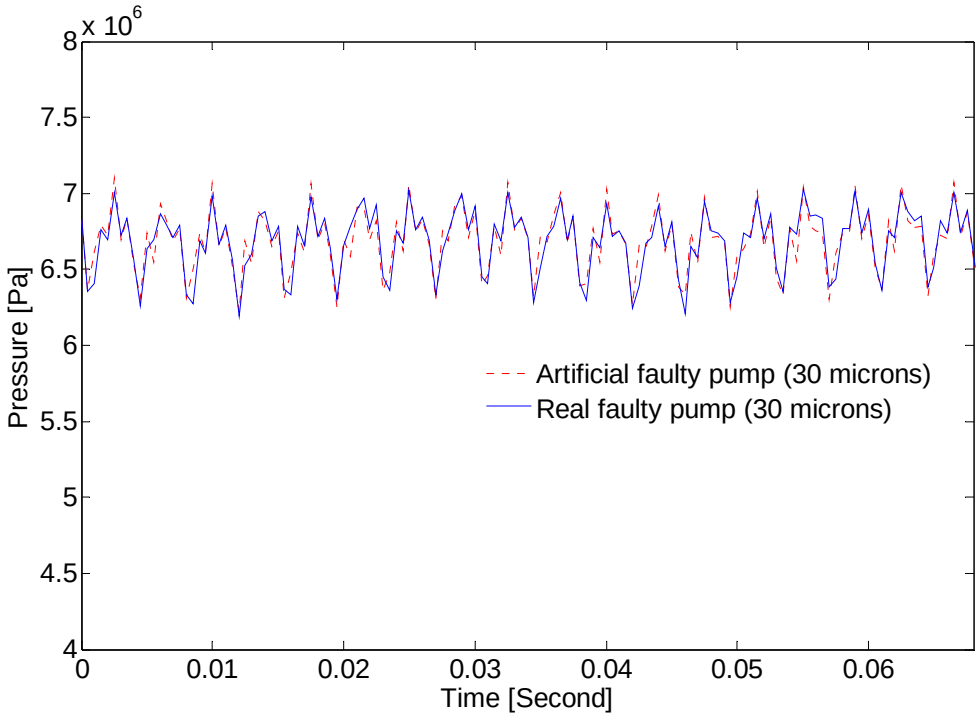

Figure 5.32 Comparison of real faulty and artificial faulty pump pressure waveforms (30 microns) (experimental)

5.6 Variable artificial leakage summary

Table 5.2 summarizes the artificial faulty data with inputs to the pressure control servo valve. From the table, it is apparent that different calibrated (magnitude and timing) inputs to the pressure control servo valve can produced different flows to simulate different leakage conditions. In addition, by comparing Table 5.2 with Table 5.3 (real fault pump data), it can be observed that the artificial faulty pressure waveform characteristics were very similar to those of the pump with the real fault. Both of them had the same ratio of normalization data, and a period of 0.034 seconds.

Table 5.2 Artificial faulty pump data

Artificial leakage	Simulation piston wear(radial clearance, micron)	Normalization data ratio (peak value)	Mean (pressure ripple) MPa
No artificial leakage	0	0um	6.74
Artificial leakage	30	0.02	6.69
Artificial leakage	60	0.05	6.57

Table 5.3 Real faulty pump data

Piston worn (radial clearance) (micron)	Normalization data ratio	Mean (pressure ripple) (MPa)
0	0	6.82
30	0.02	6.77
60	0.05	6.65

Although not presented in this report, it is anticipated that the fault simulator could readily accommodate different inputs to the pressure control servo valve to introduce different leakage values into to the pump to simulate more than one worn pistons.

5.7 Summary

In this chapter, the experimental results which demonstrate the pressure ripple waveform for a normal pump, a pump with a “physical” faulty piston and a pump with a simulated or artificial faulty piston were presented. Explanations of, and discussions about, the results were presented. In next chapter, some conclusions and suggestions for future work are forwarded.

Chapter 6 Conclusions and Future work

In this chapter, conclusions will be drawn and some future work will be recommended.

6.1 Introduction

The research objectives of this project, defined in Chapter 1 are repeated as follows:

1. To understand in detail the cause and effect of piston wear on piston leakage and, subsequently, the output performance of the pump.

2. To develop methodologies for introducing artificial wear via leakage into the pump in accordance with Objective 1 and to determine its feasibility through simulation.

3. To implement the above methodologies in order to determine their success in artificially simulating wear in pistons in a variable displacement axial piston pump.

The following section related the outcomes of this research with respect to these specific objectives.

6.2 Summary and conclusions

6.2.1 Faults in an axial piston pump, piston wear and its effect on pump performance

In Chapter 2, the operation of an axial piston pump was presented. An understanding of the operation of the axial piston pump was necessary in order to identify factors that may hinder its performance. In section 2.3, a table was listed which contained all main faults and their possible effects on an axial piston pump. In section 2.4, the change in the pump's output performance due to piston wear was addressed. Increasing piston wear would affect the overall efficiency of the hydraulic systems, and would have an effect on the pump output pressure and flow waveforms.

In order to establish what the output performance would be from a pump with a worn piston, a simplified model of the axial piston pump was developed in Chapter 3.

The simulated waveforms of the pump pressure and flow allowed visual observations of how wear in one piston would affect the shape of the waveforms. It was ascertained at this time that pressure ripple would be the variable to be observed due to the physical difficulty in actually measuring flow ripple at very small magnitudes. The pressure ripple waveform showed a concave dip with respect to the normal pump pressure ripple waveform for half of the cycle. The greater the piston wear, the larger was the magnitude of the concave dip. This simulation study and the methodology introduced in Chapters 2 and 3 were therefore believed to have met the first two objectives.

6.2.2 Methodology to introduce leakage

A methodology to introduce an artificial leakage into pump was introduced in Chapter 4. The pressure control servo valve with high response frequency was used to create a leakage path to artificially introduce leakage in the pump. The data acquisition system was described in this Chapter. The collected data showed good repeatability from experimental test to test. Because oil temperature and system pressure had significant influence on leakage, these two were held approximately constant throughout all comparative tests.

6.2.3 Experimental results

The results from experiments on the pump with the artificial fault and the pump with no fault were presented in Chapter 5. The pressure ripple waveform and the ratio of normalization data were compared. A comparison of these two characteristics for the pump with the real fault and one with the artificial fault showed very good correlation. Power spectral density was used to analyze the pressure ripple from the pump with a real fault and the pump with the artificial fault and the interpreted results substantiated the excellent correlation found from the waveform results.

6.2.4 Research conclusions

From the experimental and simulation results, some main conclusions can be drawn as follows:

- Piston wear affects the pump output flow and output pressure waveforms statically and dynamically.
- Based on a comparison of the pump with a real worn piston and the pump with an artificial fault, the excellent correlation would indicate that the use of a pressure control servo valve in an open loop configuration with a calibrated input signal (magnitude and timing) can be used to introduce artificial leakage in order to simulate the effects of piston wear in a pump.
- The test system and fault simulator so proposed can be used in studies to test various algorithms for condition monitoring schemes.

6.3 Recommendations for future work

Some future considerations that should be investigated are:

- The test should be repeated at several swash plate angles to test the ability of the system to create artificial faults under a wider range of operating conditions, in particular lower pressure conditions.
- A closed loop controller needs to be designed to eliminate the need to manually match (calibrate) the output pressure ripple to that of the actual faulty pump ripple.
- The leakage rates (based on 30 – 60 micron clearances) were quite large. It is necessary to refine the approach to be able to simulate very small leakage rates. The challenge here is to be able to actually measure the small rates to provide verification.
- A more accurate model of piston leakage should be considered to assist in the design of the input to the servo valve
- The system should be used to provide data for various condition monitoring approaches.

References:

1. Hindman, J., “Condition Monitoring of Valves and Actuators in a Mobile Hydraulic System Using an Artificial Neural Network and Expert Data”, M. Sc. Thesis University of Saskatchewan, 2002.
2. Hibberd, D. “Pump Efficiency Monitoring in the Steel Industry”, Steel Times, 216(9), 1988.
3. Sommer, Holger T. “Machine Condition Monitoring: Definition of an Oil Condition Index”, Proceedings of National Conference of Fluid Power, 2002, pp. 19-23.
4. Stecki, J. and Schoenau, G. “Application of Simulation and Knowledge Processing in Contamination Control”, SAE Transactions, Journal of Commercial Vehicle, 2000
5. Cao, H. “Parameter Estimation Using Extended Kalman Filter for the Swash Plate Assembly and the Control Piston in a Load Sensing Pump”, University of Saskatchewan, M.Sc. Thesis, 2001.
6. Ramden, T. “On Condition Monitoring of Fluid Power Pumps and Systems”, Ph.D.Thesis No. 474, Linkoping Studies in Science and Technology, Linkoping, Sweden, 1995.
7. Tan, A.C.H., Chua, P.S.K. and Lim, G.H. “Condition Monitoring of a Water Hydraulic Cylinder by Vibration Analysis”, Journal of Testing and Evaluation, Vol. 28, 2000, pp. 507-512.
8. Neill,G.D, Reuben, R.L., Sandford,P.M, Brown,E.R. and Steel, J. A. “Detection of Incipient Cavitation in Pumps Using Acoustic Emission”, Proceedings of Institution Mechanical Engineers Vol. 211, Part E, 1997, pp. 267-277.
9. Angeli, C. “An Online Expert System for Fault Diagnosis in Hydraulic Systems”, Expert Systems, Vol. 16 No. 2, May 1999, pp. 115-120.
10. Weddfelt, K. and Palmberg, I. “Condition Monitoring of Fluid Power Systems by a Thermodynamic Measurement Method”, On Modeling, Simulation and Measurements of Fluid Power Pumps and Pipelines, Linkoping Studies in Science and Technology Dissertations No. 268, Linkoping University, 1992, pp. 61-75.
11. Khoshzanban-Zavarehi, M. “On-line Condition Monitoring and Fault Diagnosis in Hydraulic System Pattern Classification”, University of British Columbia, Ph.D. Thesis, 1997.

12. Seifert, T.D., and Steele, J.P.H. “Fuzzy Logic Processing and Dynamic Alarm Handling for Real-Time Machine Health Monitoring”, Artificial Neural Networks in Engineering Conference, 1996, pp. 231-236.
13. Le, T. and Watton, J. “An Artificial Neural Network Based Approach to Fault Diagnosis and Classification of Fluid Power Systems”, Proceedings Institution Mechanical Engineers Vol. 211, Part I, 1997, pp. 307-317.
14. Crowther, W. and Edge, K. “Fault Diagnosis of a Hydraulic Actuator Circuit Using Neural Network-an Output Vector Space Classification Approach”, Proceedings Institution Mechanical Engineers Vol. 212, Part I, 1998, pp. 57-69.
15. Mourre, D. and Burton, R. “Investigation of a Neural Network/Statistical Condition Monitoring Technique for a Proportional Solenoid Valve”, Bath Workshop on Power Transmission and Motion Control (PTMC 2001), University of Bath, 2001, pp. 119-134.
16. Lu, F.X., Burton, R.T. and Schoenau, G. “Feasibility Study on the Use of a Neural Network to Detect and Locate Excess Piston Wear in an Axial Piston Pump”, Innovations in Fluid Power, 7th Bath International Fluid Power Workshop, University of Bath, 1994, pp. 25-40.
17. Pollmeier, K., Burrows, C.R., and Edge, K.A. “Condition Monitoring of an Electro-hydraulic Position Control System Using Artificial Neural Networks”, Proceedings of ASME IMECE04, Anaheim, California, USA, Nov. 13-20, 2004.
18. PAN, Ming-qing, ZHOU, Xiao-jun, LEI, Liang-yu “Machine Fault Diagnosis Using KPCA and SVM”, Proceedings of the Sixth International Conference on Fluid Power Transmission and Control ICFP 2005, Hangzhou, China, 2005, pp. 621-624.
19. Bhojkar, A., Burton, R., Schoenau, G. and Bitner, D. “Development of a Fault Simulator for Proportional Spool Valve”, 1st International Conference on Computational Method in Fluid Power Technology, Melbourne Australia, 2003 (from CD version, ISBN o-9578574-2-x).
20. Yates, M.A. “Thermodynamically Based Pump Performance Monitoring”, Proceedings of 11th International Pump Technical Conference, 1989, pp. 259-272.
21. Luo, M. and Smith, M. “Diagnosis of Rolling-Element Bearing Faults Using Demodulation Analysis”, Proceedings of COMADEM’96, Condition Monitoring and

Diagnostic Engineering Management, 1996, pp. 549-558.

22. Wang, L., Hope, A.D. and Sadek, H., "Fault Diagnosis Using Artificial Neural Networks for Waste Water Pump Bearings", Proceedings of International Conference on Condition Monitoring, 2001, pp. 291-299.
23. Domotor,F. and Tepro,G. "Early Detection of Rolling Bearing Defects in a Hot Water Circulating Pump by Vibration Analysis at Budapest-Ferihegy Airport", Condition Monitoring and Diagnostic Engineering Management, 1996, pp. 403-409.
24. Ding, G. and Hu, D. "Monitoring and Diagnosis of Typical Faults of Hydraulic Systems", Condition Monitoring'87, 1987, pp. 593-603.
25. Ukrainetz, P.R., Nikiforuk, P.N. and Bitner, D.V. "Wear of an Axial Piston Pump Under High Temperature and High Pressure Conditions", Proceedings of the 42nd National Conference on Fluid Power, 1987, pp. 9-13.
26. Ukrainetz, P.R., Nikiforuk, P.N. and Bitner, D.V. "The Effect of Elevated Fluid Temperature and Constant Loading Conditions on the Wear of an Axial Piston Pump", Proceedings of the 43rd National Conference on Fluid Power, 1988, pp. 209-216.
27. Hunt, T.M. "Condition Monitoring of British Coal High Pressure Water Pumps", Condition Monitoring' 87, 1987, pp. 910-918.
28. Chen, Dongning and Jiang, Wanlu "Application of Wavelet Analysis and Fractal Geometry for Fault Diagnosis of Hydraulic Pump", Proceedings of the Sixth International Conference on Fluid Power Transmission and Control ICFP 2005, Hangzhou, China, 2005, pp. 628-631.
29. Ivantysyn, J and Ivantysynova, M "Hydrostatic Pumps and Motors", Akademia Books International Publishers & Distributor, New Delhi, India, 2001.
30. Atkinson, R.H. "Noise Reduction in Vane and Piston Pumps", Proceedings of National Conference on Fluid Power, 1983, pp. 318-324.
31. Ivantysynova, M. "Prediction of Pump and Motor Performance by Computer Simulation", 1st International Conference on Computational Method in Fluid Power Technology, Mel borne, Australia, November, 2003.
32. Cui, P. "The Development of a High Speed Digital On-Off Valve", Master's Thesis, University of Saskatchewan, 1992.

33. Ruan, J., Ukrainetz, P. and Burton, R., “Frequency Domain Modeling and Identification of 2D Digital Servo Valve”, International Journal of Fluid Power, 2001.
34. Moog Series 15 Pressure control servo valves, Catalogue 150 1178, Moog Inc. East Aurora, New York, 1988.
35. Merritt, H., “Hydraulic Control Systems”, John Wiley & Sons, Inc. New York.
36. RAMAPO Installation and Operations Manual, Hersey Measurement Company, 1988
37. Martin, M., “Load Simulator Using Hydraulics”, M. Sc. Thesis, University of Saskatchewan, 1992.
38. http://www.eas.asu.edu/~mining03/chap2/lesson_2_1.html.

Appendix A

Reynolds Number for Piston Leakage Fluid

An assumption was made that the fluid used in this study was Esso Nuto H68 at 40 Celsius degrees. Consider the flow between cylinder block and piston, shown in Figure A.1.

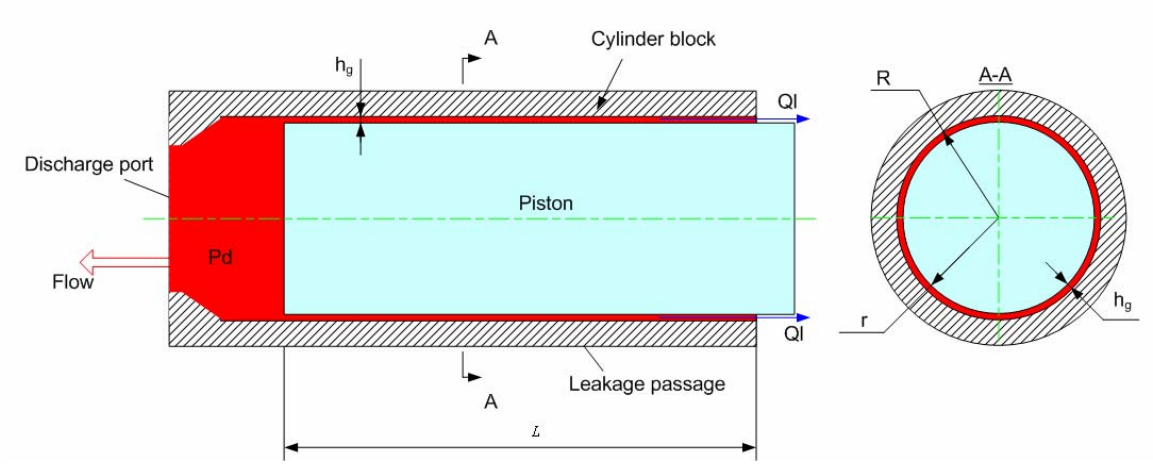

Figure A.1 The schematic for piston leakage

The radius of the cylinder block R was 5.162 mm and the radius of the piston was 5.154 mm. The hydraulic diameter of this annulus was:

$$D_h = \frac{4Area}{perimeter} = \frac{4\pi(R^2 - r^2)}{2\pi(R + r)} \tag{A.1}$$

Substituting R = 5.162 mm and r = 5.154 mm into Equation A.1, then get

D_h =1.600*10^{-5} [m]

Assuming laminar flow, the pressure drop ΔP is given by

$$\Delta P = \frac{32\mu L\ v}{D_h^{\ 2}} \tag{A.2}$$

where μ = Absolute viscosity, 5.855*10^{-2} [Pa.s]

L = Length of leakage passage 0.0229 [m]

v = Fluid velocity [m/s]

D_h = Hydraulic diameter of leakage passage $1.600*10^{-5}$ [m]

For a pressure drop of ΔP =21 MPa, the maximum for this pump, Equation A.2 can be solved to get a fluid velocity

ν =0.1253 [m/s]

The Reynolds number of this flow is

$$\mathrm{Re} = \frac{\rho \nu D_h}{\mu} \qquad \text{(A.3)}$$

where ρ = Density, 861 [kg/m^3]

ν = Velocity, 0.1253 [m/s]

D_h = Hydraulic diameter of leakage passage $1.600*10^{-5}$ [m]

μ = Absolute viscosity, $5.855*10^{-2}$ [N.sec/m^2]

From these values,

Re=0.0295,

which is rounded off to

Re=0.030.

The Reynolds number 0.030 for this fluid is much less 2000 which is the lowest Reynolds number for turbulent flow; clearly, this leakage fluid was laminar as assumed.

Appendix B Derivation of Equations

B.1 Derivation of the Equation for Total Pump "Kinematical" Flow

In order to derive the total "kinematical" flow equation for the pump, an orthogonal coordinates system was employed, as shown in Figure B.1.The barrel was assumed to be driven by a prime mover (electrical motor) at a constant angular velocity ω and the pistons executed a compounded movement, made up of two motions: one linear movement (piston stroke) in the direction of the Z- axis and one rotation motion around the Z-axis.

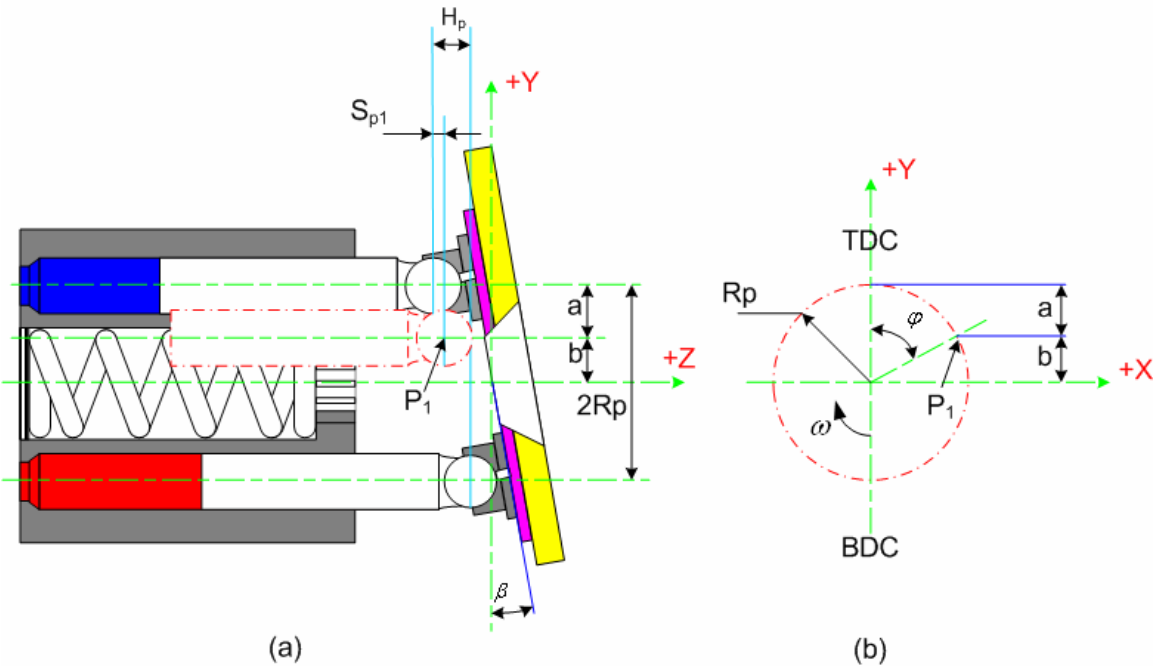

Figure B.1 Scheme of axial piston pump for derivation of the flow equation

When the piston is at Top Dead Center (TDC), the piston has zero displacement. The TDC is as the initial position for this derivation. Consider Figure B.1 a. For the "red piston P_1" the displacement S_{p1} is given by

$$S_{p1} = a \tan \beta \tag{B.1}$$

From Figure A.1.b, it follows that

$$b = R_p \cos \varphi \tag{B.2}$$

and

$$a = R_p - b \tag{B.3}$$

Substituting Equation B.2 in Equation B.3, yields

$$a = R_p(1-\cos\varphi) \tag{B.4}$$

and Equation B.4 into Equation B.1

$$S_{p_1} = R_p \tan\beta(1-\cos\varphi) \tag{B.5}$$

Equation B.5 for the piston displacement S_{p1} is dependent upon the piston angular position φ and the angle of the swash plate β. The relative velocity of the piston in the Z axis direction is

$$v_p = \frac{dS_{p1}}{dt} = \frac{dS_{p1}}{d\varphi}\cdot\frac{d\varphi}{dt} = \frac{dS_{p1}}{d\varphi}\cdot\omega \tag{B.6}$$

Therefore, the flow for this piston is

$$Q_{p1} = v_p \cdot \frac{\pi d^2}{4} = \omega \cdot \frac{\pi d^2}{4}\cdot\frac{dS_{p1}}{d\varphi} \tag{B.7}$$

By substituting Equation B.5 into Equation B.7, the flow from piston P_1 is

$$Q_{p1} = \omega\frac{\pi d^2 R_p}{4}\tan\beta\cdot\sin\varphi \tag{B.8}$$

Because the barrel rotates at a constant angular velocity ω, the piston angular position φ can be represented as

$$\varphi = \omega\cdot t \tag{B.9}$$

Substituting Equation B.9 into Equation B.8, then yields

$$Q_{p1} = \omega\frac{\pi d^2 R_p}{4}\tan\beta\cdot\sin(\omega\cdot t) \tag{B.10}$$

The flows from the other pistons are delayed because of their location on the swash plate. The phase delay α between the nearest two pistons is given by

$$\alpha = \frac{2\pi}{m} \tag{B.11}$$

Therefore, the flow for the second piston which is nearest (and follows) piston P_1 is:

$$Q_{p1} = \omega\frac{\pi d^2 R_p}{4}\tan\beta\cdot\sin(\omega\cdot t-\alpha) \tag{B.12}$$

For the third piston the flow is

$$Q_{p1} = \omega \frac{\pi d^2 R_p}{4} \tan\beta \cdot \sin(\omega \cdot t - 2\alpha) \quad \text{(B.13)}$$

…….

and for the “mth” piston is

$$Q_{p1} = \omega \frac{\pi d^2 R_p}{4} \tan\beta \cdot \sin(\omega \cdot t - (m-1)\alpha) \quad \text{(B.14)}$$

The total flow of the pump, kinematically, is the sum of all flows from all the piston, that is,

$$Q_k = \omega \frac{\pi d^2 R_p}{4} \tan \beta \sum_{k=0}^{m-1} \sin(\omega t - k\alpha) \quad \text{(B.15)}$$

where: Q_k = Total kinematical pump flow [m^3/s]

ω = Angular velocity of drive shaft [rad/s]

d = Diameter of piston [m]

R_p = Piston pitch radius on barrel [m]

β = Angle of swash plate [rad]

m = Number of piston

t = Time [sec]

k = 0, 1, 2, 3….. m-1

α = Phase delay [rad], equal to $2\pi / m$

B.2 Derivation of the Equation for Pump Output Pressure

In order to facilitate the derivation, the pump is assumed to discharge into a simply loaded system as shown in Figure B.2. In this circuit, a needle valve was used to simulate the hydraulic load.

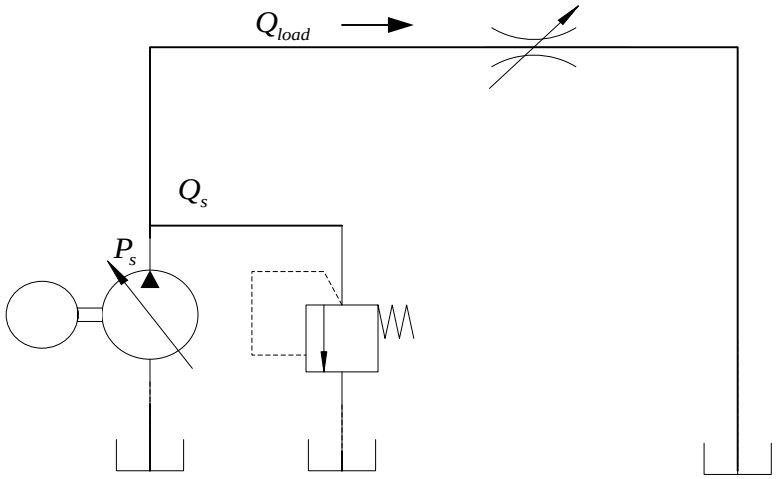

Figure B.2 Scheme for simple hydraulic circuit

In order to facilitate the derivation, the parameters used in this model are defined in Figure B.3 and B.4. Once a piston connects the pump discharge chamber, the piston starts to "push" the flow into the discharge chamber. In Figure B.3, the flow from one piston (for example P_1 piston) chamber to the discharge chamber can be expressed as [29]

$$Q_{p1} = C_{d1} A_{d1} \sqrt{\frac{2|P_{p1} - P_s|}{\rho}} \operatorname{sgn}(P_{p1} - P_s) \tag{B.16}$$

and the flow from piston P_n chamber to the discharge chamber

$$Q_{pn} = C_{d1} A_{dn} \sqrt{\frac{2|P_{pn} - P_s|}{\rho}} \operatorname{sgn}(P_{pn} - P_s) \tag{B.17}$$

where: Q_{p1} = Flow from P_1 piston chamber to discharge chamber [m^3/s]

Q_{pn} = Flow from P_n piston chamber to discharge chamber [m^3/s]

C_{d1} = Flow discharge coefficient of the discharge area for piston port opening to discharge chamber [29]

A_{d1} = The discharge area for P_1 piston port opening to the discharge chamber in valve plate [m^2]

A_{dn} = The discharge area for P_n piston port opening to the discharge chamber in valve plate [m^2]

ρ = Flow density [kg/m^3]

P_{p1} = Instantaneous pressure in P_1 piston chamber [Pa]

P_{pn} = Instantaneous pressure in P_n piston chamber [Pa]

P_s = Pump output pressure (discharge chamber pressure) [Pa]

Among the above parameters, the discharge areas A_{d1} and A_{dn} are a function of the piston angular position, φ, which will be explained later in this section.

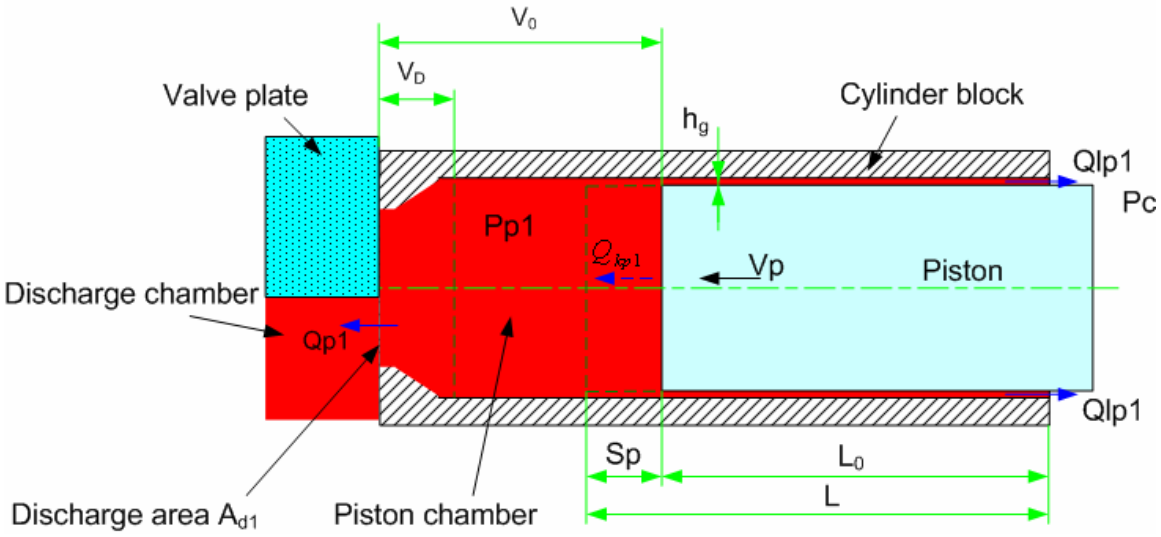

Figure B.3 Control volume for instantaneous piston flow

The sum of the flow from all the pistons to the discharge chamber is

$$Q_p = Q_{p1} + Q_{p2} + Q_{p3} + Q_{p4} + Q_{p5} + Q_{p6} + Q_{p7} + Q_{p8} + Q_{p9} \quad \text{(B.18)}$$

that is,

$$Q_p = \sum_{k=1}^{m=9} Q_{pk} \tag{B.19}$$

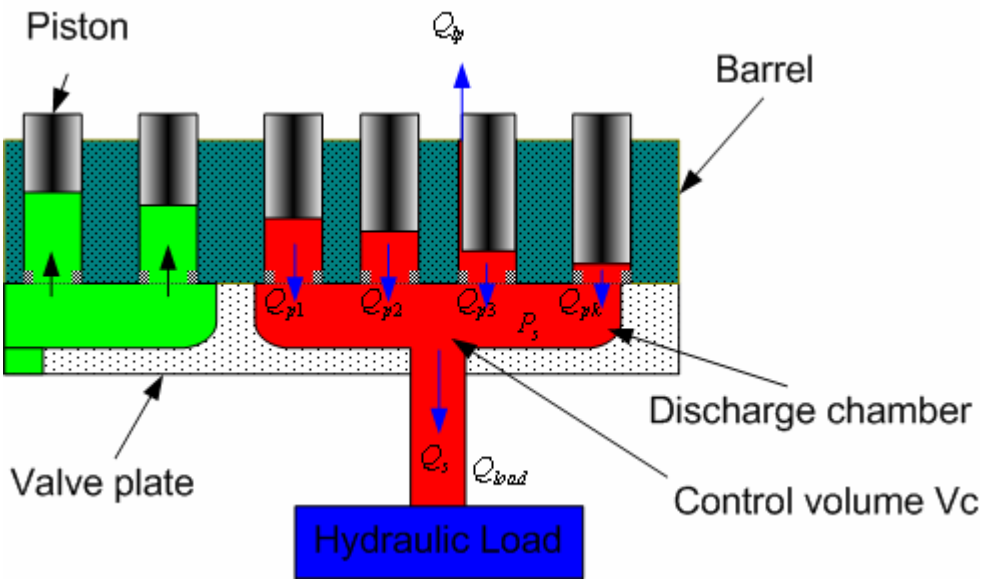

Figure B.4 Schematic for the derivation of the pump output pressure equation

In the P_1 piston chamber, the continuity equation can be given as

$$\dot{P}_{p1} = \frac{B}{V_0 - A_p S_{p1}} (Q_{kp1} - Q_{p1} - Q_{lp1}) \tag{B.20}$$

and for the P_n piston chamber

$$\dot{P}_{pn} = \frac{B}{V_0 - A_p S_{pn}} (Q_{kpn} - Q_{pn} - Q_{lpn}) \tag{B.21}$$

where: P_{p1} = Instantaneous pressure in P_1 piston chamber [Pa]

P_{pn} = Instantaneous pressure in P_n piston chamber [Pa]

B = Bulk modulus [Pa]

V_0 = Piston initial volume [m^3]

A_p = Piston area [m^2]

S_{p1} = Stroke for P_1 piston [m]

S_{pn} = Stroke for P_n piston [m]

Q_{kp1} = Kinematical flow delivered P_1 piston [m^3/s]

Q_{kpn} = Kinematical flow delivered P_n piston [m^3/s]

Q_{p1} = Flow from P_1 piston chamber to discharge chamber [m^3/s]

Q_{pn} = Flow from P_n piston chamber to discharge chamber [m^3/s]

Q_{lp1} = Internal leakage from P_1 piston to case chamber [m^3/s]

Q_{lpn} = Internal leakage from P_n piston to case chamber [m^3/s].

In the discharge chamber, the continuity equation follows

$$\dot{P}_s = \frac{B}{Vc}(Q_p - Q_s) \tag{B.22}$$

where: P_s = Pump output pressure (discharge chamber pressure) [Pa]

B = Bulk modulus [Pa]

V_c = Discharge chamber control volume [m^3]

Q_p = Flow from piston chamber to discharge chamber [m^3/s]

Q_s = Pump output flow [m^3/s].

In this specific system, the pump output flow Q_s is equal to the load flow Q_{load}, that is,

$$Q_s = Q_{load} = C_{d2}.A_v\sqrt{\frac{2P_s}{\rho}} \tag{B.23}$$

where: Q_s = Pump output flow [m^3/s]

Q_{load} = Load flow [m^3/s]

C_{d2} = Discharge coefficient of needle valve orifice

A_v = Discharge orifice area of the needle valve [m^2]

P_s = Pump output pressure (discharge chamber pressure) [Pa]

In addition, there are several equations which are required to complete the model. The internal leakage Q_{lp1} from the P_1 piston chamber to case drain chamber is given as:

$$Q_{lp1} = \frac{\pi r h_g^{\ 3}}{6\mu L_{p1}}(P_{p1} - P_c) \tag{B.24}$$

and the internal leakage Q_{lpn} for P_n piston:

$$Q_{lpn} = \frac{\pi r h_g^{\ 3}}{6\mu L_{pn}}(P_{pn} - P_c) \tag{B.25}$$

where: Q_{lp1} = Internal leakage from P_1 piston to case chamber [m^3/s]

Q_{lpn} = Internal leakage from P_n piston to case chamber [m^3/s]

r = Radius of piston [m]

h_g = Gap (radial clearance) between piston and cylinder bore [m]

P_p = Piston chamber pressure [Pa]

P_c = Case drain chamber pressure [Pa]

μ = Absolute fluid viscosity [N.sec/m^2]

L_{p1} = Length of leakage passage in P_1 piston chamber [m].

L_{pn} = Length of leakage passage in P_n piston chamber [m].

The length of the leakage passage L_{p1} and L_{pn} can be given as

$$L_{p1} = L_0 + S_{p1} \tag{B.26}$$

and

$$L_{pn} = L_0 + S_{pn} \tag{B.27}$$

where: L_{p1} = Length of leakage passage in P_1 piston chamber [m].

L_{pn} = Length of leakage passage in P_n piston chamber [m].

L_0 = Initial length of piston leakage passage[m]

S_{p1} = Piston stroke of P_1 piston [m]

S_{pn} = Piston stroke of P_n piston [m]

According to the derivation in Appendix B1, the piston strokes S_{p1} and S_{pn} are presented by

$$S_{p1} = R_p \tan\beta \cdot (1 - \cos(\omega t)) \tag{B.28}$$

and

$$S_{pn} = R_p \tan\beta \cdot (1 - \cos(\omega t - (n-1)\alpha)) \tag{B.29}$$

where: S_{p1} = Piston stroke[m]

S_{pn} = Stroke for P_n piston [m]

R_p = Piston pitch radius on barrel [m]

β = Angle of swash plate [rad]

ω = Angular velocity of the pump drive shaft [rad/s]

t = Time [sec].

In addition, the kinematical flows delivered by each piston are

$$Q_{kp1} = \omega \frac{\pi d^2 R_p}{4} \tan\beta \cdot \sin(\omega t) \tag{B.30}$$

and

$$Q_{kpn} = \omega \frac{\pi d^2 R_p}{4} \tan\beta \cdot \sin(\omega t - (n-1)\alpha) \tag{B.31}$$

where: Q_{kp1} = Kinematical flow delivered by P_1 piston [m^3/s]

Q_{kpn} = Kinematical flow delivered by P_n piston [m^3/s]

ω = Angular velocity of the pump drive shaft [rad/s]

d = Diameter of piston [m]

R_p = Piston pitch radius on barrel [m]

β = Angle of swash plate [rad]

t = Time [sec]

n = 1, 2, 3….. m (m = Number of piston)

α = Phase delay [rad], equal to $2\pi / m$

Furthermore, the piston initial volume V_0 is given by

$$V_0 = V_D + 2 \cdot R_p \cdot \tan\beta \tag{B.32}$$

where: V_0 = Piston initial volume [m^3]

V_D = Piston dead volume [m^3], shown in Figure B.3

R_p = Piston pitch radius on barrel [m]

β = Angle of swash plate [rad].

Finally, the discharge area A_d of the piston port opening to the discharge chamber in the valve plate is dynamic in each cycle, and is a function of the angular position of the piston φ [29]. Shown in Figure B.5, when piston port is at S1, close to TDC, the discharge area A_d is the small black triangle. The piston port continues to move in; when piston is at S2, the discharge area A_d is the area of the piston port. When the piston rotates to the S3 position, the discharge area becomes smaller than the piston port. Finally, when the piston moves out of the discharge chamber at "S4" the discharge area is zero.

The discharge area A_d is calculated as follows

1) If $-13^0 < \varphi < 9^0$, then A_d is given as:

$$A_d = \frac{(\varphi + 13)^2 * \pi R_p}{360 * 22}(R_1 - R_2) \tag{B.33}$$

2) If $9^0 < \varphi < 17^0$, then A_d is given as:

$$A_d = \frac{(\varphi - 9)}{360}\pi(R_1^{\,2} - R_2^{\,2}) + \frac{22}{360}\pi R_p(R_1 - R_2) \tag{B.34}$$

3) If $17^0 < \varphi < 39^0$, then A_d is given as:

$$A_d = \frac{(\varphi - 9)}{360}\pi(R_1^{\,2} - R_2^{\,2}) + (\frac{22}{360}\pi R_p(R_1 - R_2) - \frac{(\varphi - 17)^2 * \pi R_p}{360 * 22}(R_1 - R_2)) \tag{B.35}$$

4) If $39^0 < \varphi < 141^0$, then A_d is given as:

$$A_d = \frac{30}{360}\pi(R_1^{\,2} - R_2^{\,2}) \tag{B.36}$$

5) If $141^0 < \varphi < 171^0$, then A_d is given as:

$$A_d = \frac{(\varphi - 141)}{360}\pi(R_1^{\,2} - R_2^{\,2}) \tag{B.37}$$

6) If $171^0 < \varphi < 360^0\text{-}13^0$, then A_d is given as:

$$A_d = 0 \tag{B.38}$$

where: A_d = The discharge area for the P_1 piston port opening to the discharge chamber in valve plate [m^2]

φ = The angular position of the piston [rad]

R_1 = The outer radius of the discharge kidney port in the valve plate [m]

R_2 = The inner radius of the discharge kidney port in the valve plate [m]

R_p = The piston pitch radius on the barrel [m].

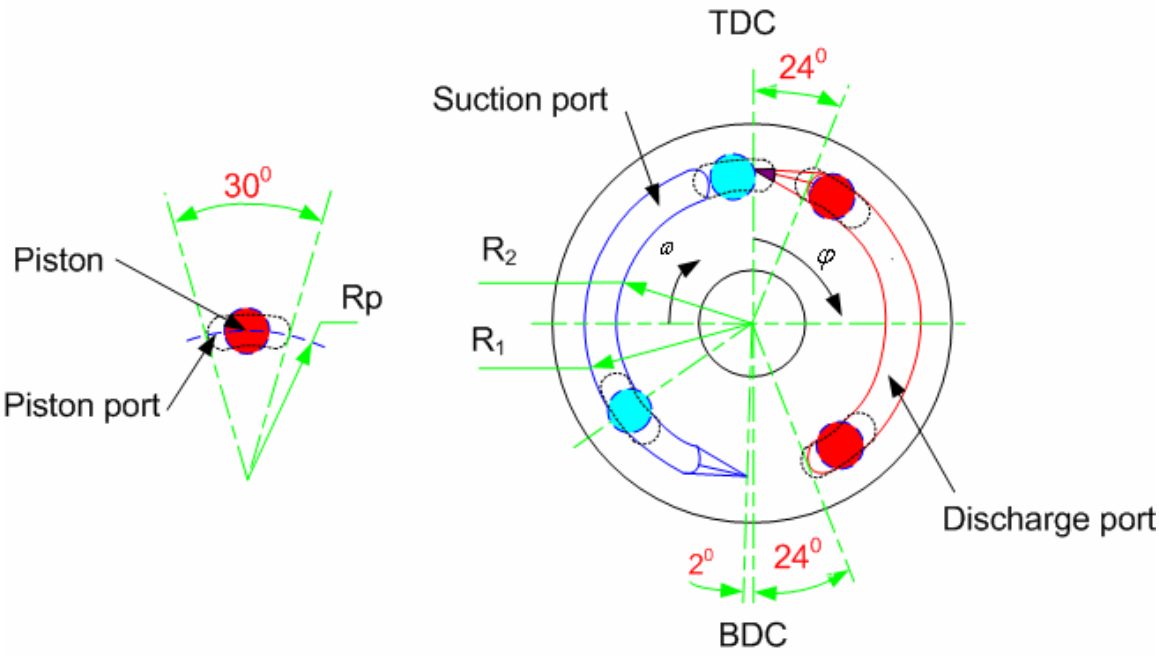

Figure B.5 Discharge area of the piston port opening to the discharge chamber in the valve plate

From the above equations, for a specified barrel angular velocity, the swash plate angle and the load needle valve area, the pump output pressure P_s and the pump output flow Q_s can be calculated. This is the model used in simulation.

Appendix C Simulation Parameters

All simulation studies were based on a Vickers PVB5 variable displacement axial piston pump and the circuit shown in Figure B.2. All parameters related to the pump were measured from the Vickers PVB5 variable displacement axial piston pump.

Table C.1 Simulation parameter value list

Parameter name	Description	Magnitude	Unit
A_p	Piston area	$8.343*10^{-5}$	m^2
A_v	The discharge orifice area of the needle valve	$4.457*10^{-6}$	m^2
α	Phase delay	0.698	rad
B	Bulk modulus	$8.547*10^{8}$	Pa
β	Angle of swash plate	0.335	rad
C_{d1}	Discharge flow coefficient	0.675	
C_{d2}	Discharge coefficient	0.610	
d	Piston diameter	$1.031*10^{-2}$	m
h_g	Gap (radial clearance) between piston and cylinder bore	$0,30,60,90*10^{-6}$	m
L_0	Initial length of piston leakage passage	0.0145	m
r	Piston radius	$5.155*10^{-3}$	m
m	Number of pistons in pump	9	
P_c	Case drain chamber pressure	0	Pa
ρ	Fluid density	860	kg/ m^3
R	Radius of cylinder bore in barrel	$5.162*10^{-3}$	m
R_1	Outer radius of the discharge kidney port in valve plate	0.0238	m

Parameter name	Description	Magnitude	Unit
R_2	Inner radius of the discharge kidney port in valve plate	0.0204	m
R_p	Piston pitch radius on barrel	0.0221	m
μ	Absolutely viscosity	$5.855*10^{-2}$	$N.sec/m^2$
V_0	Piston chamber initial volume	$1.534*10^{-6}$	m^3
V_c	Discharge chamber control volume	$3.156*10^{-5}$	m^3
V_D	Piston dead volume	$2.504*10^{-7}$	m^3
ω	Rotating speed	188.4	rad/second

Appendix D Calibration Information

In this appendix, the calibration equations for different transducers used in this study are presented.

D.1 Pressure transducer

A Sensotec model Z/6415-01ZG pressure transducer, was used to measure the pump outlet pressure. The measured output voltage is directly proportional to the applied pressure. The output voltage ranges 0~5.5VDC.

The pressure transducer was calibrated with a twin seal pressure dead weight tester (Type 5525). Selected weights (representing system pressure) were applied to the test unit and the related transducer output voltages measured. The output voltage as a function of the calibrated pressure is shown in Figure D.1. The scatter of error fell in a range of ± 0.012 MPa (0.1% full scale). The calibration equation was

$$y = 2.2972x-0.006 \quad (D.1)$$

where x was measured output, and its unit is voltage; y was pressure and its unit is MPa.

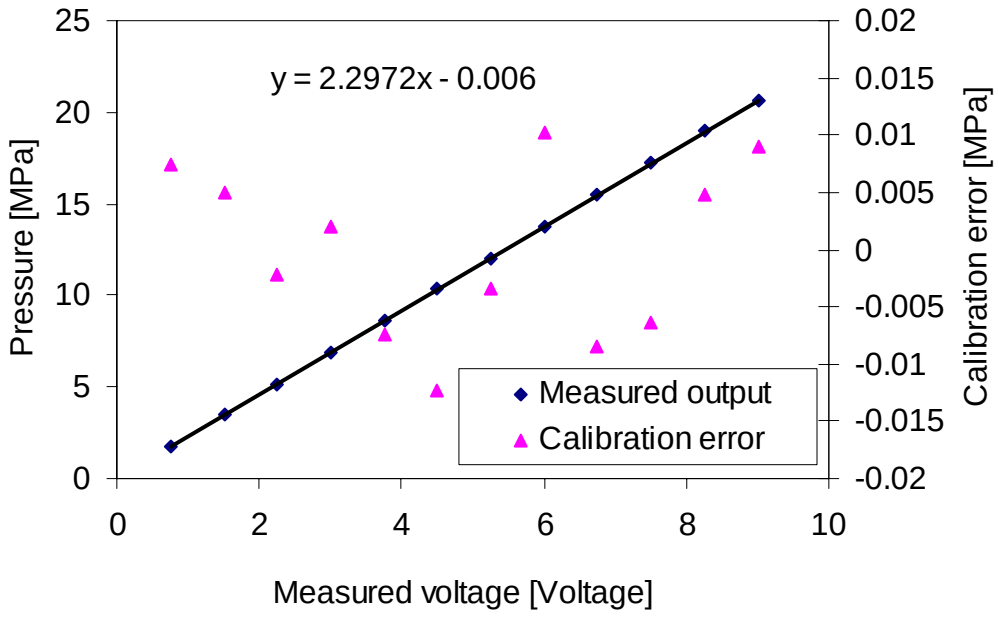

Figure D.1 Calibration of pressure transducer

D.2 Flow transducer

A Ramapo model V-.5-A0S5K6-E flow transducer was used. It measures the flow rate by measuring the force that is produced by the pressure drop across a drag element in the transducer. The output voltage is proportional to the force. According to the user manual [36], the relationship between the flow rate and the measured output voltage is a square root relationship which is given as follow:

$$Q_i = \sqrt{\frac{V_i}{V_{fs}} Q_{fs}} \tag{D.2}$$

where Q_i and Q_{fs} are the instantaneous and full scale flow rates respectively, and V_i and V_{fs} are the instantaneous and full scale voltage outputs.

To calibrate the flow transducer, an accurate flow source must be used. This was achieved by a flow rate calibration system in the Fluid Power Laboratory at the University of Saskatchewan. It consists of one computer, one 113 litre-barrel, a flow control valve, a scale system, and one computer. In this flow calibration system, data from the transducer were processed and then calibrated in a computer using a specific program developed specifically for this flow calibrator. The flow and the output voltage from the differential pressure transducer were recorded. The calibration results are shown in Figure D.2. The calibration errors fell within a range of ± 0.004 litre per second (2.5% of full scale).The calibration equation was

$$Y = 0.1488x-0.011 \tag{D.3}$$

where x was the measured output, and its unit is voltage; y was flow rate and its unit is litre per second.

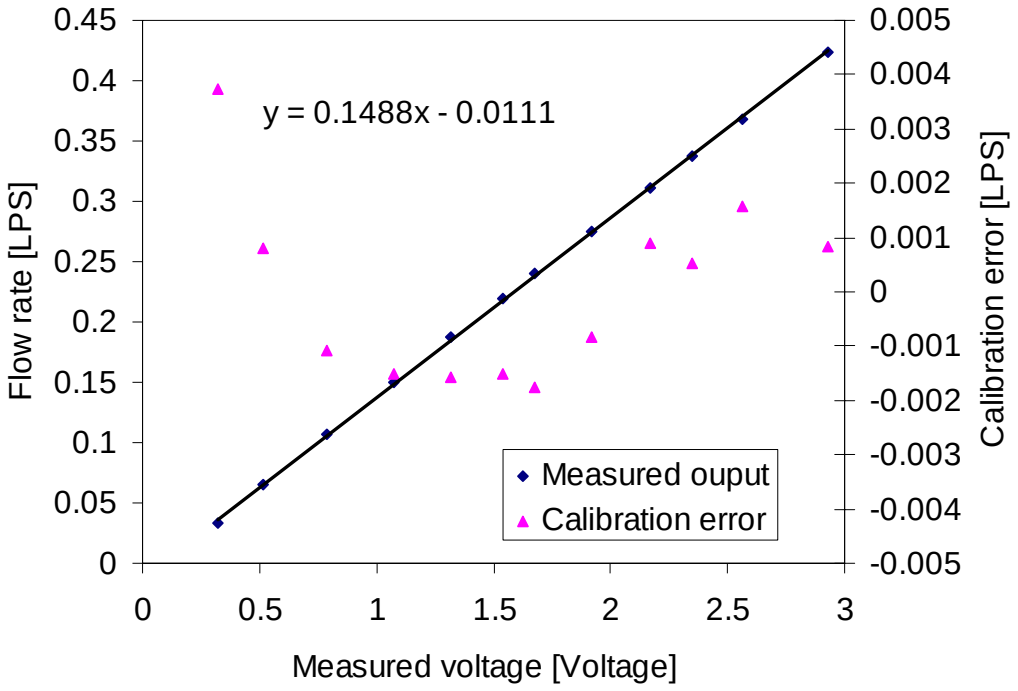

Figure D.2 Calibration of flow transducer

D.3 Diaphragm differential pressure transducer (used to measure artificial leakage flow)

A diaphragm differential pressure transducer was used to determine the flow through the pressure control servo valve by measuring the differential pressure across the needle valve. If C_d, A_{nv}, ρ and ΔP are the discharge coefficient, orifice area, oil density and differential pressure across the needle valve respectively, then the flow is represented by [35]:

$$Q = C_d A_{nv} \sqrt{\frac{2}{\rho} \Delta P} \qquad \text{(D.4)}$$

To calibrate the differential pressure/flow transducer, the accurate flow source described in Section D.2 was again used. The calibration results are illustrated in Figure D.3. The calibration errors fell within a range of ± 0.0015 litre per second. The calibration equation was

$$y = 0.014x - 0.0048 \qquad \text{(D.5)}$$

where x was the measured output, and voltage is its unit; y was the flow rate and its unit is litre per second .

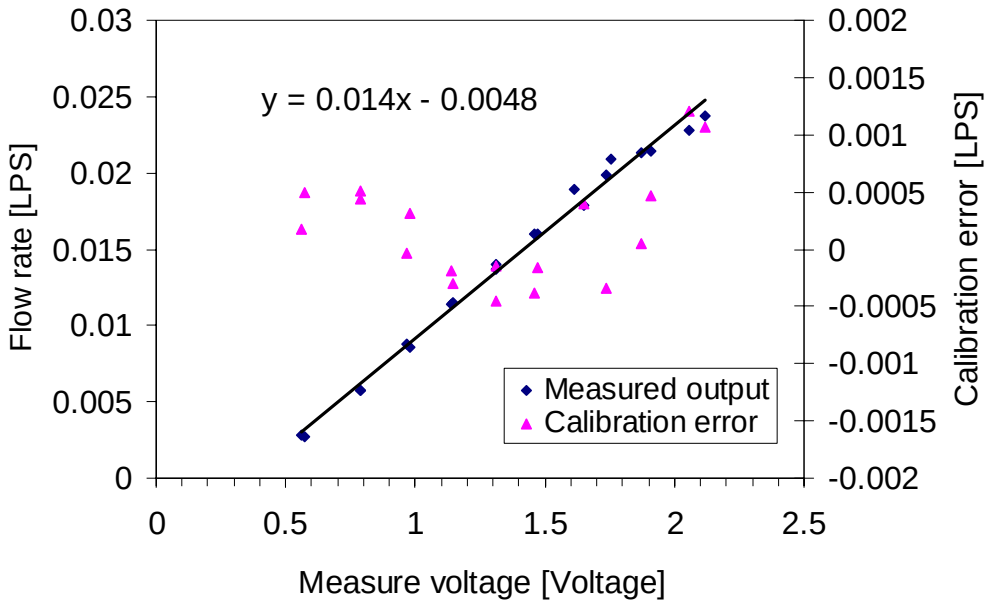

Figure D.3 Calibration of diaphragm pressure transducer

Appendix E Instrumentation Summary

Table E.1 Summary of equipment for the experiments

Instrumentation Name	Manufacture	Settings
Amplifier	Validyne model CD15	
Amplifier	Moog 2310 Signal conditioning amplifier	
Amplifier	Bell & Howell amplifier 8-115	
Amplifier of magnetic pick-up sensor	Analog devices model 950	
Diaphragm differential pressure transducer	Validyne Diaphragm model DP15TL	50 Psi diaphragm 34.5KPa
Flow transducer	Ramapo model V-.5-A0S5K6-E	0-10GPM 0-6.31*10^{-4} m^3/sec
Hydraulic pump	Vickers PVB5 RSY21 C11	5GPM 3.15*10^{-4} m^3/sec
Magnetic pick-up sensor	Aeroflex 812UI-SCT OE	
Needle valve	Parker N200S OH1044035	Max: 5000psi (3GPM) 34.5M Pa
Needle valve	Marsh 900-10000FFG	
Pressure transducer	Sensotec model Z/6415-01ZG	0-5000Psi 0-34.5 MPa
Pressure control servo valve	Moog model 15 010 series 112	
Relief valve	Sperry Vickers CT06F50	500-3000Psi 0.34-20.7 MPa
Thermometer	Extech temp alarm dual thermo	

Instrumentation Name	Manufacture	Settings
Data acquisition board	National Instruments Model PCI-6035	12 bits
DAC I/O connector	National Instruments Model BNC-2090 SN CB212B	16 input channels and 2 output channels
Computer	Pentium II 512 RAM	

Appendix F

Derivation of the Flow through the Pressure Control Servo Valve

The pressure control servo valve is a two stage valve. The first stage consists of a permanent magnet torque motor and flapper nozzle assembly. The torque motor was modelled by Martin [37] as an equivalent electrical circuit of a resistance, R_c, an inductance L_c and a back EMF voltage V_{emf}, equal to a constant K_b multiplied by the torque motor rotational speed $d\theta / dt$, as shown in Figure F.1

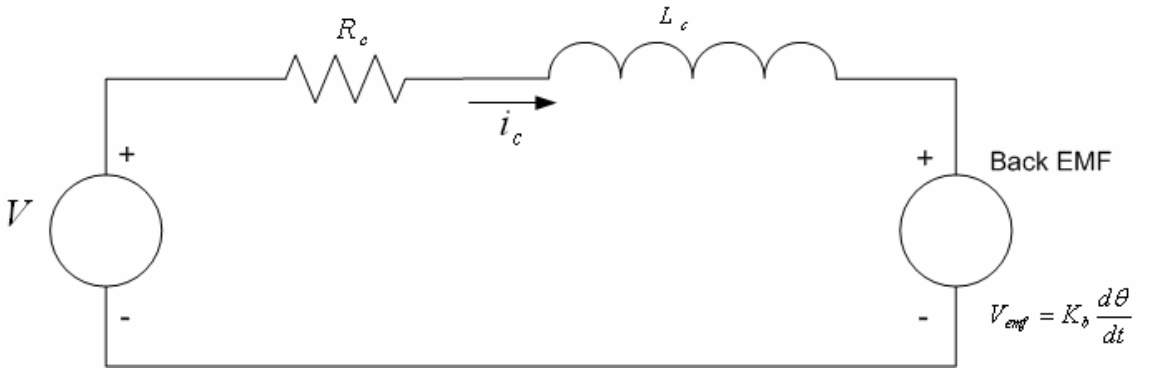

Figure F.1 Equivalent circuit of the servo valve torque motor

The equation for above equivalent circuit of the first stage shown in Figure F.1 is

$$V = V_{emf} + R_c i_c + L_c \frac{di_c}{dt} \qquad \text{(F.1)}$$

where V = Voltage across the coil of the torque motor [V],

V_{emf} = Back EMF voltage by the motion of the armature [V],

R_c = Resistance of the coil [Ohm],

L_c = Inductance of the coil [H],

i_c = Current through the coil [A].

A servo amplifier, as a simple controller, is used to control the current input by a current feedback loop. This design extended the cutoff frequency of the torque motor to a high range, at least as high as 200 Hz. Compared with the bandwidth of the rest of the

valve components, the electronic portion of the valve could be considered as a pure gain K_a'. Hence, Equation F.1 could be simplified to

$$V_c = K_a' i_c \tag{F.2}$$

Then, the coil current could be presented as

$$i_c = K_a V_c \tag{F.3}$$

where K_a = Gain of the servo valve amplifier [A/V] $0.982*10^{-3}$

The second stage of valve can be presented by the following block diagram, as shown in Figure F.2 [34].

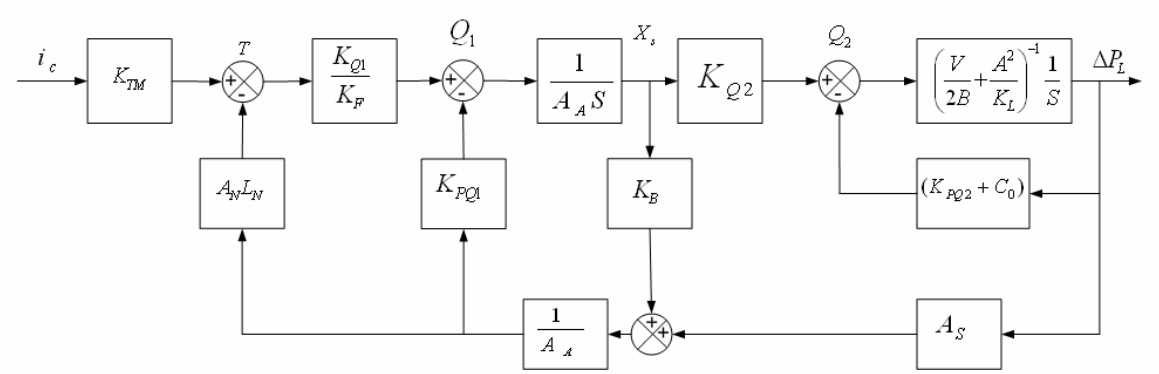

Figure F.2 Simplified block diagram Model 15-010 pressure control servo valve

The parameter values for this valve have been provided by the manufacturer and are as listed:

i_c = Input current ± 10 rated [mA]

T = Torque on armature/flapper ± 0.0165 rated [in*lb]

Q_1 = Hydraulic amplifier flow to drive the spool ± 0.23 rated [cis]

Q_2 = Servo valve flow, no-load ± 55 rated [cis]

Xs = Spool displacement ± 0.020 rated [in]

ΔP_1 = Hydraulic amplifier differential pressure ± 890 rated [Psi]

ΔP_{12} = Load differential pressure ± 3000 rated [Psi]

K_{TM} = Torque motor gain 0.0165 [in*lb/ma]

K_{Q1} = Hydraulic amplifier flow gain 65 [cis/radian]

K_{Q2} = Spool flow gain (no-load) $1.13*10^{-4}$ [cis/in]

K_{PQ1} = Hydraulic amplifier loading effect $1.26*10^{-4}$ [cis/psi]

K_{PQ2} = Spool orifice loading [cis/psi] (depend on the load, nonlinearized)

K_B = Spool Bernoulli force gradient, no-load 1040 [lb/in]

K_F = Net stiffness of armature/flapper 45 [in*lb/radian]

A_A = Spool driving area 0.041 [in^2]

A_S = Spool feedback end area 0.0122 [in^2]

A_N = Nozzle frontal area $3.14*10^{-4}$ [in^2]

L_N = Moment arm to nozzles 0.34 [in]

B = Fluid bulk modulus $1.24*10^5$ [psi]

V = Load fluid volume (per side) [in^3] (not employed in this research)

K_L = Mechanical stiffness of load [lb/in] (not employed in this research)

A = Load drive piston area [in^2] (not employed in this research)

C_0 = Bypass orifice flow (if present) [cis/psi] (not employed in this research)

s = LaPlace operator [sec^{-1}]

Since all of the parameters are in English units, the transform function was firstly derived in these units, and it was then converted to the international system of units. Mason's gain formula was used to develop the transfer function for the pressure control servo valve as follows

$$\frac{\Delta P_L}{i_c} = \frac{d}{as^2 + bs + c} \tag{F.4}$$

where $a = A_A\left(\frac{V}{2B} + \frac{A^2}{K_L}\right)K_F$

$$b = \frac{1}{A_A}\left(\frac{V}{2B} + \frac{A^2}{K_L}\right)\left(K_{Q1}K_B A_N L_N + K_B K_{PQ1} K_F\right) + A_A K_F\left(K_{PQ2} + C_0\right)$$

$$c = \frac{1}{A_A}\left(K_{Q1}K_{Q2}A_S A_N L_N + K_F K_{Q2} K_{PQ1} A_S + K_F K_{PQ1} K_B\left(K_{PQ2} + C_0\right)\right)$$

$$+ \frac{1}{A_A} K_F K_{PQ1} K_B\left(K_{PQ2} + C_0\right)$$

$$d = K_{TM} K_{Q1} K_{Q2}$$

$$\Delta P_L = \frac{K_p \omega_n^{\ 2}}{s^2 + 2\zeta\omega_n s + \omega_n^{\ 2}} i_c \qquad \text{(F.5)}$$

In this particular study, a needle valve was used to simulate the load of the pressure control servo valve. The resulting block diagram is then as follows

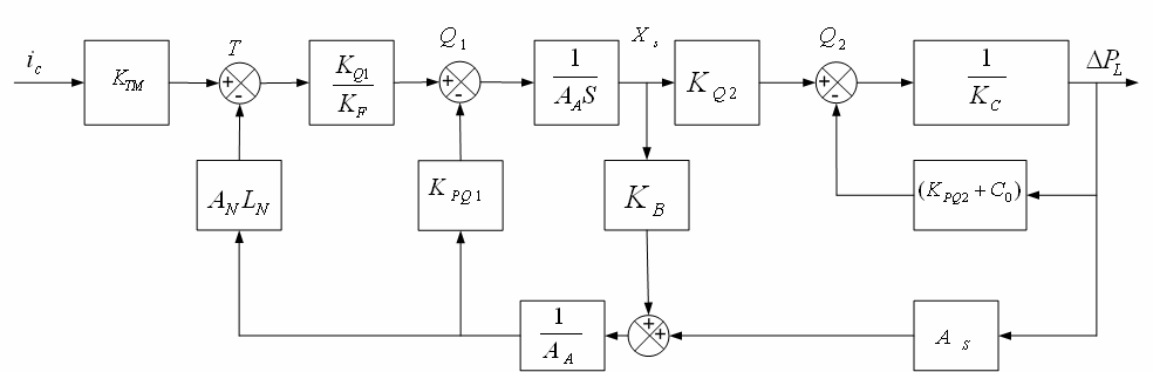

Figure F.3 Simplified block diagram Model 15-010 pressure control servo valve with needle valve as load

The transfer function of the Figure F.3 block diagram is then

$$\Delta P_L = \frac{g}{es + f} i_c \qquad \text{(F.6)}$$

where $e = A_A K_F \left(K_C + K_{PQ2} + C_0\right)$

$$f = \frac{A_S}{A_A}\left(K_{Q1}K_{Q2}A_N L_N + K_F K_{Q2} K_{PQ1}\right)$$

$$+ \frac{1}{A_A}\left(K_{Q1}K_B A_N L_N + K_F K_{PQ1} K_B\right)\left(K_{PQ2} + C_0\right)$$

$$+ \frac{K_C}{A_A}\left(K_{Q1}K_B A_N L_N + K_F K_B K_{PQ1}\right)$$

$$g = K_{TM} K_{Q1} K_{Q2}$$

and K_c is flow-pressure coefficient of the restrictor, equal to 1.718*10^{-4}[in^3/sec/psi], which was calculated from the needle valve,

K_{PQ2} = 1.002*10^{-4} [cis/psi], which was calculated from the needle valve too

C_0 = 0, due to no bypass orifice flow in this circuit.

Substituting all the given parameters into Equation 4.16, yields

$$\Delta P_L = \frac{1.212*10^{-4}}{5.015*10^{-4}s + 8.694*10^{-2}} i_c = \frac{1.394*10^{-3}}{5.700*10^{-3}s + 1} i_c \text{ [Psi]} \quad \text{(F.7)}$$

By converting unit Psi into Pa

$$\Delta P_L = \frac{9.608}{5.700*10^{-3}s + 1} i_c \text{ [Pa]} \quad \text{(F.8)}$$

In this specific system, the load differential ΔP_L is the differential pressure ΔP_{12} across the needle valve (component 19 in Figure 4.2). Hence, the flow through control servo valve is the flow through the needle valve (component 19 in Figure 4.2), which was given as

$$Q_{nv} = C_d A_{nv} \sqrt{\frac{2}{\rho} \Delta P_{12}} \quad \text{(F.9)}$$

where Q_{nv} = Flow through the needle valve, or flow through servo valve [m^3/s]

C_d = Discharge coefficient of needle valve orifice, 0.61

A_{nv} = Orifice area of needle valve, 4.052*10^{-7} [m^2]

ρ = Density of oil, 860 [kg/m^3]

ΔP_{12} = Differential pressure across needle valve (component 19 in Figure4.2) [Pa]

Substituting all parameters into Equation F.9, then gives,

$$Q_{nv} = 1.192*10^{-8} \sqrt{\Delta P_{12}} \text{ [m}^3\text{/s]} \quad \text{(F.10)}$$

From Equations F.3 to F.10, with all the given parameters, the flow Q_{nv} through control valve could be solved. The introduced artificial leakage could then be calculated from the valve flow.

Appendix G

Power Spectral Density

Power spectral density analysis is a useful method to quantify the performance of a rotating machine. It is sometimes very difficult to obtain useful information from time domain signals. On the other hand, the frequency domain may contain useful information. One method of obtaining frequency domain information is by means of power spectral density (PSD). PSD describes how the power (or variance) of a time series is distributed with frequency. Mathematically, it is defined as the Fourier transform of the autocorrelation sequence of the time series. The Fourier transform *X(f)* of the signal *x(t)* is given by

$$X(f) = \int_{-\infty}^{+\infty} x(t) e^{-j2\pi ft} dt \qquad -\infty < f < +\infty \tag{G.1}$$

X(f) contains all the information of the original signal, and *x(t)* can be obtained from *X(f)* by the inverse Fourier transformation:

$$x(t) = \int_{-\infty}^{+\infty} X(f) e^{j2\pi ft} df \qquad -\infty < t < +\infty \tag{G.2}$$

To deal with discrete time-series *x(n)*, the discrete-time Fourier transform (DFT) is used

$$X(k) = \sum_{n=0}^{N-1} x(n) e^{-j2\pi kn/N} \tag{G.3}$$

Computationally efficient algorithms for the calculation of the discrete-time Fourier transform are called Fast Fourier Transform (FFT) algorithms. The FFT can be easily calculated in Matlab® by the following function

$$X = fft(x, n) \tag{G.4}$$

where X is the DFT of x(n) computed with FFT algorithms, and n is the number of FFT points.

The Matlab® program used to calculate the power spectral density in this study is as the follows:

```
X = M0;                    % Name of input signal
Fs = 2000;                 % Sampling frequency (Hz)
N = 2001;                  % No. of points for input signal
Y = fft(x,N);              % N-point FFT operation of x
```

```
  P = Y.*conj(Y)/(N*Fs);                          % Calculating the Power spectral density
Pyy =10*log10(P);                                 % Calculating the decibels
    f = Fs*(0:(N/2-1))/N;                         % Frequency range of the X axis
plot(f,Pyy(1:N/2));                               % Plot the PSD magnitude vs. frequency
xlabel('Frequency [Hz]');                         % Labelling the X-axis
ylabel('Power spectral density [dB/Hz]');         % Labelling the Y-axis
title('Normal pump power spectral density');      % Titling  the plot
```

Appendix H

Data Normalization Method

In order to facilitate the analysis and comparison of the data it was decided to normalize the pressure ripple data. The method using in this study is called Min-Max normalization [38]. Assuming that the data is taken at the same point in the cycle, and at the same operating conditions, the definition of the "normalized data" is:

Pressure normalized data Pnd = (Normal pump pressure Pnp -faulty pump pressure Pfp)/Normal pump pressure Pnp , or

$$Pnd = \frac{Pnp - Pfp}{Pnp} \tag{H.1}$$

where: Pnd = Pressure normalized data

Pnp = Normal pump pressure ripple [Pa]

Pfp = Faulty pump pressure ripple [Pa]

For example, in Figure H.1, the normalized data at 0.02 second is:

$$Rnd = \frac{Pnp - Pfp}{Pnp} = \frac{6.95MPa - 6.57MPa}{6.95MPa} = 0.05 \tag{H.2}$$

This process is repeated at each sample point on the two traces for a specified period

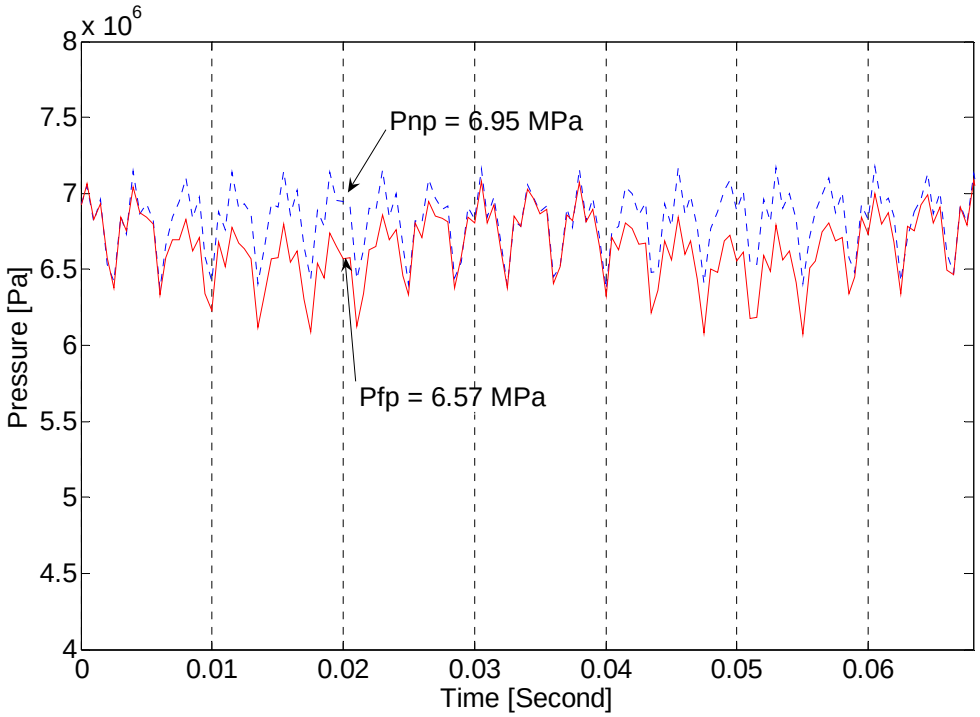

Figure H.1 Definition of data normalization

The follow figure shows the normalized data for the data in Figure H.1.

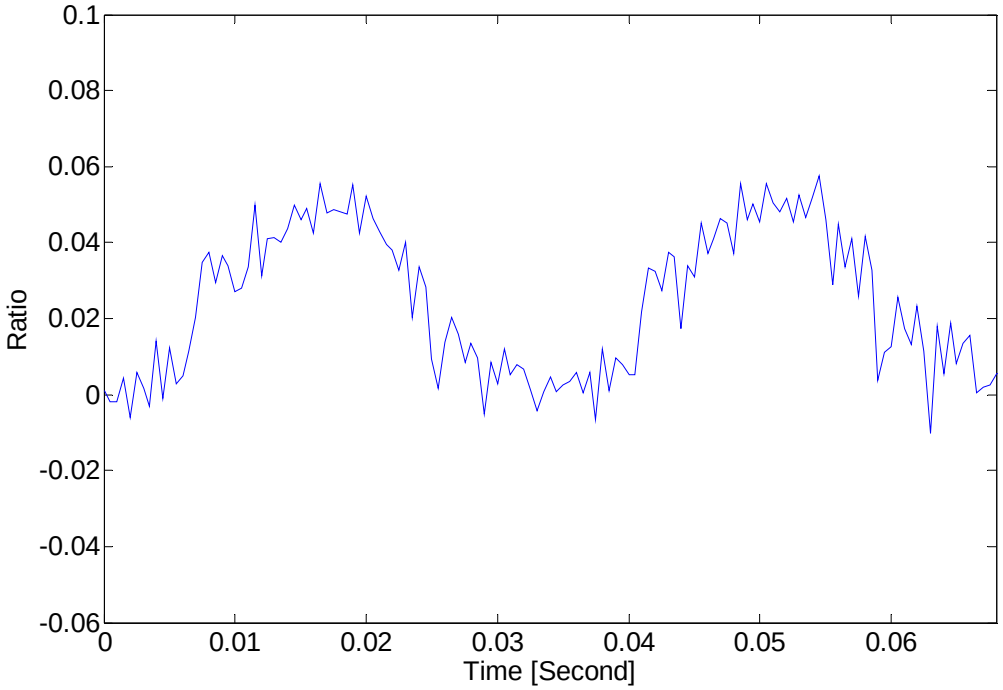

Figure H.2 Normalized data plot